Aeroelastic Loads Modeling
for
Composite Aircraft Design Support

Aeroelastic Loads Modeling
for
Composite Aircraft Design Support

Proefschrift

ter verkrijging van de graad van doctor
aan de Technische Universtiteit Delft,
op gezag van de Rector Magnificus prof.dr.ir. J.T. Fokkema,
voorzitter van het College voor Promoties,
in het openbaar te verdedigen op vrijdag 24 april 2009 om 12:30 uur

door

Haroon Awais BALUCH

Master in Mechanical Engineering, College of EME, NUST, Pakistan
geboren te Peshawar, Pakistan

Dit proefschrift is goedgekeurd door de promotor:
Prof.dr.ir. M.J.L. van Tooren

Samenstelling promotiecommissie:

Rector Magnificus	voorzitter
Prof.dr.ir. M.J.L. van Tooren	Technische Universiteit Delft, promotor
Prof.dr.ir. D. Rixen	Technische Universiteit Delft
Prof.dr.ir. Z. Gürdal	Technische Universiteit Delft
Prof.dr.ir. J.E. Cooper	University of Liverpool
Asst.prof.dr.ir. I. Tuzcu	California State University, Sacramento
Dr.ir. J. Hofstee	Loads and Aeroelastics Department, Airbus Germany
Prof.dr.ir. J.A. Mulder	Technische Universiteit Delft, reservelid

ISBN 978-90-8559-507-6

keywords: flexible aircraft, modeling and simulation, composite airframe, material anisotropy, coupled vibrations, gust, maneuvers, dynamic loads

Printed in the Netherlands.

Nomenclature

A	state coefficient matrix
AR	aspect ratio
ASF	aircraft shape functions
A_x	$\left[[C^{(1)}_{V\Omega}(t)]M^{(1)^{-1}}_{\xi\xi} + B_x - B_u G\right]$
$A_{V\Omega}$	coefficient matrix w.r.t aerodynamic damping
A_{ij}	components of membrane stiffness matrix A in Eqs. (1.3–1.8)
B_x	coefficient matrix w.r.t aerodynamic stiffness
B_u	coefficient matrix w.r.t control inputs
C	full order damping matrix
CTC	conventional tail configuration
C_i	component rotation matrix w.r.t O_f
C_d	drag coefficient
C_{d_α}	$\frac{\partial C_d}{\partial \alpha}$
C_l	vertical lift coefficient
C_{l_α}	$\frac{\partial C_l}{\partial \alpha}$
C_{l_β}	roll stiffness
C_{l_δ}	$\frac{\partial C_l}{\partial \delta}$
C_{m_α}	pitch stiffness
C_{n_β}	yaw stiffness
C_s	side force coefficient
C_{s_β}	$\frac{\partial C_s}{\partial \beta}$
D_m	matrix of eigenvectors
$D.o.F$	degree of freedom
D_i	represents over the length or span integration
EI	bending stiffness of a section
F_f	resultant force vector at O_f
G	closed loop gain matrix
GJ	torsional stiffness of a section
H	gust gradient in meters
J	cost function
J_f	inertia matrix of the whole aircraft

J_i	local inertia matrix at a node of comp. i
K	full order stiffness matrix
K_ξ	reduced order stiffness matrix
L	total length of a beam or a component
LTI	linear time invarient
LTV	linear time varient
L_f	generalized loads at O_f
L_η	reduced order generalized structural loads
M	full order global mass matrix
M_f	resultant moment vector at O_f
M_j	resultant bending moment due to component shear loads in Fig 4.2
M_{xi}	external torsion moment on a node
M_ξ	reduced order mass matrix
O_i	component origin
P_d	dynamic pressure
Q, R	weighting matrices in performance index
Q_j	resultant shear as component internal loads in Fig 4.2
Q_u	generalized force vector in bending
Q_ψ	generalized force vector in torsion
R_f	position vector $[R_{f_x} \;\; R_{f_y} \;\; R_{f_z}]^T$ w.r.t inertial axes
$\tilde{S}$	first moment of inertia
T	kinetic energy
TTC	T-tail configuration
U_i	potential energy
V_f	rigid-body velocity vector in translation along O_f, $[V_{f_x} \;\; V_{f_y} \;\; V_{f_z}]^T$
$\bar{V}_i$	rigid-body velocity vector in translation on a particular node of a component i
V_{zi}	external shear force on a node
$a.c$	aerodynamic center
b	wing span
c_i	chord length of a particular section of a component
$e.a$	elastic axis
e_1	null vector of size (1×3)
e_2	null matrix of size (6×6)
e_3	null vector of size (6+m×1)
e_4	null vector of size ($1 \times m$)
d	eigenvector
f_i	vector of resultant forces on a certain section of a component i
h	height of a box structure in Eqs. (1.12–1.14) or a thickness of a ply in Eq. (1.4)
k	stiffness due to the material anisotropy
k_i	induced drag factor
l_i	moment arm vector in aerodynamic dampipng matrices (i.e. Eqs. (3.10–3.24)
m	mass of the aircraft
n_z	load factor

p	generalized momenta
q	vector of full order generalized coordinates
r	position $[r_x \;\; r_y \;\; r_z]^T$ of a node w.r.t a component origin
$r.a$	reference axis
s	vector of full order generalized velocities
s_i	side force on a certain section of a component i
t	time
t_f	final time of the simulation
u	control vector $[\delta_{el} \;\; \delta_a \;\; \delta_r \;\; \delta_T]^T$
w	width of a box structure
$w.r.t.$	with respect to
w_g	vertical discrete gust function
w_{g0}	peak or design vertical discrete gust velocity
x_g	distance penetrated into the gust in meters
y_i	distance between reference and elastic axes
z_i	total structural deflection of a particular section of a component i
α_{f_i}	rotation angles due to aft fuselage bending
α_i	anagle of attack at O_f
β_i	side-slip angle at O_f
δ_i	control input vector
η	vector of reduced-order generalized velocities
ρ	air density
Ω_f	rigid-body rotational rates along O_f in roll, pitch, and yaw
θ_f	position vector in roll, pitch, and yaw $[\theta_{f\Phi} \;\; \theta_{f\Theta} \;\; \theta_{f\Psi}]^T$ w.r.t inertial axes
Φ	eigenfunctions given in Table 3.1
ϕ	eigenfunctions or shape functions of a component
λ	eigenvalue
ξ	vector of reduced-order generalized coordinates

Subscripts

E	engine
T	thrust
a	aileron
a	represents resultant aerodynamic loads due to lift and drag in Eq. (2.37)
dof	degree of freedom
d	represents drag in Eqs. (2.31–2.37)
d	represents dynamic loads in Eqs. (4.4–4.10)
e	empennage
el	elevator
f	fuselage
g	gravity
h	horizontal tail
i	referring to a particular component

ij	rows and column in a matrix
l	ply number on the webs of box structure in Eqs. (1.9–1.11)
l	represents lift in Eqs. (2.31–2.37)
m	no. of shape functions in reduced-order
n	ply number on the flanges of box structure in Eqs. (1.3–1.11)
n	no. of sections over the length of a beam in Eqs. (2.19–2.21)
r	rudder
s	represents static loads in Eq. (4.3)
s	represents side force in Eqs. (2.32–2.37)
u	degree of freedom (D.o.F) in bending
v	vertical tail
w	wing
ψ	degree of freedom (D.o.F) in torsion

Superscripts

(0)	zero-order
(1)	first-order
$1, 2$	represents upper and lower sides of a box beam in Eqs. (1.6–1.14)
$3, 4$	represents right and left sides of a box beam in Eqs. (1.6–1.14)
A	aft
F	fore
L	left
M	total number of plies on the webs of box structure in Eqs. (1.9–1.11)
N	total number of plies on the flanges of box structure in Eqs. (1.3–1.14)
MDM	mode displacement method
R	right
SFM	summation of forces method
V	vertical
T	transpose
$\sim$	represents a skew symmetric matrix of a particular vector

Contents

Chapter 1

Introduction

The mathematical modeling of maneuvering flexible aircraft is in "constant evolution". Previously the limitations of hardware and numerical techniques in terms of computing time needed for large scale problem solving forced the engineers to make several far reaching approximations in the mathematical modeling of aircraft dynamics. However, the ongoing reduction in computational cost resulting from the decreasing cost of hardware and the increasing efficiency of numerical techniques allows todays engineers to simulate efficiently not only simple models based on rigid-body flight mechanics but also complex models incorporating many of the details associated with the trinity of flight dynamics, controls and aero-elasticity. Current aircraft development like the emergence of high-altitude and long-endurance Unmanned Aerial Vehicles (UAVs) with very high aspect ratio flexible wings, subject to large wing deflections and rigid-body perturbations in flight, has opened a new paradigm in the modeling and simulation of highly flexible aircraft, requiring inclusion of the structural nonlinearities, both geometry and material related, in the mathematical model [1, 2, 3]. However, it is not the objective of the current research to focus on large geometric perturbations characterizing the flight of these specialized aircraft. The aim is to develop a linear model, considering only the small perturbations around the steady state condition, that allows the analysis of elastically tailored composite aircraft, both business jets [4] and large civil transport airplanes [5]. Although such a linear model is only valid close to the steady state condition, it can be used in many cases to support compliance finding to loads related aviation requirements found in FAR/CS part 23 and part 25, applicable to light and large aeroplanes respectively.

The beginning of this century shows a new trend in airframe design for large civil transport aircraft. There is a paradigm shift from fully metal based structures to those dominated by the choice for fiber composites as baseline material. The

Boeing B787, approaching certification, and the Airbus A350, under full scale development, are clear examples in this regard. The fuselage shells of the B787, frames excluded, are made of carbon fiber reinforced epoxy. The A350 fuselage is expected to show an even larger dominance of fiber composites. Previously fiber composites usage in primary aircraft structure was restricted mainly to the tail section (i.e. tail section A340). Today we are not far away from a fully fiber composite dominated airframe on a commercial passenger aircraft being airworthy. Although many light aircraft are already flying with fiber composite airframes, the criticality increases for large size, highly utilized aircraft, especially for the pressurized fuselages in those airplanes. The increasing use of composite material demands some steps in the evolution of the mathematical modeling of the flexible aircraft, some of which are explained in the next sections of this chapter.

1.1 The saga of elastic axis

To solve the dynamics of flexible aircraft, it is common among aeroelasticians and flight loads engineers to use the elastic axis of an equivalent beam model of an aircraft component as a reference for vibrations of that particular component. For a beam element with isotropic material properties, the shear center of a particular section of a beam element is assumed to decouple the bending and torsional deformations, where the coupling becomes a cross-sectional property, independent of the loads [6]. The elastic axis intersects with these centers and acts as a reference. Figure 1.1(a) shows a deflected wing (i.e. u in bending and ψ in torsion) with isotropic material properties, where the x-axis of the axes system x, y, z represents the elastic axis $e.a$ of the wing from root to tip. It shows that the vertical lift force F_Z acting on the aerodynamic center $a.c$ of a section, creates a torsional moment M_x around the $e.a$ and a bending moment M_y on the highlighted section. Eq. (1.1) gives us an expression of static aeroelasticity where the inverse of the stiffness matrix is multiplied with the load vector to give the deflection curvatures. It is to be noted that due to both isotropic material properties and the use of $e.a$ as the reference of deformation, a diagonal stiffness matrix results that decouples the bending and torsion degrees of freedom (D.o.F).

$$\begin{bmatrix} u'' \\ \psi' \end{bmatrix} = \begin{bmatrix} EI & 0 \\ 0 & GJ \end{bmatrix}^{-1} \begin{bmatrix} M_y \\ M_x \end{bmatrix} \tag{1.1}$$

where u'' or $\frac{du^2}{dx^2}$ is the bending curvature and ψ' or $\frac{d\psi}{dx}$ is the twist curvature. Now the wing shown in Fig. 1.1 is assumed to be made of fiber composite material, where the principal axes of the laminates around the wing-box, espe-

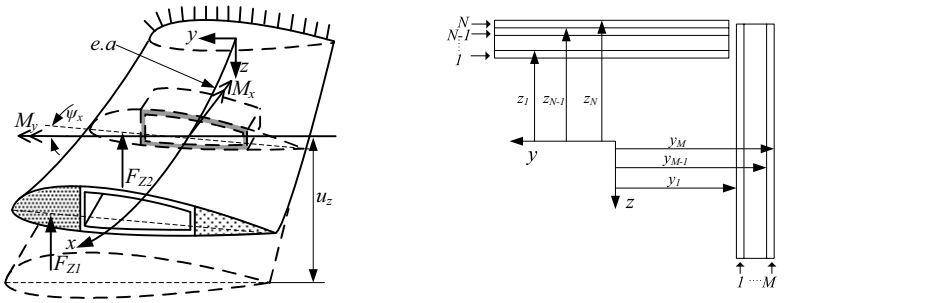

(a) Deflected wing. (b) Laminate geometry of flanges and webs.

Figure 1.1: A deflected wing with the elastic axis as a reference of vibrations.

cially on the webs (i.e. left and right sides of the wing-box), are not aligned with the reference axes for the loads. This misalignment results into a coupling between bending and torsion and makes the stiffness matrix nondiagonal thus introducing off-diagonal k term:

$$\begin{bmatrix} z'' \\ \psi' \end{bmatrix} = \begin{bmatrix} EI & k \\ k & GJ \end{bmatrix}^{-1} \begin{bmatrix} M_y \\ M_x \end{bmatrix} \tag{1.2}$$

where z'' is curvature of the total deflection due to coupling of bending and torsion D.o.F. (i.e. $z = u + y\psi$ and y is the distance between the shear center and the aerodynamic center). It is quite evident from Eq. (1.2) that the use of elastic axis $e.a$ as a reference of vibration does not decouple the bending and torsion deformations, and the off-diagonal k term term naturally causes a coupling.

1.1.1 k term and stiffness matrix: a brief overview

As mentioned above the misalignment of fiber principal axes with the reference load axes around the wing-box gives the coupling term in the stiffness matrix. Before discussing how a bending-torsion coupling k comes into being in a fiber composite wing-box, it is appropriate to briefly describe the process of constructing a stiffness matrix from a ply level to a laminate and finally to a box structure. The stiffness matrix of a laminate is normally constructed by first multiplying the stiffness matrix of material with the ply thickness, which are further added in a global stiffness matrix of a laminate, normally known as A_{ij} matrix. The 3×3 stiffness of a ply at $\Theta = 0$ direction and A_{ij} matrix for N

number of plies are defined as [7]:

$$[Q]^{\Theta=0} = \begin{bmatrix} \frac{E_{11}}{1-\mu_{12}\mu_{21}} & \frac{\mu_{12}E_{22}}{1-\mu_{12}\mu_{21}} & 0 \\ \frac{\mu_{12}E_{22}}{1-\mu_{12}\mu_{21}} & \frac{E_{22}}{1-\mu_{12}\mu_{21}} & 0 \\ 0 & 0 & G_{12} \end{bmatrix} \tag{1.3}$$

$$A_{ij} = \sum_{n=1}^{N} \bar{Q}_n^{\Theta} h_n \tag{1.4}$$

in which E_{11} and E_{12} represent the moduli of extension in each direction. G_{12} and μ_{12} represents the shear moduli and Poisson's ratio, respectively. Θ and h_n are the ply angle w.r.t. the laminate reference axes and ply thickness, respectively. The $\bar{Q}$ represents the transformed stiffness matrix of a particular ply in a direction with a $\Theta \neq 0$. For example, the $[Q]^{\Theta=0}$ and $[Q]^{\Theta=15}$ matrices of a ply with material properties given in the footnotes of Table 1.1 are found to be:

$$[Q]^0 = \begin{bmatrix} 1.6159 & 0.4687 & 0 \\ 0.4687 & 1.1160 & 0 \\ 0 & 0 & 0.6140 \end{bmatrix} 10^{10} \tfrac{N}{m^2}, \quad [Q]^{15} = \begin{bmatrix} 1.5470 & 0.5041 & 0.2476 \\ 0.5041 & 1.1140 & 0.0023 \\ 0.2476 & 0.0023 & 0.6848 \end{bmatrix} 10^{10} \tfrac{N}{m^2} \tag{1.5}$$

The above example shows that the slight change in the direction of the ply w.r.t. the laminate reference axes fills the zero terms of the Q matrix (i.e. Q_{13} and Q_{23}), which give couplings between the shear and extension D.o.F. By putting the $[Q]$ matrices of Eq. (1.5) in Eq. (1.4) gives the A_{ij} matrix of a two ply laminate. For a 4-sided (i.e. upper, lower, left, and right) wing-box structure with a straight laminate on each side, the A_{ij} matrices of upper and lower side laminates are transformed to a uniaxial stiffness w.r.t. left and right sides as follows [7, 8]:

$$K_{11}^{(1,2)} = \sum_{n=1}^{N} A_{11}^{(1,2)} - (A_{12}^{(1,2)})^2 / A_{22}^{(1,2)} \tag{1.6}$$

$$K_{16}^{(1,2)} = \sum_{n=1}^{N} A_{16}^{(1,2)} - \left(A_{12}A_{26}\right)^{(1,2)} / A_{22}^{(1,2)} \tag{1.7}$$

$$K_{66}^{(1,2)} = \sum_{n=1}^{N} A_{66}^{(1,2)} - (A_{26}^{(1,2)})^2 / A_{22}^{(1,2)} \tag{1.8}$$

in which the superscripts 1 and 2 represent upper and lower sides. With the help of the matrices K_{ij} of upper and lower sides, and A_{ij} of left and right sides the equivalent bending stiffness EI, torsion stiffness GJ, and bending-torsion

stiffness k are expressed as [8]:

$$EI = \sum_{n=1}^{N} \int\int_{1,2} K_{11}^{(n)} (z_{(n)})^2 dxdy + \sum_{l=1}^{M} \int\int_{3,4} A_{11}^{(l)} (z_{(l)})^2 dxdy \tag{1.9}$$

$$GJ = \sum_{n=1}^{N} \int\int_{1,2} K_{66}^{(n)} (z_{(n)})^2 dxdy + \sum_{l=1}^{M} \int\int_{3,4} A_{66}^{(l)} (y_{(l)})^2 dxdy \tag{1.10}$$

$$k = \sum_{n=1}^{N} \int\int_{1,2} K_{16}^{(n)} (y_{(l)})^2 dxdy \tag{1.11}$$

in which z_n and y_l are the distances of each ply of flanges (i.e. upper and lower side) and webs (i.e. left and right side), respectively, to the reference axes of the wing-box, see Fig. 1.1(b). Eqs. (1.9–1.11) can be simplified as [7]:

$$EI = \frac{w \times h}{4} \left[K_{11}^{(1)} + K_{11}^{(2)} \right] \tag{1.12}$$

$$GJ = \frac{w^2 \times h^2}{\left(w+h\right)^2} \left[\left(K_{22}^{(1)} + K_{22}^{(2)} \right) w + \left(A_{66}^{(3)} + A_{66}^{(4)} \right) h \right] \tag{1.13}$$

$$k = \frac{w^2 \times h^2}{2\left(w+h\right)} \left[K_{22}^{(1)} + K_{22}^{(2)} \right] \tag{1.14}$$

where w and h are width and height of the cross-section, respectively. The above equations are then used to calculate the stiffness properties of a box beam given in Table 1.1. It shows that first lay-up configuration (i.e. $[0/90]_6$) has symmetric[1] laminates on all the four sides, which give no coupling in torsion and bending D.o.F (i.e. $k = 0$). The second lay-up configuration (i.e. $[15]_6$ and $[15/-15]_3$) has symmetric-unbalanced laminates on the flanges and symmetric-balanced[2] laminates on the webs, which give the coupling (i.e. $k \neq 0$). This example shows that coupling arises due to balanced laminates on the webs, where the principal axes of the fiber directions around a close section are not aligned with the reference axes for the loads.

The elements of a stiffness matrix depend upon cross-sectional properties and, as stated above, the material properties (i.e. A_{ij} of each laminate). The moduli of metal alloys are well determined and published in the literature. In case of fiber composite, as shown above, it largely depends upon the lay-up configuration of the fibers and requires some analytical formulas to construct the stiffness matrix. In addition to Eqs. (1.3–1.14), two excellent papers by Hong

[1] A laminate is called *symmetric* around its midplane if the ply located at a position $+z$ is identical to the ply at -z [9].

[2] A laminate is called *balanced* for every ply in the $+\Theta$ direction there is an identical ply at in the -Θ direction [9].

Table 1.1: Wing-box layers configuration and stiffness properties

Configuration[a]		Ref. 8[b]			MSC.Nastran[b]		
Flanges	Webs	EI	GJ	k	EI	GJ	k
$[0/90]_3$	$[0/90]_3$	13.1	2.34	0	12.73	2.02	0
$[15]_6$	$[15/-15]_3$	22.53	5.26	5.85	14.90	2.51	3.0

[a] Mechanical properties: $E_{11} = 14.19$GPa, $E_{22} = 9.8$GPa, $G_{12} = 6.14$GPa, $\mu_{12} = 0.42$, ply thickness = 0.127mm, width = 0.0242m, height = 0.014m.

[b] Units: kg-m^2.

and Chopra [10], and Smith and Chopra [11] also give a detailed analytical model of constructing the stiffness matrix for a thin-walled fiber composite helicopter blade. Although this model takes care of calculating stiffness along bending-extension degree of freedom, which is generally not incorporated in a fixed wing aircraft, one can use the model by omitting the bending-extension coupling in the stiffness matrix. Moreover, Lottati [12] also gives an overview on how to construct the stiffness matrix for a composite wing-box. As shown in Table 1.1 the results from Ref. 8 are compared to the equivalent stiffness values calculated from the static condensation in MSC.Nastran software. Equivalent stiffness values for a box type structure can be obtained quite simply by solving the above equations but for complex and large structures like a fuselage section, the usage of static condensation techniques included in a state of art FEA software like MSC.Nastran becomes inevitable. Static condensation of a finite element model gives the equivalent stiffness values at the chosen condensation points and constructs the beam model for further aeroelastic analysis, see Appendix A for a brief description on this account.

Now the question arises how does the coupling affect the dynamics of the aircraft. In aeroelastic tailoring, e.g. to increase the divergence and flutter speeds, the optimized design often suggests different combinations of fiber lay-up [13]. It shows that the flutter speed in case of asymmetric-balanced and symmetric-balanced laminates of a wing-box is increased as much as 20% compared to those of from purely symmetric-unbalanced laminates, but, as stated in Section 1.1, balanced laminates introduce cross coupling term k in the stiffness matrix. Previously, research on a box beam of a helicopter blade shows that the symmetric-balanced laminates on each flange and web contribute to the cross coupling terms with an appreciable influence on stability of the blade [10]. Later on, the deformations calculated analytically in Ref. 10 were correlated with experimental results with satisfactory conformity [8].

1.2 The problem identification

As stated above, the shear center of a particular section plays a significant role in decoupling the bending and torsion deformations, and the intersection of shear centers over the length of beam makes the elastic axis [6]. It is also shown that the effectiveness of the *e.a* in decoupling is reduced if a nondiagonal stiffness matrix comes into being, as Eq. (1.2) makes it quite clear that the cross coupling terms in the stiffness matrix gives a torsional deformation due to bending moment. In this particular case the shear center does not remain to be a cross-sectional property, rather becomes a local beam property (i.e. a beam with constant cross-section will not have the same point of the shear center in each of the cross-section and the resultant elastic axis might not be exhibiting a straight line from root to tip). To assert this claim, a mathematical example is presented in this regard [6, 8]; the vertical aerodynamic force F_Z in Fig. 1.1 applies the torsion load around the shear center of the highlighted section as $F_Z \times y$, where y is the distance between the *a.c* and shear center[3]. Bending moment is applied as $F_Z \times (L - x)$, where L is the total length of the wing. By integrating Eq. (1.2) total twist due to both bending and torsion loads is expressed as [8]:

$$\psi(x) = \frac{-k\left[F_Z \times (2Lx - x^2)\right] + 2EI\left[F_Z \times y\right]x}{2\left[EI \times GJ - k^2\right]} \tag{1.15}$$

A shear center is a point where the application of a force will not lead to torsional deformation (i.e. $\psi = 0$), so the above equation takes the form as:

$$y(x) = \frac{k(2L - x)}{2EI} \tag{1.16}$$

where the length L can be written as a function of x, so the above equations takes the form as follows:

$$y(x) = \frac{kx}{2EI} \tag{1.17}$$

Eq. (1.17) makes it quite clear that the shear center does not remain to be a cross-sectional property anymore and it is dependent on the stiffness terms and moreover over the length position in the wing (i.e the position of shear center y is proportional to the length, so as the length of the wing is increased, the shear center at the tip will tend to go out of the structural boundaries). Otherwise, as suggested by Hodges [6], the locus of mass centroids as being a reference line can be an alternative to the elastic axis, but the straightness of this line is also not guaranteed due to structural discontinuities in fixed-wing

[3]It is to be noted that in Chapter 2 the symbol y represents the distance between the *r.a* and the shear center, and that should not to be mixed up with the definition given in this section.

aircraft. So keeping in mind the increasing use of fiber composite material in aircraft structures, a mathematical model is looked for that does not have the necessity of using the *e.a* as references for vibrations in aircraft components. The use of the *e.a* of a component is to be replaced by a "practical" reference axis *r.a* and its location on each component of the aircraft is fixed at a certain position relative to the aircraft body axes. The use of *r.a* was already shown in Ref. 12. But the mathematical modeling was restricted only to a wing structure for flutter analysis. The aim of this research is to address the dynamics of the whole aircraft, which, as stated, includes the trio of flight dynamics, controls and aeroelasticity in one simulation. The preference is to modify the existing mathematical model, rather than "reinventing the wheel". In the next section we discuss the choices made for the existing mathematical model for the inclusion of a practical *r.a* on each component and its effects on the component stiffness matrix alongside the anisotropic material properties.

1.3 A search for a mathematical model

Upon looking at the existing linear models which address the three different disciplines of flight dynamics, controls, and aeroelasticity, we find a few models in the published archives and their characteristics are briefly described here by categorizing them into inertially decoupled equations of motion and inertially coupled equations of motion.

1.3.1 Inertially decoupled equations of motion

Inertially decoupling of equations of motion means that different forms of motion, whether elastic or rigid-body, and translational or rotational are not coupled to each other. In short a vibrating fuselage does not affect the wings or tail planes through inertial terms and, vice-versa. Also the rigid-body motion of the aircraft does not affect the structural vibrations through inertial terms and, vice-versa. The reason is, as stated earlier, the mathematical models of flexible aircraft are approximated for the simplifications. The foremost simplifications comes through the use of such reference axes as aircraft stability axes, usually called as "mean axes", which are not fixed with a material point on the fuselage [14, 15, 16]. The resulting inertial decoupling by using the mean axes is explained as under:

1. Omission of the linear and angular momenta due to elastic deformation in the total kinetic energy of the aircraft, i.e. the derivatives of the Lagrangian of the whole aircraft with respect to local structural velocities are zero in those equations that belong to the rigid-body motion of the

aircraft, hence it inertially decouples the two sets of equations i.e. flight and structural dynamics. The only coupling between these two sets of equations is achieved through the aerodynamic forces [5, 14].

2. The use of free-free orthogonal mode shapes that decouple the structural dynamics equations and constructs a diagonal[4] mass matrix [5, 14]. As stated, a vibrating fuselage does not affect the wings or tail planes through inertial terms and, vice-versa.

Inertially decoupled equations of motion derived in Ref. 14 are reproduced in Appendix B with a brief description. The Eq. (B.4) of Appendix B expresses the use of orthogonality criteria. Here it is important to note that though the structural dynamics equations are inertially decoupled but in the case of elastic coupling, as given in Eq. (1.2), these equations are not truly fully decoupled rather these equations remain intact through the stiffness terms. However, these equations are solved as a function of natural frequencies, which can also be determined through ground vibrational tests (GVT) and in that case too, that during the system modeling, the stiffness matrix is also diagonalized by using the orthogonal modes [18].

1.3.2 Inertially coupled equations of motion

In contrary to the mean axes system, by using the quasi-coordinate approach, Meirovitch and Tuzcu [4] show the replacement of mean axes by another kind of aircraft body axes, called as "body fixed axes", which are fixed to a material point on the fuselage. The aircraft structural components like fuselage, wings, and empennage are represented in the form of equivalent beams with fixed-free mode shapes. The equations of motion are inertially coupled by taking into account the effects of linear and angular momenta due to elastic deformation in the total kinetic energy of the aircraft, hence giving a non diagonal mass matrix. However in this case too, the use of elastic axes makes a diagonal stiffness matrix. Most recently these inertially coupled equations of motion are extended to the simulation of dynamic loads during atmospheric turbulence [19].

1.4 The scope of the present work

After identifying the problem in using *e.a* as a reference for vibrations it is time to describe the scope of the work presented here. As stated above, it is intended

[4] In this report a diagonal or non diagonal matrix means a "block" diagonal or non diagonal matrix, respectively. A block diagonal matrix is defined as a square matrix in which the diagonal elements are square matrices of any size, and the off-diagonal elements are zero. [17]

to come up with such a mathematical model that should address all the main areas related to the aircraft dynamics and moreover should also take care of the new challenges as state above. It is proposed to modify the existing state of the art mathematical model so in this regard the model derived by Meirovitch and Tuzcu [4] is considered to be the most suitable as it is the latest version and closer to reality than to those of models derived in Ref. 14 and 16. Once the equations of motion are updated with the modifications, the equations are expanded to the structural loads, which are one of the primary factors in the sizing of structural parts during the preliminary design phase. In addition to the inclusion of bending-torsion coupling it is also thought to transform the given equations of motion to an aircraft model with horizontal tails mounted on a vertical tail, see Fig. 1.2. This requirement comes through an industrial project [20] on the flight loads simulation of a regional jet. Moreover, it is also thought that while looking at the current market trends in the business and regional jet designs the T-Tail configuration is quite common [21] and the present work will serve for the aeroelastic and loads analysis in the preliminary design of composite airframes of both conventional and T-tail configuration. The steps taken during the modification are summarized as:

- Inclusion of k term in the stiffness matrix.
- The use of fixed axes as reference of vibrations on each component of the aircraft.
- Transforming the model into a configuration that the horizontal tail is attached to vertical tail.
- Extending the resultant equations of motion to structural loads equations.

However, the chosen mathematical model is based on a purely analytical approach. So it starts by redefining the deflection of a beam section in bending to incorporate the torsion effects. The result is expanded to the modified expressions of beam generalized velocities. The modified expressions of generalized velocities and deflections affect the whole mathematical model from top to bottom (i.e. from the equations of kinetic and strain energies to the global mass and stiffness matrices, respectively, and further down to state-space coefficient matrices and structural loads equations). Lastly, flight loads simulations are presented in two different maneuvers and gust conditions, while programming the whole mathematical model presented herewith in MATLAB language software.

Figure 1.2: T-Tail configuration in Fokker 100 aircraft

1.5 Thesis breakdown

The structure of the thesis is as follows. Chapter 2 presents the mathematical modeling with all those steps that are taken during the modification process and which are believed necessary to be included in this thesis. Chapter 3 presents the state-space form of the linearized equations of motion. Dynamic loads equations are presented in the Chapter 4. Presenting a complete structural optimization problem, which also includes finding the cross-sectional and material properties, is out of the scope of this thesis but the modified equations of motion do present a viable basis to do so. Moreover, due to the non availability of the structural data of the aircraft made of fiber composite, it is not possible to include the actual anisotropic material properties in the stiffness matrix. However, the coupling effects are simulated by manipulating the $e.a$ of each wing and horizontal tail of a twin jet metal aircraft in five different cases of numerical examples in Chapters 5 and 6. In first three cases, the $e.a$ of each wing and horizontal tail is drawn parallel to the $r.a$ of that particular component, where the $e.a$ with respect to $r.a$ of each component is placed in three different positions. In the fourth and fifth case, the $e.a$ of each wing and tail is drawn by intersecting the shear centers of each section from root to tip, where the shear center of a section is calculated by using Eq. (1.17). In Chapter 5 this is done for steady level flight and in Chapter 6 for discrete gust and pilot induced maneuvers. Finally, conclusions are drawn in Chapter 7.

Chapter 2

Mathematical Modeling

In this chapter the mathematical model regarding the dynamics of the fully flexible aircraft is modified to accommodate the new aspects related to the coupled vibrations. It starts with the description of the generic Lagrange's equations of motion, the basis for the rest of the mathematical modeling presented in this chapter. The modeling is divided into two main domains; structural dynamics and aerodynamics, where the structures part covers the structural discretization of aircraft components into lumped mass and stiffness elements, and the aerodynamics part covers the discretization of lifting surfaces into quasi-steady strips. On the basis of the structural discretization the kinetic energy and potential energy expressions are formulated. On the basis of kinetic and potential energies mass and stiffness matrices are derived, respectively. Kinetic and potential energies of the whole system are assembled in the Lagrangian and the equations of both rigid-body and elastic motions are driven through the generalized aerodynamic forces. Consequently the full-order model is reduced to a lower numbers of degrees of freedom by the eigenvalue solution of global stiffness and mass matrices.

2.1 Lagrange's equation of motion

Motions of a system can be solved through the Langrange's equation of motion as [22]:

$$\frac{d}{dt}\frac{\partial L}{(\partial \dot{q}_i)} - \frac{\partial L}{\partial q_i} + \frac{\partial \mathcal{F}}{\partial \dot{q}_i} = Q_i \quad i = f, e, w \tag{2.1}$$

in which $L = T - U$ is the Lagrangian, which is a function of kinetic energy T and potential energy U of the system. $\mathcal{F}$ is the Rayleigh dissipation density function, which gives the structural damping due to friction between the structural components during vibrations. Generalized coordinates vector q_i holds

the information of several variables related to aircraft motion (i.e. both rigid-body motion w.r.t. inertial and body axes, and elastic motion of the structural components w.r.t. to their particular local axes system), see Section 2.2 for a brief description in this account. Q_i is the vector of generalized conservative forces[1] due to aerodynamic and gravity loads. Eq. (2.1) gives us a guideline to proceed further in deriving a complete mathematical model of the flexible aircraft, which includes the derivations of kinetic and potential energies, dissipation density function, and the generalized forces.

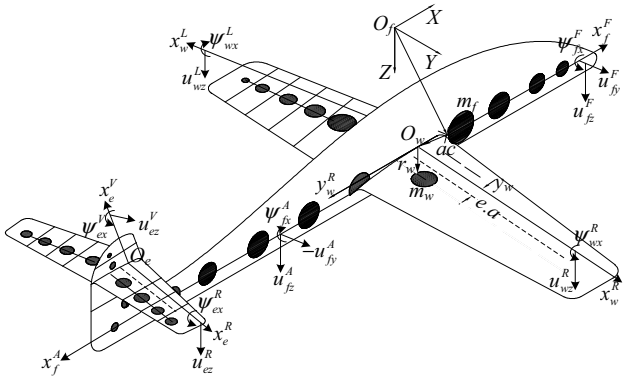

Figure 2.1: Aircraft discretized model.

2.2 Modeling of aircraft structural dynamics

In the structural dynamics part we discuss the structural discretization of the aircraft. On the basis of the discretization the kinetic and potential energy expressions and consequent mass and stiffness matrices, respectively, are derived.

2.2.1 Structural discretization

The structure of a flexible aircraft can be discretized into a number of beams. Fig. 2.1 shows a sample aircraft modeled with seven beams to represent fore and aft fuselage structures, one beam per half wing and half horizontal tail, and one beam for the vertical tail, where the aircraft body axes O_f lies on the juncture of aft and fore fuselages beams. Each beam over its length is further discretized

[1] We can classify friction as nonconservative force (i.e. it does not changes the potential energy of the system), whereas gravitational and aerodynamic forces as conservative, which changes the potential energy of a system through the structural deformations or change in the position of the aircraft.

into several sections with lumped mass elements m_i at their mass centers ($c.g$). These mass elements are attached to each other with springs of average stiffness over the two neighboring sections. For each fuselage beam there are two bending degrees of freedom (D.o.F) u along each y and z directions of the aircraft body axes O_f and one torsion ψ along the longitudinal axis of O_f [4]. For each wing and empennage beam there is one bending D.o.F normal to the plane of the lifting surface and one torsion D.o.F. along the $r.a$, i.e. longitudinal axis of their respective coordinate axes at O_i. Local axes O_i are normally positioned w.r.t. O_f. Fig. 2.2 shows the position of the wing local axes O_w w.r.t. O_f and moreover the position of a node on the wing w.r.t O_w, where the position vector r_w is divided into its three components (i.e. r_{w_x}, r_{w_y}, and r_{w_z}). Same analogy is also used for the rest of the components (i.e. horizontal and vertical tails).

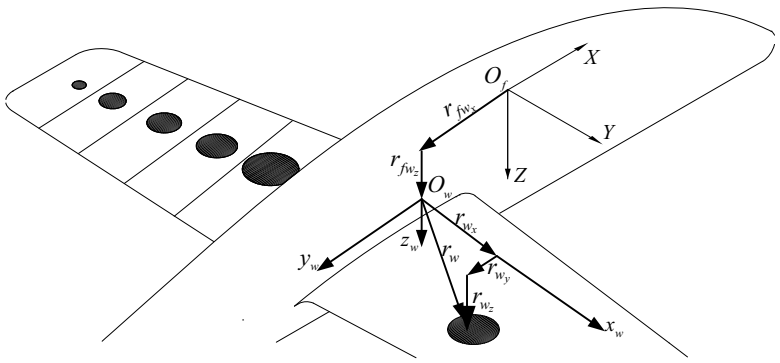

Figure 2.2: Position of a node on the wing w.r.t its local axes.

2.2.2 Kinetic energy

To derive the kinetic energy of a maneuvering aircraft, the motion of the aircraft is defined. The rigid-body motion of the aircraft is normally observed w.r.t. two types of the axes system (i.e. inertial and aircraft body axes). The positions of the aircraft in translation R_f and rotation θ_f are defined w.r.t to the inertial axes, whereas aircraft motion in the form of rigid-body velocities (i.e. V_f as translational velocity vector and Ω_f as angular velocity vector) are defined w.r.t aircraft body axes O_f. Elastic motion in the form of structural generalized velocities (i.e. s_u in bending and s_ψ in torsion) of the aircraft components are defined w.r.t. a component's local axes system. The total kinetic energy T w.r.t. O_f due to both rigid and elastic motions of the aircraft will be as follows [4]:

$$T = \frac{1}{2}\int \bar{V}_f^T \bar{V}_f dm_f + \frac{1}{2}\int \bar{V}_w^T \bar{V}_w dm_w + \frac{1}{2}\int \bar{V}_e^T \bar{V}_e dm_e$$
$$= \frac{1}{2} V^T M V \tag{2.2}$$

where the velocity vector V is discretized as follows:

$$V = \begin{bmatrix} V_f^T & \Omega_f^T & s_{u_f}^T & s_{uw}^T & s_{u_e}^T & s_{\psi_f}^T & s_{\psi_w}^T & s_{\psi_e}^T \end{bmatrix}^T \tag{2.3}$$

in which the first two subvectors, as stated above, are the rigid-body velocities, next three subvectors represent the generalized velocities in bending s_{u_i}. Last three subvectors are the generalized velocities in torsion $s_{\psi i}$. The subvectors of s_{u_i} in bending and s_{ψ_i} in torsion are further discretized into component level e.g. empennage in bending and torsion is discretized into vertical tail, right and left horizontal tail components and expressed as:

$$s_{u_e} = \begin{bmatrix} s_{uv}^T & s_{u_h}^{R^T} & s_{u_h}^{L^T} \end{bmatrix}^T \qquad s_{\psi_e} = \begin{bmatrix} s_{\psi_v}^T & s_{\psi_h}^{R^T} & s_{\psi_h}^{L^T} \end{bmatrix}^T \tag{2.4}$$

Similarly for fuselage into fore and aft, while wing into right and left components can be expressed as:

$$s_{u_f} = \begin{bmatrix} s_{u_f}^{F^T} & s_{u_f}^{A^T} \end{bmatrix}^T \qquad s_{\psi_f} = \begin{bmatrix} s_{\psi_f}^{F^T} & s_{\psi_f}^{A^T} \end{bmatrix}^T \tag{2.5}$$

$$s_{u_w} = \begin{bmatrix} s_{u_w}^{R^T} & s_{u_w}^{L^T} \end{bmatrix}^T \qquad s_{\psi_w} = \begin{bmatrix} s_{\psi_w}^{R^T} & s_{\psi_w}^{L^T} \end{bmatrix}^T \tag{2.6}$$

2.2.3 Generalized velocities

As given in Eq. (2.3), the local elastic motion of a component i is expressed in the form of vectors $s_{u,\psi}$. Before defining the expressions of each subvector of structural velocities, first the structural deflections of a section of a component 'i', placed at a position 'r_i' from its origin 'O_i', are defined. Fig. 2.3 shows a deformed section, where 'z_i', 'u_i', and 'ψ_i' represent the total vertical deflection, pure bending and torsion, respectively. While assuming no deformation due to shear [23] and using the small angle approximation in conjunction with the Galerkin method [23], the deformations with respect to the $r.a$ of a component are expressed as a function of two eigenfunctions or shape functions $\phi_{u,\psi}$ per D.o.F of a fixed-free beam and the corresponding vector of generalized coordinates '$q_{u,\psi}$':

$$\begin{aligned} z_i(r_i,t) &= u_i(r_i,t) + y_i \sin(\psi_i(r_i,t)) \\ &\approx \phi_{ui}(r_i)\, q_{u_i}(t) + y_i \phi_{\psi i}(r_i)\, q_{\psi_i}(t) \\ \psi_i(r_i,t) &= \phi_{\psi_i}(r_i)\, q_{\psi_i}(t) \end{aligned} \tag{2.7}$$

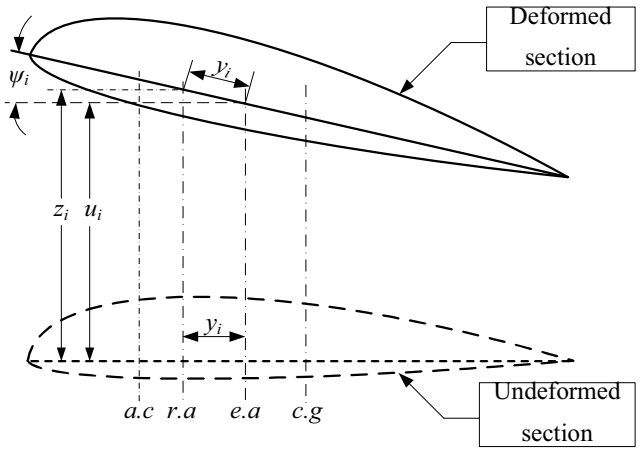

Figure 2.3: Deformed section.

A brief description of eigenfunctions is given in Appendix C. By taking the time derivative of the generalized coordinates, the corresponding structural velocities will be as follows:

$$\begin{aligned} \dot{z}_i(r_i,t) &= \phi_{u_i}(r_i)\, s_{u_i}(t) + y_i \phi_{\psi_i}(r_i)\, s_{\psi_i}(t) \\ \dot{\psi}_i(r_i,t) &= \phi_{\psi_i}(r_i)\, s_{\psi_i}(t) \\ s_{u_i,\psi_i}(t) &= \dot{q}_{u_i,\psi_i}(t) \end{aligned} \tag{2.8}$$

The vector of total absolute velocity $\bar{V}_f(r_f,t)$ on a node is the sum of rigid-body velocities at O_f and the generalized structural velocities at that node. From Eqs. (2.7–2.8), the velocity vector on a node of the fuselage is expressed as the sum of rigid-body translational velocity $C_f V_f$ of the aircraft, absolute velocity due to aircraft rigid-body angular velocity[2] $(\tilde{r}_f + \tilde{z}_f)^T C_f \Omega_f$, the absolute velocity due to torsional velocity $\tilde{r}_f^T \dot{\psi}_f$, and the structural bending velocity $\dot{z}_f$ of the node [4]:

$$\begin{aligned} \bar{V}_f(r_f,t) &= C_f V_f + (\tilde{r}_f + \tilde{z}_f)^T C_f \Omega_f + \tilde{r}_f^T \dot{\psi}_f + \dot{z}_f \\ &= C_f V_f + \tilde{r}_f^T C_f \Omega_f + \left(\widetilde{C_f \Omega_f}\right)\left(\phi_{u_f} q_{u_f} + \tilde{y}_f \phi_{\psi_f} q_{\psi_f}\right) \\ &+ \left(\tilde{r}_f + \tilde{y}_f{}^T\right)\phi_{\psi_f} s_{\psi_f} + \phi_{u_f} s_{u_f} \end{aligned} \tag{2.9}$$

[2]Absolute velocity V_i due to a angular velocity is normally expressed as the cross-product $r \times \Omega_f$, in which r is the distance from the origin of the rotation to the point where the absolute velocity is measured. For a generalized distance, r is summed with the instantaneous structural deflection z in Eq. (2.9). Similarly the torsional structural velocity is also converted to the absolute velocity by using the same analogy shown in the case of rigid-body velocities. The cross-product of two vectors is solved in matrix form by multiplying the skew symmetric matrix of one of the vector, represented as $\sim$ over that vector, to the other vector. The property of skew symmetry is $\tilde{a}^T b = \tilde{b} a$.

in which C_f is the rotation matrix of the fuselage, which transforms the vectors from O_f to the component's local axes system[3]. The deflection of the attachment point of wings or empennage on the fuselage is a function of rotation angles due to deflections in bending and torsion of the fuselage. Figure 2.4 shows the kinematics of the attachment point 'O_w' of the two halves of the wing on the aft fuselage, where the beams representing the aft fuselage and the left wing are depicted with their lumped mass elements 'm_f' and 'm_w', respectively,

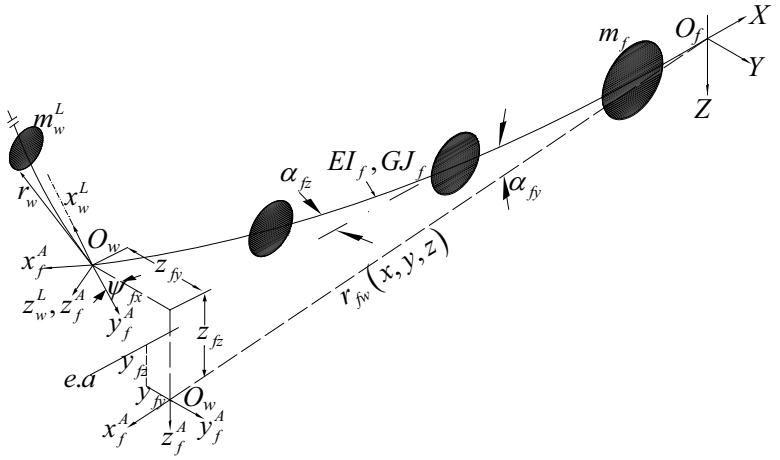

Figure 2.4: Deflected aft fuselage and left wing beams.

and their respective stiffness elements. The other components are not shown for the sake of brevity. The point 'O_w' is deflected by 'z_{f_y}' and 'z_{f_z}' in 'y' and 'z' directions, respectively, with a torsion angle of 'ψ_{fx}' along the x-axis. By using the first expression of Eq. (2.7), the rotation angle along the y-axis due to bending about z-axis is as follows:

$$\alpha_{f_y}\left(r_{f_{x_i}},t\right) = -\frac{\partial z_{f_z}}{\partial r_{f_{x_i}}} = -\left(\frac{\partial \phi_{u_f}\left(r_{f_{x_i}}\right) q_{u_{zf}}(t)}{\partial x_f} + y_{f_z}\frac{\partial \phi_{\psi_f}\left(r_{f_i}\right) q_{\psi_f}(t)}{\partial x_f}\right) \tag{2.10}$$

Similarly the rotation angle along the z-axis due to bending about y-axis is as follows:

$$\alpha_{f_z}\left(r_{f_{x_i}},t\right) = \frac{\partial z_{f_y}}{\partial r_{f_{x_i}}} = \left(\frac{\partial \phi_{u_f}\left(r_{f_i}\right) q_{u_{yf}}(t)}{\partial x_f} + y_{f_y}\frac{\partial \phi_{\psi_f}\left(r_{f_i}\right) q_{\psi_f}(t)}{\partial x_f}\right) \tag{2.11}$$

The generalized rotational velocities due to bending can be written in a vector

[3]It is to be noted that in Eq. (2.9) the rigid-body velocities are only required to transform, whereas the structural velocities (i.e. $\dot{z}$ and $\dot{\psi}$) are already expressed in the local axes system.

form as:

$$
\begin{aligned}
\dot{\alpha}\left(r_{f_i},t\right) &= \Delta\phi_{u_{fi}}s_{uf} + \tilde{y}_f\Delta\phi_{\psi_{fi}}s_{\psi f}\\
\Delta &= \begin{bmatrix} \partial/\partial x_f & 0 & 0\\ 0 & 0 & -\partial/\partial x_f\\ 0 & \partial/\partial x_f & 0 \end{bmatrix}\\
\phi_{u_{fi}}\left(r_{f_i}\right) &= \begin{bmatrix} 0 & 0 & 0\\ 0 & \phi_{u_{fy}} & 0\\ 0 & 0 & \phi_{u_{fz}} \end{bmatrix}\\
\phi_{\psi_{fi}}\left(r_{f_i}\right) &= \begin{bmatrix} \phi_{\psi_f} & 0 & 0 \end{bmatrix}^T\\
s_{u_f} &= \begin{bmatrix} 0 & \dot{q}_{u_{yf}} & \dot{q}_{u_{zf}} \end{bmatrix}^T\\
y_f &= \begin{bmatrix} 0 & y_{fz} & y_{fy} \end{bmatrix}^T
\end{aligned}
\tag{2.12}
$$

The vector of total absolute velocity on a node of either the wing or the vertical tail is the sum of rigid-body and structural velocities of the aft fuselage, structural velocities of the attachment point 'O_i' and finally the structural velocities of the node itself. It is given as follows:

$$
\begin{aligned}
\bar{V}_i\left(r_i,t\right) = C_iV_f &+ \left[C_i\left(\tilde{r}_{fi}+\tilde{z}_{fi}\right)^T + \left(\tilde{r}_i+\tilde{z}_i\right)^TC_i\right]\Omega_f\\
&+ C_i\left(\dot{z}_{fi}+\tilde{r}_{fi}^T\dot{\psi}_{fi}\right) + \tilde{r}_i^TC_i\left(\dot{\alpha}_{fi}+\dot{\psi}_{fi}\right)\\
&+ \dot{z}_i+\tilde{r}_i^T\dot{\psi}_i \qquad i=w,v
\end{aligned}
\tag{2.13}
$$

Figure 2.4 is expanded to Fig. 2.5, where it is shown that the horizontal tail is attached to the vertical tail at a position of 'r_{vh}' and the effects of fuselage deformation comes through the vertical tail. The vector of total absolute velocity for a mass element 'm_h', located at a position 'r_h', on one of the horizontal tails is a function of rigid-body and structural velocities of fuselage, vertical tail, and the node itself. It is expressed as follows:

$$
\begin{aligned}
\bar{V}_h\left(r_h,t\right) = C_hC_vV_f &+ \begin{bmatrix} C_hC_v\left(\tilde{r}_{fv}+\tilde{z}_{fv}\right)^T + C_h\left(\tilde{r}_{vh}+\tilde{z}_{vh}\right)^TC_v\\ +\left(\tilde{r}_h+\tilde{z}_h\right)^TC_hC_v \end{bmatrix}\Omega_f\\
&+ C_h\left[C_v\dot{z}_{fv}+C_v\tilde{r}_{fv}^T\dot{\psi}_{fv}\right] + C_h\left[\tilde{r}_{vh}^TC_v\left(\dot{\alpha}_{fv}+\dot{\psi}_{fv}\right)\right]\\
&+ C_h\left[\dot{z}_{fh}+\tilde{r}_{vh}^T\dot{\psi}_{vh}\right] + \tilde{r}_h^TC_h\left(\dot{\alpha}_{vh}+\dot{\psi}_{vh}\right) + \dot{z}_h+\tilde{r}_h^T\dot{\psi}_h
\end{aligned}
\tag{2.14}
$$

By using Eqs. (2.7–2.8), and (2.12), the Eqs. (2.13) and (2.14) are expanded and linearized as given in Appendix H, see Eqs. (H.5– H.8).

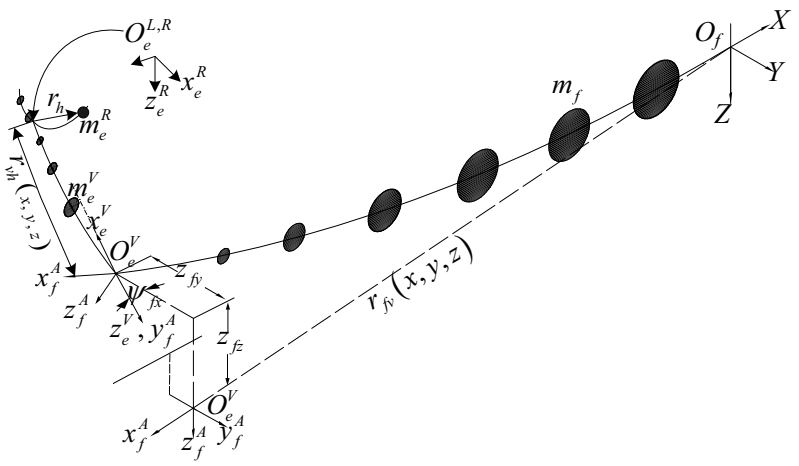

Figure 2.5: Deflected aft fuselage and empennage beams.

2.2.4 Mass Matrix

The velocity terms in Eqs. (2.9) and (2.13– 2.14) are sorted out in vector form of Eq. (2.3) and then used in Eq. (2.2). The coefficients resulting from the product of velocities construct the global mass matrix $M = [M_{ij}]$, which is a function of a structural displacements:

$$M = \begin{bmatrix} \begin{bmatrix} m & & \\ & m & \\ & & m \end{bmatrix} & \tilde{S}^T & M_{13} & \dots & M_{18} \\ \tilde{S} & J_f & M_{23} & \dots & M_{28} \\ M_{31} & M_{32} & M_{33} & \cdots & M_{38} \\ \vdots & \vdots & \vdots & \vdots & \vdots \\ M_{81} & M_{82} & M_{83} & \cdots & M_{88} \end{bmatrix} \tag{2.15}$$

in which m, $\tilde{S}$, and J_f are the aircraft mass, and first moment of inertia and moment of inertia matrices of the flexible aircraft, respectively. Readers are referred to Ref. 4 for the complete listing of the submatrices $[M_{ij}]$ of the mass matrix except for the modified submatrices due to bending-torsion coupling and T-Tail configuration. These are given in Eqs.(E.2–E.54) in Appendix E.

2.2.5 Stiffness matrix

As assumed in Section 2.2.3 that there are no deformations due to shear, whereas only bending and torsion deformations are taken into account. So

the potential energy is presented in the form of strain energy [12, 24]:

$$U = \sum_{i=f,e,w} \int \frac{1}{2} \left[\begin{array}{l} EI_i \left(z_i''\right)^2 - 2k_i \left(z_i''\right)\left(\psi_i'\right) \\ +GJ_i \left(\psi_i'\right)^2 \end{array} \right] dD_i \tag{2.16}$$

in which dD_i represents the integration over the length of the beam. The global stiffness matrix of the aircraft is a function of the strain energy [22]:

$$K = \left[\begin{array}{cccccc} K_{u_f} & 0 & 0 & K_{u\psi_f} & 0 & 0 \\ 0 & K_{u_w} & 0 & 0 & K_{u\psi_w} & 0 \\ 0 & 0 & K_{u_e} & 0 & 0 & K_{u\psi_e} \\ K_{\psi u_f} & 0 & 0 & K_{\psi_f} & 0 & 0 \\ 0 & K_{\psi u_w} & 0 & 0 & K_{\psi_w} & 0 \\ 0 & 0 & K_{\psi u_e} & 0 & 0 & K_{\psi_e} \end{array} \right] \tag{2.17}$$

where

$$[K_{jk}] = \left[\frac{\partial^2 U}{\partial q_j \partial q_k} \right] \tag{2.18}$$

Using Eqs. (2.7) and (2.16–2.17), the stiffness in bending and torsion are stated, respectively, as:

$$\begin{aligned} K_{u_i} &= \left[\frac{\partial^2 U}{\partial q_{u_i} \partial q_{u_i}} \right] \\ &= \left[\phi_{u_i}''\right] diag \left[EI_{i(dof)1} \cdots EI_{i(dof)n}\right] \left[\phi_{u_i}''\right]^T \end{aligned} \tag{2.19}$$

$$\begin{aligned} K_{\psi_i} &= \left[\frac{\partial^2 U}{\partial q_{\psi_i} \partial q_{\psi_i}} \right] \\ &= \left[\phi_{\psi_i}'\right] diag \left[GJ_{i(dof)1} \cdots GJ_{i(dof)n}\right] \left[\phi_{\psi_i}'\right]^T \end{aligned} \tag{2.20}$$

The cross coupling term in the form of a submatrix of the global stiffness matrix is as follows:

$$\begin{aligned} K_{u\psi_i} &= \left[\frac{\partial^2 U}{\partial q_{u_i} \partial q_{\psi_i}} \right] \\ &= \overbrace{\left[\phi_{u_i}''\right] diag \left[EI_{i(dof)1} \cdots EI_{i(dof)n}\right] diag \left[y_{i_1} \cdots y_{i_n}\right] \left[\phi_{\psi_i}''\right]^T}^{\text{due to the use of } r.a} \\ &\quad \underbrace{- \left[\phi_{u_i}''\right] diag \left[k_{i_1} \cdots k_{i_n}\right] \left[\phi_{\psi_i}'\right]^T}_{\text{due to the material properties}} \end{aligned} \tag{2.21}$$

where the matrix of two shape functions or mode shapes[4] of a beam in bending 'u' or torsion 'ψ' is given as:

$$[\phi_i] = \left[\begin{array}{ccc} \phi_{1,1} & \cdots & \phi_{1,n} \\ \phi_{2,1} & \cdots & \phi_{2,n} \end{array} \right], i = u, \psi \tag{2.22}$$

[4]Two shape functions or mode shapes of a cantilever beam means to consider only the first two lowest frequencies, see Appendix C.

In conjunction with the subvectors of generalized structural velocities in Eqs. (2.3–2.6), and two shape functions per D.o.F in Eq. (2.7), the vector of structural generalized coordinates is defined as:

$$q = [\overbrace{q_{uf}^T \quad q_{uw}^T \quad q_{ue}^T}^{q_u} \quad \overbrace{q_{\psi f}^T \quad q_{\psi w}^T \quad q_{\psi e}^T}^{q_\psi}]^T \tag{2.23}$$

The length of q is 32, in which, the first eight elements belong to fuselage in bending, the next four elements belong to wings in bending and so on with the last six elements belong to torsion in empennage i.e. a vertical tail and two halves of horizontal tail.

2.3 Damping matrix

Friction between the vibrating components dissipates energy, which damps the vibrations. By using Eq. (2.16) the structural damping in the form of dissipation density '$\mathcal{F}$' is written as [22]:

$$\mathcal{F} = \sum_{i=f,e,w} \frac{2\zeta}{\sqrt{\Lambda_{u,\psi_i}}} \int \frac{1}{2} \begin{bmatrix} EI_i \left(\dot{z}_i''\right)^2 - 2k_i \left(\dot{z}_i''\right)\left(\dot{\psi}_i'\right) \\ +GJ_i \left(\dot{\psi}_i'\right)^2 \end{bmatrix} dD_i \tag{2.24}$$

in which the $\sqrt{\Lambda_{u,\psi_i}}$ is the lowest natural frequency of a component, computed from the eigenvalue solution of the particular mass and stiffness matrices of that component, ζ is the structural damping factor. From Eq. (2.16) we can write Eq. (2.24) as:

$$\mathcal{F} = \sum_{i=f,e,w} \frac{2\zeta}{\sqrt{\Lambda_{u,\psi_i}}} \dot{U} \tag{2.25}$$

and by using Eq. (2.8), Eq.(2.24) can be expanded as follows:

$$\mathcal{F} = \sum_{i=f,e,w} \frac{2\zeta}{\sqrt{\Lambda_{u,\psi_i}}} \int \begin{pmatrix} s_{u_i}^T \left[\phi_{u_i}''\right] diag\left[EI_{i(dof)1} \cdots EI_{i(dof)n}\right] \left[\phi_{u_i}''\right]^T s_{u_i} \\ +s_{u_i}^T \left[\phi_{u_i}''\right] diag\left[EI_{i(dof)1} \cdots EI_{i(dof)n}\right] \\ \times diag\left[y_{i_1} \cdots y_{i_n}\right] \left[\phi_{\psi_i}''\right]^T s_{\psi_i} \\ -s_{u_i}^T \left[\phi_{u_i}''\right] diag\left[k_{i_1} \cdots k_{i_n}\right] \left[\phi_{\psi_i}'\right]^T s_{\psi_i} \\ +s_{\psi_i}^T \left[\phi_{\psi_i}'\right] diag\left[GJ_{i(dof)1} \cdots GJ_{i(dof)n}\right] \left[\phi_{\psi_i}'\right]^T s_{\psi_i} \end{pmatrix} dD_i \tag{2.26}$$

and now by substituting Eqs. (2.20–2.21) into Eq. (2.26) $\mathcal{F}$ is expressed as:

$$\mathcal{F} = \sum_{i=f,e,w} \frac{2\zeta}{\sqrt{\Lambda_{u,\psi_i}}} \left(s_{u_i}^T K_{u_i} s_{u_i} - s_{u_i}^T K_{u\psi_i} s_{\psi_i} + s_{\psi_i}^T K_{\psi_i} s_{\psi_i}\right) \tag{2.27}$$

The structural damping matrix 'C' is proportional to the stiffness matrix i.e. $C = \frac{2\zeta K}{\sqrt{\Lambda_{u,\psi_i}}}$, where the Rayleigh dissipation density $\mathcal{F}$ is finally expressed as [22]:

$$\mathcal{F} = \sum_{i=f,e,w} \left(s_{u_i}^T C_{u_i} s_{u_i} - s_{u_i}^T C_{u\psi_i} s_{\psi_i} + s_{\psi_i}^T C_{\psi_i} s_{\psi_i} \right) \tag{2.28}$$

The global damping matrix of the aircraft is expressed similar to the stiffness matrix in Eq. (2.17) as:

$$C = \begin{bmatrix} C_{u_f} & 0 & 0 & C_{u\psi_f} & 0 & 0 \\ 0 & C_{u_w} & 0 & 0 & C_{u\psi_w} & 0 \\ 0 & 0 & C_{u_e} & 0 & 0 & C_{u\psi_e} \\ C_{\psi u_f} & 0 & 0 & C_{\psi_f} & 0 & 0 \\ 0 & C_{\psi u_w} & 0 & 0 & C_{\psi_w} & 0 \\ 0 & 0 & C_{\psi u_e} & 0 & 0 & C_{\psi_e} \end{bmatrix} \tag{2.29}$$

where the individual submatrix in Eq. (2.29) is given as:

$$[C_{jk}] = \left[\frac{\partial^2 \mathcal{F}}{\partial \dot{q}_j \partial \dot{q}_k} \right] \tag{2.30}$$

2.4 Aerodynamic and gravity loads

The aerodynamic model is essentially a two dimensional model, presented in the form of several strips, as shown in Fig. 2.1, with lift, sideforce, moment, and drag slopes i.e. C_{l_α}, C_{s_β}, C_{m_α}, and C_{d_α}, respectively. It is well known that aeroelastic predictions are usually conservative when using the quasi-steady strip theory [23], but at the same time the use of aerodynamic coefficients suits the quasi-coordinate approach [4]. Otherwise the aerodynamic data from a high fidelity analysis (e.g. computational fluid dynamics) can also be converted to aerodynamic derivatives and the same form of the equations of motion can be used [25].

The quasi-steady lift f_{l_i} on the aerodynamic center of each strip of either fuselage, wings or horizontal tails is a function of the aerodynamic lift slope and the local angle of attack of the strip [4, 25]:

$$\begin{aligned} f_{l_f} &= P_d c_f C_{l\alpha_f} \alpha_f = P_d c_f C_{l_f} \\ f_{l_w} &= P_d c_w \left(C_{l\alpha_w} \alpha_w + C_{l\delta_a} \delta_a \right) \\ f_{l_h} &= P_d c_h \left(C_{l\alpha_h} \alpha_h + C_{l\delta_e} \delta_e \right) \end{aligned} \tag{2.31}$$

in which P_d, c_i, α_i, and δ are dynamic pressure, chord length, angle of attack, and control deflection, respectively. Similarly the lateral force f_{s_i} per unit strip

of either fuselage or vertical tail can be expressed as:

$$\begin{aligned} f_{s_f} &= P_d c_f C_{s\beta f} \beta_f = P_d c_{sf} C_{sf} \\ f_{s_v} &= P_d c_v \left(C_{s\beta_v} \beta_v + C_{s\delta r} \delta_r \right) \end{aligned} \tag{2.32}$$

The dynamic pressure p_d, angle of attack α_i, and side-slip angle β_i are defined as:

$$P_d = \frac{1}{2} \rho V_{f_x}^2 \tag{2.33}$$

$$\alpha_i = \theta_{\Theta_f} + \frac{V_{f_z} - V_\xi + l_i \Omega_{f_\Theta} + \dot{q}_i}{V_{f_x}} + \psi, \quad i = f, h, w \tag{2.34}$$

$$\beta_i = \theta_{\Psi_f} + \frac{V_{f_y} + l_i \Omega_{f_\Psi} + \dot{q}_i}{V_{f_x}} + \psi, \quad i = f, v \tag{2.35}$$

in which V_ξ, θ_{Θ_f}, and θ_{Ψ_f} are the vertical component of the downwash in horizontal tail only, pitch attitude, and yaw attitude, respectively. The instantaneous local angle of attack of a strip is determined from the torsion angle 'ψ' of that strip and the angles produced by both rigid-body and elastic motions, see Appendix F for the definitions. Pitching velocity Ω_{f_Θ} multiplied with the moment arm l_i from O_f to the particular strip gives the vertical absolute velocity. As given in Eq. (2.8), $\dot{q}_i$ is the generalized velocity vector. The drag f_{d_i} per unit strip of either fuselage, wings, or empennage is expressed as [4]:

$$f_{d_i} = P_d c_i \left(C_{d0_i} + k_i C_{l\alpha i}^2 \alpha^2 \right) \tag{2.36}$$

in which the 2-D profile drag coefficients C_{d0_i} corresponds to $\alpha = 0$ and k_i is the induced drag factor. The resultant aerodynamic force $f_{a_{li}}$ and $f_{a_{si}}$ on fuselage, wings, empennage with respect to the local coordinate axes O_i are expressed in vector form as:

$$\begin{aligned} f_{a_{lf}} &= \begin{bmatrix} f_{l_f} \sin\alpha_f - f_{d_f} \cos\alpha_f \\ 0 \\ -f_{l_f} \cos\alpha_f - f_{d_f} \sin\alpha_f \end{bmatrix}, \qquad f_{a_{sf}} = \begin{bmatrix} f_{s_f} \sin\beta_f \\ -f_{s_f} \cos\beta_f \\ 0 \end{bmatrix} \\ f_{a_{li}}^L &= \begin{bmatrix} 0 \\ f_{l_i} \sin\alpha_i - f_{d_i} \cos\alpha_i \\ -f_{l_i} \cos\alpha_i - f_{d_i} \sin\alpha_i \end{bmatrix}, \quad f_{a_{li}}^R = \begin{bmatrix} 0 \\ -f_{l_i} \sin\alpha_i + f_{d_i} \cos\alpha_i \\ -f_{l_i} \cos\alpha_i - f_{d_i} \sin\alpha_i \end{bmatrix} \\ f_{a_{sv}} &= \begin{bmatrix} 0 \\ f_{s_v} \sin\beta_v \\ -f_{s_v} \cos\beta_v \end{bmatrix} \end{aligned} \tag{2.37}$$

It is to be noted that the sign convention for aerodynamic forces on left and right wing or horizontal tail in Eq. (2.37) is referred to the respective coordinate

axes 'O_i', as shown in Fig. 2.1. The gravitational forces per unit volume of a component are as follows [26]:

$$f_{g_f} = m_f C_{If} \begin{bmatrix} 0 \\ 0 \\ g \end{bmatrix}$$
$$f_{g_i} = m_i C_i C_{If} \begin{bmatrix} 0 \\ 0 \\ g \end{bmatrix}, \quad i = e, w \tag{2.38}$$

in which C_{If} is the transformation from inertial axes to the aircraft body axes and given in Appendix D. Gravity g is taken as $9.81 m/sec^2$. The total force on a node of a component is the summation of air and gravitational forces:

$$f_i = f_{a_{li}} + f_{a_{si}} + f_{g_i}, \quad i = f, e, w \tag{2.39}$$

2.5 Thrust model

The thrust f_E for a single engine is expressed as [26]:

$$f_E = f_{E_{SL}} \left(\frac{\rho}{1.225}\right)^{0.7} \left(1 - \exp^{-(\frac{R_{f_z}+17000}{2000})}\right) \delta_T \tag{2.40}$$

where δ_T, $f_{E_{SL}}$, ρ, and R_{f_z} are the pilot input on thrust, static thrust at the sea level, air density, and altitude, respectively.

2.6 Generalized forces

The distributed forces on a component as given in Eq. (2.39) are converted to generalized forces, which are to be used in conjunction with the equations of motion, see section 2.7. The actual forces are generalized by means of virtual work $\delta\bar{W}$, which in terms of rigid-body and elastic deformations can be written as [4]:

$$\delta\bar{W} = F_f^T \delta R_f + M_f^T \delta\theta_f + \sum_{i=f,e,w} \left(Q_{ui}^T \delta q_{u_i} + Q_{\psi_i}^T \delta q_{\psi_i}\right) \tag{2.41}$$

while using the Eqs. (2.9), (2.13), and (2.14), the generalized forces for the rigid-body motion can be defined as:

$$
\begin{aligned}
F_f &= \int_{D_f} \left[f_E \delta \left(r - r_{f_E} \right) \right] dD_f + \sum_{i=f,e,w} C_i^T \int_{D_i} f_i dD_i \\
M_f &= C_f^T \int_{D_f} \left(\tilde{r}_f + \tilde{z}_f \right) \left[f_f + f_E \delta \left(r - r_{fE} \right) \right] dD_f \\
&\quad + \int_{D_h} \begin{bmatrix} \left(\tilde{r}_{f_v} + \tilde{z}_{f_v} \right) \left(C_h C_v \right)^T + C_v^T \left(\tilde{r}_{v_h} + \tilde{z}_{v_h} \right) C_h^T \\ + \left(C_h C_v \right)^T \left(\tilde{r}_h + \tilde{z}_h \right) \end{bmatrix} f_h dD_h \\
&\quad + \int_{D_i} \left[\left(\tilde{r}_{f_i} + \tilde{z}_{f_i} \right) C_i^T + C_i^T \left(\tilde{r}_i + \tilde{z}_i \right) \right] f_i dD_i, \quad i = w, v
\end{aligned}
\tag{2.42}
$$

in which $\delta \left(r - r_{f_E} \right)$ is a direct delta function and r_{f_E} is the location of the engines on the fuselage [4][5]. By using the Eqs. (2.9), (2.13), and (2.14), the generalized forces acting on the fuselage are expressed as:

$$
\begin{aligned}
Q_{u_f} &= \int_{D_f} \phi_{u_f}^T \left[f_f + f_E \delta \left(r - r_{fE} \right) \right] dD_f + \int_{D_i} \left[\tilde{r}_i^T C_i \Delta \phi_{u_{fi}} + C_i \phi_{u_{fi}} \right]^T f_i dD_i \\
&\quad + \int_{D_h} \left[\tilde{r}_{v_h}^T C_v \Delta \phi_{u_{fv}} + C_v \phi_{u_{fv}} \right]^T C_h^T f_h dD_h, \quad i = w, v \\
Q_{\psi_f} &= \int_{D_f} \phi_{\psi_f}^T \tilde{r_f} \left[f_f + f_E \delta \left(r - r_{fE} \right) \right] dD_f \\
&\quad + \int_{D_i} \left[\tilde{r}_i^T C_i \left(\tilde{y}_f \Delta \phi_{\psi fi} + \phi_{\psi fi} \right) + C_i \left(\tilde{y}_f + \tilde{r}_{f_i}^T \right) \phi_{\psi_{fi}} \right]^T f_i dD_i \\
&\quad + \int_{D_h} \left[\tilde{r}_{v_h}^T C_v \left(\tilde{y}_f \Delta \phi_{\psi_{fv}} + \phi_{\psi_{fv}} \right) + C_v \left(\tilde{y}_f + \tilde{r}_{f_v}^T \right) \phi_{\psi_{fv}} \right]^T C_h^T f_h dD_h
\end{aligned}
\tag{2.43}
$$

[5]The aircraft used in Chapters 5 and 6 has fuselage mounted engines. Otherwise, in case of wing mounted engines, their location and direct delta function will be accommodated as $\delta \left(r - r_{w_E} \right)$ in the integrals of generalized forces acting on the wings.

Similarly using the equations, as stated above, the generalized forces on the vertical tail are expressed as follows:

$$\begin{aligned} Q_{u_v} &= \int_{D_v} \phi_{u_v}^T f_v dD_v + \int_{D_h} \left[\tilde{r}_h^T C_h \Delta\phi_{uvh} + C_h \phi_{u_{vh}}\right]^T f_h dD_h \\ Q_{\psi_v} &= \int_{D_h} \left[\tilde{r}_h^T C_h \left(\tilde{y}_v \Delta\phi_{\psi_{vh}} + \phi_{\psi_{vh}}\right) + C_h \left(\tilde{y}_v + \tilde{r}_{v_h}^T\right) \phi_{\psi_{vh}}\right]^T f_h dD_h \\ &\quad + \int_{D_v} \phi_{\psi_v}^T \tilde{r_v} f_v dD_v \end{aligned} \tag{2.44}$$

and the generalized forces on wings and horizontal tails are given as:

$$\begin{aligned} Q_{u_i} &= \int_{D_i} \phi_{u_i}^T f_i dD_i \\ Q_{\psi_i} &= \int_{D_i} \phi_{\psi_i}^T \tilde{r}_i f_i dD_i, \quad i = h, w \end{aligned} \tag{2.45}$$

In conjunction with the generalized coordinates in Eq. (2.23), the generalized forces with regard to elastic deformations are arranged as:

$$Q = \begin{bmatrix} Q_{u_f}^T & Q_{u_w}^T & Q_{u_e}^T & Q_{\psi_f}^T & Q_{\psi_w}^T & Q_{\psi_e}^T \end{bmatrix}^T \tag{2.46}$$

The above equation can be further partitioned into the subvectors in the same way as in the case of generalized velocities in Eqs. (2.4–2.6).

2.7 Equations of motion

The generalized momenta 'p' can be expressed as a partial derivative of the Lagrangian "$L = T - U$" w.r.t the velocity [4, 22]:

$$\begin{aligned} p &= {}^{\partial L}/_{\partial V} = MV \\ p &= \begin{bmatrix} p_{V_f}^T & p_{\Omega_f}^T & p_{u_f}^T & \cdots & p_{\psi_e}^T \end{bmatrix} \end{aligned} \tag{2.47}$$

By using the generic form of the equations of motion [4], the equations of motion for the whole aircraft can be expressed as follows:

$$\begin{aligned} \dot{R}_f &= C_{If}^T V_f, \qquad \dot{\theta}_f = E_{If}^{-1} \Omega_f \\ \dot{q}_{u_i} &= s_{ui}, \qquad \dot{q}_{\psi i} = s_{\psi i} \\ \dot{p}_{V_f} &= -\tilde{\Omega}_f p_{V_f} + F_f \\ \dot{p}_{\Omega_f} &= -\tilde{V}_f p_{V_f} - \tilde{\Omega}_f p_{\Omega_f} + M_f \end{aligned} \tag{2.48}$$

The first two expressions in Eq. (2.48) belong to the rigid-body motions with respect to the inertial axes, where C_{If} and E_{If} are the transformation matrices from inertial axes to the aircraft body axes. The third and fourth solve the generalized coordinates, which are then used in Eq. (2.7) to get the subsequent elastic deformations. The last two expressions in Eq. (2.48) solve the momenta in rigid-body translations and rotations, respectively. By using the generic form of Lagrange's equation, as given in Eq. (2.1), the expressions for the generalized momenta for elastic motion in bending and torsion are given as:

$$\begin{aligned}
\dot{p}_{u_i} &= \frac{\partial T}{\partial q_{u_i}} - K_{\psi i} q_{u_i} - C_{u_i} s_{u_i} + Q_{u_i} \\
\dot{p}_{\psi_i} &= \frac{\partial T}{\partial q_{\psi_i}} - K_{\psi_i} q_{\psi_i} - C_{\psi_i} s_{\psi_i} + Q_{\psi_i} \qquad i = f, e, w
\end{aligned} \tag{2.49}$$

As the kinetic energy in Eq. (2.2) is a function of the absolute velocity $\bar{V}_i$, which in turn, as given in Eqs. (2.9), (2.13), and (2.14), is a function of the structural generalized coordinates q_{u_i} in bending and q_{ψ_i} in torsion. So by using the chain rule for differentiation, the partial derivatives of kinetic energy T with respect to a vector of generalized coordinates in bending is expresses as:

$$\begin{aligned}
\frac{\partial T}{\partial q_{u_i}} &= \frac{\partial \bar{V}_f^T}{\partial q_{u_i}} \frac{\partial T}{\partial \bar{V}_f^T} + \frac{\partial \bar{V}_w^T}{\partial q_{u_i}} \frac{\partial T}{\partial \bar{V}_w^T} + \frac{\partial \bar{V}_e^T}{\partial q_{u_i}} \frac{\partial T}{\partial \bar{V}_e^T} \\
\frac{\partial T}{\partial q_{u_f}} &= \int_{D_f} \phi_{u_f}^T \widetilde{C_f \Omega_f}^T \bar{V}_f dm_f + (C_f^T \phi_{u_{fw}})^T \tilde{\Omega}_f^T C_w^T \int_{D_w} \bar{V}_w dm_w \\
&\quad + (C_f^T \phi_{u_{fv}})^T \tilde{\Omega}_f^T \left[C_v^T \int_{D_v} \bar{V}_v dm_v + (C_h C_v)^T \int_{D_h} \bar{V}_h dm_h \right] \\
\frac{\partial T}{\partial q_{u_w}} &= \int_{D_w} \phi_{u_w}^T (\widetilde{C_w \Omega_f})^T \bar{V}_w dm_w \\
\frac{\partial T}{\partial q_{u_v}} &= \int_{D_v} \phi_{u_v}^T (\widetilde{C_v \Omega_f})^T \bar{V}_v dm_v + \phi_{u_{vh}}^T C_h^T (\widetilde{C_v \Omega_f})^T \int_{D_h} \bar{V}_h dm_h \\
\frac{\partial T}{\partial q_{u_h}} &= \int_{D_h} \phi_{u_h}^T (\widetilde{C_h C_v \Omega_f})^T \bar{V}_h dm_h
\end{aligned} \tag{2.50}$$

Similarly, by using the analogy of the first expression of Eq. (2.50) the partial derivatives of kinetic energy w.r.t a vector of generalized coordinates q_{ψ_i} in

torsion are given as:

$$
\begin{aligned}
\frac{\partial T}{\partial q_{\psi_i}} &= \frac{\partial \bar{V}_f^T}{\partial q_{\psi_i}}\frac{\partial T}{\partial \bar{V}_f^T} + \frac{\partial \bar{V}_h^T}{\partial q_{\psi_i}}\frac{\partial T}{\partial \bar{V}_h^T} + \frac{\partial \bar{V}_i^T}{\partial q_{\psi_i}}\frac{\partial T}{\partial \bar{V}_i^T} \\
\frac{\partial T}{\partial q_{\psi_f}} &= \int_{D_f} (\tilde{y}_f \phi_{\psi_f})^T \widetilde{C_f \Omega_f}^T \bar{V}_f dm_f + (C_f^T \tilde{y}_f \phi_{\psi_{fw}})^T \tilde{\Omega}_f^T C_w^T \int_{D_w} \bar{V}_w dm_w \\
&\quad + (C_f^T \tilde{y}_f \phi_{\psi_{fv}})^T \tilde{\Omega}_f^T \left[C_v^T \int_{D_v} \bar{V}_v dm_v + (C_h C_v)^T \int_{D_h} \bar{V}_h dm_h \right] \\
\frac{\partial T}{\partial q_{\psi_w}} &= \int_{D_w} (\tilde{y}_w \phi_{\psi_w})^T (\widetilde{C_w \Omega_f})^T \bar{V}_w dm_w \\
\frac{\partial T}{\partial q_{\psi_v}} &= \int_{D_v} (\tilde{y}_v \phi_{\psi_v})^T (\widetilde{C_v \Omega_f})^T \bar{V}_v dm_v + (\tilde{y}_v \phi_{\psi_{vh}})^T C_h^T (\widetilde{C_v \Omega_f})^T \int_{D_h} \bar{V}_h dm_h \\
\frac{\partial T}{\partial q_{u_h}} &= \int_{D_h} (\tilde{y}_h \phi_{\psi_h})^T (\widetilde{C_h C_v \Omega_f})^T \bar{V}_h dm_h
\end{aligned}
\tag{2.51}
$$

2.8 Model reduction

The equations of motion in Eqs. (2.48–2.49) solve a state-vector of 76 elements which include 38 generalized coordinates, 6 rigid-body translations and rotations, and 32 elastic deformations. The equations contain all lower and higher frequency modes. To determine the lower frequencies and corresponding aircraft shape functions (ASF), the mathematical modal is reduced to a lower number of D.o.F by the eigenvalue solution of global stiffness and mass matrices:

$$\left[K - \lambda M_{(7:38,7:38)}|_{q=0}\right] d = 0 \tag{2.52}$$

The reduced-order mass matrix is given as [27, 28]:

$$M_\xi = U_{u\psi}^T M_q U_{u\psi} \tag{2.53}$$

in which the transformation matrix $U_{u\psi}$ is given as:

$$U_{u\psi} = \begin{bmatrix} I & & 0 \\ & \ddots & \\ 0 & & D_m \end{bmatrix}$$

$$D_m = \left[d_{(\,:\,,1:m)}\right] = \begin{bmatrix} D_{uf} \\ D_{uw} \\ \vdots \\ D_{\psi e} \end{bmatrix} = \begin{bmatrix} D_{m(1:8,1:m)} \\ D_{m(9:12,1:m)} \\ \vdots \\ D_{m(27:32,1:m)} \end{bmatrix} \tag{2.54}$$

(2.55)

and I is an identity matrix of order 6. The reduced-order stiffness and damping matrices are computed by using the analogy of mass matrix as given in Eq. (2.53):

$$K_\xi = D_m^T K D_m \tag{2.56}$$

$$C_\eta = D_m^T C D_m \tag{2.57}$$

Similarly the generalized force vector Q in Eq. (2.46) is reduced as:

$$Q_\xi = D_m^T Q \tag{2.58}$$

It is important to note that the ASF in the matrices of $U_{u,\psi}$ and D_m linearly transform the model into a reduced-order "similar" [29] model, which does not change the properties of the system i.e. both the resulting mass and stiffness matrices remain to be the non diagonal matrices that maintain the inertial and elastic coupling, respectively. The expressions for generalized coordinates and momenta in Eqs. (2.48) and (2.49) are rewritten after the reduction as:

$$\dot{\xi} = \eta \tag{2.59}$$

$$\dot{p}_\eta = \frac{\partial T}{\partial \xi} - K_\xi \xi - C_\eta \eta + Q_\xi \tag{2.60}$$

The reduced-order generalized coordinates and momenta vector from above equation can be expanded as:

$$q = D_m \xi \qquad p = D_m p_\eta \tag{2.61}$$

Similarly, the partial derivative $\frac{\partial T}{\partial \xi}$ in Eq. (2.60) is expressed by using the submatrices of D_m in Eqs (2.50) and (2.51):

$$\begin{aligned}\frac{\partial T}{\partial \xi} = {} & D_{u_f}^T \frac{\partial T}{\partial q_{u_f}} + D_{u_w}^T \frac{\partial T}{\partial q_{u_w}} + D_{u_v}^T \frac{\partial T}{\partial q_{u_v}} + D_{u_h}^T \frac{\partial T}{\partial q_{u_h}} \\ & + D_{\psi_f}^T \frac{\partial T}{\partial q_{\psi_f}} + D_{\psi_w}^T \frac{\partial T}{\partial q_{\psi_w}} + D_{\psi_v}^T \frac{\partial T}{\partial q_{\psi_v}} + D_{\psi_h}^T \frac{\partial T}{\partial q_{\psi_h}}\end{aligned} \tag{2.62}$$

2.9 Synopsis

The aircraft structure is discretized into several beams, where each beam is further discretized into lumped mass and stiffness elements. The aerodynamic lifting surfaces are presented in the form of quasi-steady panels or strips with lift, moment, and drag coefficients. The deflection of a beam section in bending with torsion effects is presented. The result is expanded to the modified expressions of beam generalized velocities. The nondiagonal mass matrix is formulated as a product of the coefficients of generalized velocities when used in

kinetic energy expression. Structural stiffness and damping matrices are formulated by using the strain energy of whole aircraft with coupled bending torsion deformations. Based on the principle of virtual work, the generalized forces due to aerodynamics and gravity loads are derived. After that, by using the generic equations of motion of a flexible aircraft, derived through the Lagrange principle of motion, the equations of motion to be used in the present study are derived, in which the positions are presented in the form of generalized coordinates and motion in the form of generalized momenta. Finally, a common modal reduction technique is used to reduce the degrees of freedom.

Chapter 3

State-Space Representation and Linearization

In this chapter the equations of motion are linearized and presented in the form of state-space equations. These will be used in the next chapters on loads equations, computer coding and finally the flight loads simulation.

Before deriving the matrices of the state-space equation it is necessary to discuss some important aspects of linearization in the equations of motion. It is common practice in rigid-body flight dynamics to linearize the equations about the steady-state condition, assuming that the disturbances are very small and aerodynamics effects are linear functions of the disturbances [30,31]. The small perturbation theory in case of a fully-flexible aircraft looks reasonably valid when the external disturbances (e.g. due to a gust input) cause small perturbations around the trim state, where the forward air speed and inertia matrix are assumed constant. But during certain maneuvers (e.g, due to abrupt elevator inputs), the angle of attack can increase significantly [32]. In such cases the idea of perturbation around the trim condition does not seem valid but at the same time it is quite difficult to solve the nonlinear equations of motion of relatively large order (i.e. integrating the rigid-body and elastic D.o.F. concurrently). A special form of perturbation theory, called the "extended aeroelasticity theory" [4, 27, 28], addresses the nonlinearities in the dynamics of the flexible aircraft by first solving the rigid-body dynamics problem, called the zero-order problem, and the solution of a zero-order problem enters into linearized equations, called the first-order problem, which solves the vibrations and their effects on the rigid-body motion. Another method, known as the Generalized-α method is also used to solve the equations of motion of the flexible aircraft by integrating the rigid-body and elastic D.o.F concurrently, where the equations of motion are not linearized around the steady-state condition [33].

However in the present study the linear model (i.e. extended aeroelasticity approach) is used, which, as stated in Chapter 1, is acceptable in verifying the loads conditions given in aviation regulations.

A constant inertia matrix for a purely rigid aircraft in a short period maneuver seems very practical but for flexible aircraft, subject to structural deformations during the maneuvers, the inertia matrix should be updated for every time step of the solution. The equations of motion of a flexible aircraft presented in Ref. 5 and 14 lack this particular capability and the inertia matrix is assumed to be constant during a maneuver. However, the inertially coupled equations of motion presented in Ref. 4 and the modified version presented in this report or in Ref. 34 are solved with updated inertia matrix for each time step, see Eqs. (E.2–E.54) where the inertia matrices are functions of the generalized coordinates q_u and q_ψ. The "extended aeroelasticity theory", as stated above, linearizes the nonlinear effects of flexibility around a certain time step of a given maneuver. As stated, it divides the solution into two parts, i.e. zero-order and first-order problems. The linearization of the equations of motion into first-order state in Ref. 4 makes the equations symbolically quite complex and a small error during the computer coding can make the results erroneous. To make the linearization process easy to implement, the equations of motion are linearized in two stages. In the first stage the most commonly known flight mechanics and aeroelasticity terms are used to differentiate the equations into a few coefficient matrices [30, 31, 35, 36] that are ultimately collected in a generic state-space equation of motion of a flexible aircraft in perturbation. In conjunction with the theory of extended aeroelasticity, the generic state-space equation is further segregated into a zero-order state and, while using the Taylor's series expansion [29], the coefficient matrices are further linearized into first-order state equations in the second stage.

3.1 Generic state-space equations

As given in the Eq. (2.47), the inverse of the mass matrix multiplied by the momenta eliminates the velocities in Eqs. (2.48–2.49) and the generic state-space form of Eqs. (2.48–2.49) is given as:

$$\dot{x}(t) = \Big[\big[A(t) + C_{V\Omega}(t)\big]\, M_{\xi\xi}^{-1}(t) + B_x(t)\Big]\, x(t) + B_u u(t) \tag{3.1}$$

in which the state-vector 'x' is defined as $\begin{bmatrix} R_f^T & \theta_f^T & \xi^T & p_{Vf}^T & p_{\Omega f}^T & p_\eta^T \end{bmatrix}^T$. Matrices $C_{V\Omega}$, B_x, and B_u are related to the aerodynamic damping, aerodynamic stiffness and control stiffness, respectively, and these are defined in this chapter.

The inverse of $M_{\xi\xi}^{-1}$ in matrix form is defined as:

$$M_{\xi\xi}^{-1} = \begin{bmatrix} 0 & M_{\xi}^{-1} \\ 0 & M_{\xi}^{-1} \end{bmatrix} \tag{3.2}$$

where the state-space matrix A is expressed as:

$$A = \begin{bmatrix} 0 & 0 & 0 & C_f^T & 0 & 0 \\ 0 & 0 & 0 & 0 & E_f^{-1} & 0 \\ 0 & 0 & 0 & 0 & 0 & s_\eta \\ 0 & 0 & 0 & 0 & \widetilde{p_{Vf}} & 0 \\ 0 & 0 & 0 & \widetilde{p_{Vf}} & \widetilde{p_{\Omega f}} & 0 \\ 0 & 0 & A_\xi - K_\xi & A_V & A_\Omega & A_\eta - C_\eta \end{bmatrix} \tag{3.3}$$

in which the submatrices A_ξ, A_V, A_Ω, and A_η are derived by using the Eqs. (2.9), (2.13), and (2.14) in Eqs. (2.50) and (2.51), see Appendix H.

3.2 The $\alpha - \beta$ derivatives

The derivatives with respect to angle of attack 'α' and side slip angle 'β' are defined in this section, which are to be used extensively in the aerodynamic damping and stiffness matrices in the later sections of this chapter. Expanding Eq. (2.37) by using Eqs. (2.31–2.36), the drag coefficient can be expressed as a function of α for a aerodynamic strip on fuselage, left wing, or left horizontal tail:

$$\begin{aligned} \frac{\partial f_{a_d}(r_i)}{\partial \alpha} &= P_d c_i(r_i) \frac{\partial \left(C_{l\alpha} \alpha \sin\alpha - \left(C_{d0} + k C_{l\alpha}^2 \alpha^2 \right) \cos\alpha \right)}{\partial \alpha} \\ &= P_d c_i(r_i) \begin{pmatrix} C_{l\alpha} \sin\alpha + C_{l\alpha} \alpha \cos\alpha - C_{d0_\alpha} \cos\alpha + C_{d0} \sin\alpha \\ -2k C_{l\alpha}^2 \alpha \cos\alpha + k C_{l\alpha}^2 \alpha^2 \sin\alpha \end{pmatrix} \end{aligned} \tag{3.4}$$

Using the small angle approximation i.e. $\sin\alpha \approx \alpha$ and $\cos\alpha \approx 1$ and also removing the higher order terms Eq. (3.4) can be written as:

$$\frac{\partial f_{a_d}(r_i)}{\partial \alpha} = -P_d c_i(r_i) C_{d0_\alpha} \tag{3.5}$$

in which C_{d0_α} for a strip can be written as $\left(\frac{\partial C_d}{\partial \alpha}\right)_0 = \frac{2C_{l0}}{\pi A R k_i} C_{l_\alpha}$. The sign convention in case of right wing and horizontal tail will be opposite to that of given in Eq. (3.5). Similarly, by using the same assumption as used in the case of Eq. (3.4), the derivative of lift and side force w.r.t α and β, respectively, are as follows:

$$\frac{\partial f_{a_l}(r_i)}{\partial \alpha} = -P_d c_i(r_i) \left[C_{l\alpha} + C_{d0} \right] \tag{3.6}$$

$$\frac{\partial f_s(r_i)}{\partial \beta} = -P_d c_i(r_i) C_{s\beta} \tag{3.7}$$

3.3 Aerodynamic damping matrix

Based on the expressions of instantaneous angles α and β, given in Appendix F, the aerodynamic damping matrix $C_{V\Omega}$ in Eq (3.1) is expressed as follows:

$$C_{V\Omega} = \left[\begin{array}{ccccc|c} 0 & 0 & 0 & 0 & 0 & 0 \\ 0 & 0 & 0 & 0 & 0 & 0 \\ 0 & 0 & 0 & 0 & 0 & 0 \\ 0 & 0 & 0 & Z_V & Z_\Omega & Z_\eta \\ 0 & 0 & 0 & M_V & M_\Omega & M_\eta \\ \hline 0 & 0 & 0 & Q_V & Q_\Omega & Q_\eta \end{array}\right] \tag{3.8}$$

3.3.1 Damping due to V

In Eq. 3.8 the aerodynamic damping matrices Z_V, M_V, and Q_V due to rigid-body motion in translation are expressed as:

$$Z_V = \frac{\rho V_{fx}}{2}\left[\begin{array}{c|c|c} e_1^T & \left\{\int C_f^T c_f \overbrace{\begin{bmatrix} C_{d0_{\beta f}} \\ C_{s\beta_f} \\ 0 \end{bmatrix}}^{Z_{V_{\beta f}}} dD_f + \int C_v^T c_v \underbrace{\begin{bmatrix} 0 \\ C_{d0_{\beta v}} \\ C_{s\beta_v} \end{bmatrix}}_{Z_{V_{\beta v}}} dD_v \right\} & e_1^T \end{array}\right]$$

$$+\frac{\rho V_{fx}}{2}\left[\begin{array}{c|c|c} e_1^T & e_1^T & \left\{\begin{array}{c} \int C_w^T c_w \overbrace{\begin{bmatrix} 0 \\ C_{d0_{\alpha w}} \\ C_{l\alpha_w} + C_{d0_w} \end{bmatrix}}^{Z_{V_{\alpha w}}} dD_w \\ + \int (C_h C_v)^T c_h \underbrace{\begin{bmatrix} 0 \\ C_{d0_{\alpha h}} \\ C_{l\alpha_h} + C_{d0_h} \end{bmatrix}}_{Z_{V_{\alpha h}}} dD_h \end{array}\right\} \end{array}\right] \tag{3.9}$$

$$M_V = \frac{\rho V_{fx}}{2}\left(\sum_{i=f,v}\int_{D_i} \tilde{l}_i c_i \begin{bmatrix} e_1 \\ Z_{V_{\beta i}}^T \\ e_1 \end{bmatrix}^T dD_i + \sum_{i=h,w}\int_{D_i} \tilde{l}_i c_i \begin{bmatrix} e_1 \\ e_1 \\ Z_{V_{\alpha h}}^T \end{bmatrix}^T dD_i\right) \tag{3.10}$$

in which e_1 is a null vector of size (1×3). By using the Eqs. (2.43–2.45), the moment arm vectors l_f, l_i, and l_h from aircraft body axes O_f to a particular node of fuselage, wings or vertical tails, and horizontal tails respectively are expressed in Eq. (3.10) as:

$$\tilde{l_f} = \tilde{r}_f C_f^T + C_f^T\left(\widetilde{\phi_{u_f} D_{u_f}} + \tilde{y}_f \widetilde{\phi_{\psi_f} D_{\psi_f}}\right)\xi \tag{3.11}$$

$$\tilde{l_i} = \left[\tilde{r_{fi}} + \left(C_f^T \widetilde{\phi_{u_f}} D_{u_f} + C_f^T \widetilde{\tilde{y}_f \phi_{\psi_f}} D_{\psi_f}\right)\xi\right] C_i^T + C_i^T \left[\tilde{r_i} + \left(\widetilde{\phi_{u_i} D_{u_i}} + \widetilde{\tilde{y}_i \phi_{\psi_i} D_{\psi_i}}\right)\xi\right] \quad i = w, v \tag{3.12}$$

$$\begin{aligned}\tilde{l_h} = &\left[\tilde{r_{fv}} + \left(C_f^T \widetilde{\phi_{u_{fv}}} D_{u_f} + C_f^T \widetilde{\tilde{y}_f \phi_{\psi_{fv}}} D_{\psi_f}\right)\xi\right] (C_h C_v)^T \\ &+ C_v^T \left[\tilde{r_{vh}} + \left(\widetilde{\phi_{u_{vh}} D_{u_v}} + \widetilde{\tilde{y}_v \phi_{\psi_{vh}}} D_{\psi_v}\right)\xi\right] C_h^T \\ &+ (C_h C_v)^T \left[\tilde{r_h} + \left(\widetilde{\phi_{u_h} D_{u_h}} + \widetilde{\tilde{y}_h \phi_{\psi_h}} D_{\psi_h}\right)\xi\right]\end{aligned} \tag{3.13}$$

The reduced-order generalized damping matrix Q_V is given as:

$$Q_V = \frac{\rho V_{fx}}{2} \sum_{i=f,e,w} Q_{V_i} \tag{3.14}$$

By using Eqs.(2.43–2.45), the reduced-order generalized damping matrices Q_{V_i} of each component in Eq. (3.14) are defined as:

$$Q_{V_i} = \int_{D_i} \left[\Phi_{u_i} + \Phi_{\psi_i}\right]^T c_i \begin{bmatrix} e_1 \\ e_1 \\ Z_{V_{\alpha i}}^T \end{bmatrix}^T dD_i, \quad i = h, w \tag{3.15}$$

$$Q_{V_v} = \int_{D_v} \left[\Phi_{u_v} + \Phi_{\psi_v}\right]^T c_v \begin{bmatrix} e_1 \\ Z_{V_{\beta v}}^T \\ e_1 \end{bmatrix}^T dD_v + \int_{D_h} \left[\Phi_{u_{vh}} + \Phi_{\psi_{vh}}\right]^T c_h \begin{bmatrix} e_1 \\ e_1 \\ Z_{V_{\alpha h}}^T \end{bmatrix}^T dD_h \tag{3.16}$$

$$\begin{aligned}Q_{V_f} = &\int_{D_f} \left[\Phi_{u_f} + \Phi_{\psi_f}\right]^T c_f \begin{bmatrix} e_1 \\ Z_{V_{\beta i}}^T \\ e_1 \end{bmatrix}^T dD_f + \int_{D_v} \left[\Phi_{u_{fv}} + \Phi_{\psi_{fv}}\right]^T c_v \begin{bmatrix} e_1 \\ Z_{V_{\beta v}}^T \\ e_1 \end{bmatrix}^T dD_v \\ &+ \int_{D_w} \left[\Phi_{u_{fw}} + \Phi_{\psi_{fw}}\right]^T c_w \begin{bmatrix} e_1 \\ e_1 \\ Z_{V_{\alpha w}}^T \end{bmatrix}^T dD_w + \int_{D_h} \left[\Phi_{u_{fh}} + \Phi_{\psi_{fh}}\right]^T C_h^T c_h \begin{bmatrix} e_1 \\ e_1 \\ Z_{V_{\alpha h}}^T \end{bmatrix}^T dD_h\end{aligned} \tag{3.17}$$

The expressions for eigenfunctions Φ_{u_i} and Φ_{ψ_i} in Eqs. (3.15–3.17) are given in Table 3.1.

3.3.2 Damping due to Ω

The aerodynamic damping due to rigid-body rotational rates in pitch and yaw (i.e. $\dot{\theta}_{\Theta_f}$ and $\dot{\theta}_{\Psi_f}$, respectively) are dominated by empennage effects (i.e. horizontal tails and vertical tail). The effects of wings and fuselage are simply

ignored in this case only [30, 36]. Similarly the damping due to a roll rate (i.e. $\dot{\theta}_{\Phi_f}$) is affected by the wings only. The damping matrices Z_Ω, M_Ω, and Q_Ω due to rigid-body motion in rotation are therefore expressed as:

$$Z_\Omega = \frac{\rho V_{fx}}{2}\left(\begin{array}{c} \int\limits_{D_v} \|l_v\| c_v \begin{bmatrix} e_1 \\ e_1 \\ \left(C_v^T Z_{V_{\beta v}}\right)^T \end{bmatrix}^T dD_v + \int\limits_{D_w} \|l_w\| c_w \begin{bmatrix} \left(C_v^T Z_{V_{\alpha w}}\right)^T \\ e_1 \\ e_1 \end{bmatrix}^T dD_w \\ + \int\limits_{D_h} \|l_h\| c_h \begin{bmatrix} e_1 \\ \left(C_h C_v\right)^T Z_{V_{\alpha h}}\right)^T \\ e_1 \end{bmatrix}^T dD_h \end{array}\right) \tag{3.18}$$

$$M_\Omega = \frac{\rho V_{fx}}{2}\left(\begin{array}{c} \int\limits_{D_v} \tilde{l}_v \|l_v\| c_v \begin{bmatrix} e_1 \\ e_1 \\ Z_{V_{\beta v}}^T \end{bmatrix}^T dD_v + \int\limits_{D_w} \tilde{l}_w \|l_w\| c_w \begin{bmatrix} Z_{V_{\alpha w}}^T \\ e_1 \\ e_1 \end{bmatrix}^T dD_w \\ + \int\limits_{D_h} \tilde{l}_h \|l_h\| c_h \begin{bmatrix} e_1 \\ Z_{V_{\alpha h}}^T \\ e_1 \end{bmatrix}^T dD_h \end{array}\right) \tag{3.19}$$

$$Q_\Omega = \frac{\rho V_{fx}}{2} \sum_{i=h,v} Q_{\Omega_i} \tag{3.20}$$

in which $\|l_i\|$ is the Euclidean norm[1] of the moment arm vector. Similar to the damping matrices Q_{V_i} in Eqs. (3.15–3.17), the reduced-order generalized damping matrices Q_{Ω_i} of each component are defined as:

$$Q_{\Omega_h} = \int\limits_{D_h} \left[\Phi_{u_h} + \Phi_{\psi_h}\right]^T \|l_h\| c_h \begin{bmatrix} e_1 \\ Z_{V_{\alpha h}}^T \\ e_1 \end{bmatrix}^T dD_h, \tag{3.21}$$

$$Q_{\Omega_v} = \int\limits_{D_v} \begin{bmatrix} \Phi_{u_v} \\ +\Phi_{\psi_v} \end{bmatrix}^T \|l_v\| c_v \begin{bmatrix} e_1 \\ e_1 \\ Z_{V_{\beta v}}^T \end{bmatrix}^T dD_v + \int\limits_{D_h} \begin{bmatrix} \Phi_{u_{vh}} \\ +\Phi_{\psi_{vh}} \end{bmatrix}^T \|l_h\| c_h \begin{bmatrix} e_1 \\ Z_{V_{\alpha h}}^T \\ e_1 \end{bmatrix}^T dD_h \tag{3.22}$$

[1] Euclidean norm of a vector $[x\ y\ z]$ is $\sqrt{x^2 + y^2 + z^2}$

3.3.3 Damping due to η

The aerodynamic damping matrices Z_η, M_η, and Q_η due to structural generalized velocities are expressed as:

$$Z_\eta = \frac{\rho V_{fx}}{2} \sum_{i=f,e,w} \int_{D_i} C_i^T Z_{\eta_i} dD_i \tag{3.23}$$

$$M_\eta = \frac{\rho V_{fx}}{2} \sum_{i=f,e,w} \int_{D_i} \tilde{l}_i Z_{\eta_i} dD_i \tag{3.24}$$

$$Q_\eta = \frac{\rho V_{fx}}{2} \sum_{i=f,e,w} \int_{D_i} \Phi_i^T Z_{\eta_i} dD_i \tag{3.25}$$

where the rotation matrix C_i of the horizontal tail in Eq. (3.23), as given in several expression before, is $C_h C_v$. The reduced-order generalized damping matrices Z_{η_i} of each component are defined as:

$$Z_{\eta_h} = c_h \begin{bmatrix} e_1 \\ e_1 \\ Z_{V_{\alpha h}}^T \end{bmatrix}^T \overbrace{\left[\Phi_{u_h} + \Phi_{\psi_h} + \Phi_{u_{vh}} + \Phi_{\psi_{vh}} + \Phi_{u_{fh}} + \Phi_{\psi_{fh}}\right]}^{\Phi_h} \tag{3.26}$$

$$Z_{\eta_w} = c_w \begin{bmatrix} e_1 \\ e_1 \\ Z_{V_{\alpha w}}^T \end{bmatrix}^T \overbrace{\left[\Phi_{u_w} + \Phi_{\psi_w} + \Phi_{u_{fw}} + \Phi_{\psi_{fw}}\right]}^{\Phi_w} \tag{3.27}$$

$$Z_{\eta_v} = c_v \begin{bmatrix} e_1 \\ Z_{V_{\beta v}}^T \\ e_1 \end{bmatrix}^T \overbrace{\left[\Phi_{u_v} + \Phi_{\psi_v} + \Phi_{u_{fv}} + \Phi_{\psi_{fv}}\right]}^{\Phi_v} \tag{3.28}$$

$$Z_{\eta_f} = c_f \begin{bmatrix} e_1 \\ Z_{V_{\beta f}}^T \\ e_1 \end{bmatrix}^T \overbrace{\left[\Phi_{u_f} + \Phi_{\psi_f}\right]}^{\Phi_f} \tag{3.29}$$

3.4 Aerodynamic stiffness matrix

The aerodynamic stiffness in Eq. (3.1) is defined as:

$$B_x = \left[\begin{array}{cc:cccc} 0 & 0 & 0 & 0 & 0 & 0 \\ 0 & 0 & 0 & 0 & 0 & 0 \\ 0 & 0 & 0 & 0 & 0 & 0 \\ Z_{R_f} & Z_{\theta_f} & Z_\xi & 0 & 0 & 0 \\ M_{R_f} & M_{\theta_f} & M_\xi & 0 & 0 & 0 \\ \hdashline Q_{R_f} & Q_{\theta_f} & Q_\xi & 0 & 0 & 0 \end{array}\right] \tag{3.30}$$

Table 3.1: Eigenfunctions used in aerodynamic damping and mass matrices

$\Phi_{u_{fi}}$	$\left[\tilde{r}_i^T C_i \Delta\phi_{u_{fi}} + C_i \phi_{u_{fi}}\right] D_{u_f}, \quad i = w, v$
$\Phi_{u_{fh}}$	$\left[\left(\tilde{r}_h^T C_h + C_h \tilde{r}_{vh}^T C_v\right) \Delta\phi_{u_{fv}} + C_h C_v \phi_{u_{fv}}\right] D_{u_f}$
$\Phi_{u_{vh}}$	$\left[\tilde{r}_h^T C_h \Delta\phi_{u_v} + C_h \phi_{u_{vh}}\right] D_{u_v}$
Φ_{u_i}	$\phi_{u_i} D_{u_i}, \quad i = f, e, w$

$\Phi_{\psi_{fi}}$	$\left[\tilde{r}_i^T C_i \left(\tilde{y}_f \Delta\phi_{\psi_{fi}} + \phi_{\psi_{fi}}\right) + C_i \left(\tilde{y}_f + \tilde{r}_{fi}\right)^T \phi_{\psi_{fi}}\right] D_{\psi_f}, \quad i = w, v$
$\Phi_{\psi_{fh}}$	$\left[\left(\tilde{r}_h^T C_h + C_h \tilde{r}_{vh}^T C_v\right) \left(\tilde{y}_f \Delta\phi_{\psi_{fv}} + \phi_{\psi_{fv}}\right) + C_h C_v \left(\tilde{y}_f + \tilde{r}_{fv}\right)^T \phi_{\psi_{fv}}\right] D_{\psi_f}$
$\Phi_{\psi_{vh}}$	$\left[\tilde{r}_h^T C_h \left(\tilde{y}_v \Delta\phi_{\psi_{vh}} + \phi_{\psi_{vh}}\right) + C_h \left(\tilde{y}_v + \tilde{r}_{vh}\right)^T \phi_{\psi_{vh}}\right] D_{\psi_v}$
Φ_{ψ_i}	$\left(\tilde{y}_i + \tilde{r}_i\right)^T \phi_{\psi_i} D_{\psi_i}, \quad i = f, e, w$

[a] As given in Eq. (2.12), $\phi_{u_{fi}}$ or $\phi_{\psi_{fi}}$, and $\phi_{u_{vh}}$ or $\phi_{\psi_{vh}}$ correspond to shape function values at the position of wings or vertical tail on fuselage, and horizontal tails on vertical tail, respectively.

3.4.1 Stiffness due to R_f

The stiffness due to the rigid-body translation is mainly attributed to the engine thrust, which, as given in Eq. (2.40), is a function of the altitude. But in the present study we assume that during short period maneuvers the change in aircraft altitude is small and has a minimum effect on the air density and so is the engine thrust. So the aerodynamic stiffness due to the R_f is simply ignored, however if one feel it necessary to include the derivative then Eq. (2.40) can be differentiated w.r.t. R_f.

3.4.2 Stiffness due to θ_f

The aircraft attitude in roll and pitch (i.e. θ_{Φ_f} and θ_{Θ_f}) affects the aerodynamic and gravity loads in Eq. (2.38). The submatrices Z_{θ_f}, M_{θ_f}, and Q_{θ_f} are functions of the derivatives of w.r.t. θ_{Φ_f}, θ_{Θ_f}, and θ_{Ψ_f} and expressed as follows:

$$Z_{\theta_f} = \sum_{i=f,e,w} \int_{D_i} \left(\frac{\rho V_{fx}^2}{2} c_i \begin{bmatrix} e_1 \\ C_i^T Z_{V_{\alpha_i}}^T \\ C_i^T Z_{V_{\beta_i}}^T \end{bmatrix}^T dD_i + \begin{bmatrix} \frac{\partial C_{If}}{\partial \theta_{\Phi_f}} & \frac{\partial C_{If}}{\partial \theta_{\Theta_f}} & \frac{\partial C_{If}}{\partial \theta_{\Psi_f}} \end{bmatrix} \begin{bmatrix} 0 \\ 0 \\ g \end{bmatrix} dm_i \right) \tag{3.31}$$

$$M_{\theta_f} = \sum_{i=f,e,w} \int_{D_i} \tilde{l}_i \left(\frac{\rho V_{fx}^2}{2} c_i \begin{bmatrix} e_1 \\ C_i^T Z_{V_{\alpha_i}}^T \\ C_i^T Z_{V_{\beta_i}}^T \end{bmatrix}^T dD_i + \begin{bmatrix} \frac{\partial C_{If}}{\partial \theta_{\Phi_f}} & \frac{\partial C_{If}}{\partial \theta_{\Theta_f}} & \frac{\partial C_{If}}{\partial \theta_{\Psi_f}} \end{bmatrix} \begin{bmatrix} 0 \\ 0 \\ g \end{bmatrix} dm_i \right)$$
$$+ \sum_{i=f,e,w} \int_{D_i} \frac{\rho V_{fx}^2 c_i}{2} \begin{bmatrix} 0 & 0 & C_{l_{\beta_i}} \\ 0 & C_{m_{\alpha_i}} & 0 \\ 0 & 0 & C_{n_{\beta_i}} \end{bmatrix} dD_i \tag{3.32}$$

$$Q_{\theta_f} = \sum_{i=f,e,w} \int_{D_i} \phi_i^T \left(\begin{array}{c} \frac{\rho V_{fx}^2}{2} c_i \begin{bmatrix} e_1 \\ C_i^T Z_{V_{\alpha_i}}^T \\ C_i^T Z_{V_{\beta_i}}^T \end{bmatrix}^T dD_i + \begin{bmatrix} \frac{\partial C_{If}}{\partial \theta_{\Phi_f}} & \frac{\partial C_{If}}{\partial \theta_{\Theta_f}} & \frac{\partial C_{If}}{\partial \theta_{\Psi_f}} \end{bmatrix} \begin{bmatrix} 0 \\ 0 \\ g \end{bmatrix} dm_i \\ + \frac{\rho V_{fx}^2 c_i}{2} \begin{bmatrix} 0 & 0 & C_{l_{\beta_i}} \\ 0 & C_{m_{\alpha_i}} & 0 \\ 0 & 0 & C_{n_{\beta_i}} \end{bmatrix} \end{array} \right) \tag{3.33}$$

3.4.3 Stiffness due to ξ

The stiffness due to a local torsion of a section on the wings, horizontal tails and the vertical tail is as follows, whereas the fuselage is simply ignored:

$$Z_\xi = -\frac{\rho V_{fx}}{2} \sum_{i=f,e,w} \int_{D_i} C_i^T Z_{\xi_i} dD_i \tag{3.34}$$

$$M_\xi = -\frac{\rho V_{fx}}{2} \sum_{i=f,e,w} \int_{D_i} \tilde{l}_i Z_{\xi_i} dD_i \tag{3.35}$$

$$Q_\xi = -\frac{\rho V_{fx}}{2} \sum_{i=f,e,w} \int_{D_i} \Phi_i^T Z_{\xi_i} dD_i \tag{3.36}$$

The reduced-order generalized aerodynamic stiffness matrices Z_{ξ_i} of each component are defined as:

$$Z_{\xi_v} = \begin{bmatrix} Z_{V_\beta}^T \\ e_1 \\ e_1 \end{bmatrix}^T \Phi_{\psi_v} D_{\psi_v} \tag{3.37}$$

$$Z_{\xi_i} = \begin{bmatrix} Z_{V_\alpha}^T \\ e_1 \\ e_1 \end{bmatrix}^T \Phi_{\psi_i} D_{\psi_i} \quad i = h, w \tag{3.38}$$

in which Φ_{ψ_i} is given in Table 3.1.

3.5 Control stiffness matrix

The aerodynamic stiffness due to pilot input (i.e. control surface deflections and thrust changes) can be written as:

$$B_u = \begin{bmatrix} 0 & 0 & 0 & 0 \\ 0 & 0 & 0 & 0 \\ 0 & 0 & 0 & 0 \\ Z_{\delta_{el}} & Z_{\delta_a} & Z_{\delta_r} & Z_{\delta_T} \\ M_{\delta_{el}} & M_{\delta_a} & M_{\delta_r} & M_{\delta_T} \\ \hline Q_{\delta_{el}} & Q_{\delta_a} & Q_{\delta_r} & Q_{\delta_T} \end{bmatrix} \tag{3.39}$$

The next four subsections describe the different contributions.

3.5.1 Stiffness due to δ_{el}

The aerodynamic stiffness as a result of an elevator deflection is expressed as:

$$Z_{\delta_{el}} = \frac{\rho V_{fx^2}}{2} \int_{D_h} c_h C_v^T C_h^T \begin{bmatrix} 0 & 0 & C_{l_{\delta_{el}}} \end{bmatrix}^T dD_h \tag{3.40}$$

$$M_{\delta_{el}} = \frac{\rho V_{fx^2}}{2} \int_{D_h} c_h \tilde{l}_h \begin{bmatrix} 0 & 0 & C_{l_{\delta_{el}}} \end{bmatrix}^T dD_h \tag{3.41}$$

$$Q_{\delta_{el}} = \frac{\rho V_{fx^2}}{2} \int_{D_h} c_h \Phi_h^T \begin{bmatrix} 0 & 0 & C_{l_{\delta_{el}}} \end{bmatrix}^T dD_h \tag{3.42}$$

in which Φ_h is expressed in Eq. (3.26).

3.5.2 Stiffness due to δ_a

Similar to Eqs. (3.40–3.42), the aerodynamic stiffness due to aileron deflections is expressed as:

$$Z_{\delta_a} = \frac{\rho V_{fx}^2}{2} \int_{D_w} c_w C_w^T \begin{bmatrix} 0 & 0 & C_{l_{\delta_a}} \end{bmatrix}^T dD_w \tag{3.43}$$

$$M_{\delta_a} = \frac{\rho V_{fx}^2}{2} \int_{D_w} c_w \tilde{l}_w \begin{bmatrix} 0 & 0 & C_{l_{\delta_a}} \end{bmatrix}^T dD_w \tag{3.44}$$

$$Q_{\delta_a} = \frac{\rho V_{fx}^2}{2} \int_{D_w} c_w \Phi_w^T \begin{bmatrix} 0 & 0 & C_{l_{\delta_a}} \end{bmatrix}^T dD_w \tag{3.45}$$

in which Φ_w is expressed in Eq. (3.27).

3.5.3 Stiffness due to δ_r

The aerodynamic stiffness due to a rudder deflection is expressed as:

$$Z_{\delta_r} = \frac{\rho V_{fx}^2}{2} \int_{D_v} c_v C_v^T \begin{bmatrix} 0 & C_{l_{\delta_r}} & 0 \end{bmatrix}^T dD_v \tag{3.46}$$

$$M_{\delta_r} = \frac{\rho V_{fx}^2}{2} \int_{D_v} c_v \tilde{l}_v \begin{bmatrix} 0 & C_{l_{\delta_r}} & 0 \end{bmatrix}^T dD_v \tag{3.47}$$

$$Q_{\delta_r} = \frac{\rho V_{fx}^2}{2} \int_{D_v} c_v \Phi_v^T \begin{bmatrix} 0 & C_{l_{\delta_r}} & 0 \end{bmatrix}^T dD_v \tag{3.48}$$

in which Φ_v is expressed in Eq. (3.28).

3.5.4 Stiffness due to δ_T

The aerodynamic stiffness due to thrust changes is expressed as:

$$Z_{\delta_T} = \int_{D_f} \delta\left(r - r_{f_E}\right) \begin{bmatrix} C_{x_{\delta_T}} & 0 & 0 \end{bmatrix}^T dD_f \tag{3.49}$$

$$M_{\delta_T} = \int_{D_f} \tilde{l}_f \delta\left(r - r_{f_E}\right) \begin{bmatrix} C_{x_{\delta_T}} & 0 & 0 \end{bmatrix}^T dD_f \tag{3.50}$$

$$Q_{\delta_T} = \int_{D_f} \Phi_f^T \delta\left(r - r_{f_E}\right) \begin{bmatrix} C_{x_{\delta_T}} & 0 & 0 \end{bmatrix}^T dD_f \tag{3.51}$$

in which, from Eq. (2.40) $C_{x_{\delta_T}} = \frac{\partial f_E}{\partial \delta_T}$.

3.6 Linearization

After the formulation of the state-space equations, the model is linearized further into a zero-order problem (i.e. the rigid-body motion) and a first-order problem (i.e. vibrations and their effects on the rigid-body response).

3.6.1 Zero-order problem

The zero-order problem represents the rigid-body motion and is represented with superscript (0):

$$\dot{x}^{(0)}(t) = \left[\left[A^{(0)}(t) + C_{V\Omega}^{(0)}(t)\right] M_{rr}^{(0)^{-1}} + B_x(t)^{(0)}\right] x^{(0)}(t) + B_u^{(0)} u^{(0)}(t) \tag{3.52}$$

Eq. (3.52) is a generic form of the zero-order problem. For a typical steady-state solution (i.e. to find the trim variables such as controls inputs $u^{(0)}$ and aircraft attitude angles $\theta_f^{(0)}$) it is assumed that the aircraft exhibits no perturbations around the steady-state. Eq. (3.52) is therefore transformed as:

$$\dot{x}^{(0)}(t) = \left[A^{(0)} M_{rr}^{(0)^{-1}} + B_x^{(0)}\right] x^{(0)} + B_u^{(0)} u^{(0)} + B_\xi \xi^{(0)} \tag{3.53}$$

Although Eq. (3.53) solves the zero-order state, at the same time static structural deflections $\xi^{(0)}$ are present[2] and their effects on the aerodynamic forces are taken care in the last term of Eq. (3.53), see Section 4.2 for a brief description on finding a steady-state. After finding the trim condition (i.e. $x^{(0)}$, $u^{(0)}$, and $\xi^{(0)} =$ constant, where $\dot{\xi} = 0$) at the given speed ($V_{f_x}^{(0)}$), the perturbation in zero-order is stated as:

$$\Delta\dot{x}^{(0)}(t) = \left[C_{V\Omega}^{(0)}(V_{f_x}^{(0)}) M_{rr}^{(0)^{-1}} + B_x^{(0)}(V_{f_x}^{(0)})\right] \Delta x^{(0)}(t) + B_u^{(0)}(V_{f_x}^{(0)}) \Delta u^{(0)}(t) \tag{3.54}$$

In Eqs. (3.52–3.54), the zero-order state-vector $x^{(0)}$ is defined as $\begin{bmatrix} R_f^{(0)^T} & \theta_f^{(0)^T} & p_{Vf}^{(0)^T} & p_{\Omega f}^{(0)^T} \end{bmatrix}^T$. The state matrix $A^{(0)}$ from Eq. (3.3) is reduced to the following form [28]:

$$A^{(0)} = \left[\begin{array}{c:c} e_2 & \begin{bmatrix} C_f^{(0)T} & 0 \\ 0 & E_f^{(0)^{-1}} \end{bmatrix} \\ \hdashline e_2 & \begin{bmatrix} 0 & \widetilde{p_{Vf}^{(0)}} \\ \widetilde{p_{Vf}^{(0)}} & \widetilde{p_{\Omega f}^{(0)}} \end{bmatrix} \end{array}\right] \tag{3.55}$$

in which the e_2 is the null matrix of size (6×6). The inverse of the zero-order mass matrix $M_{rr}^{(0)^{-1}}$ in Eqs. (3.53–3.54) has the same form as given in Eq. (3.2) (i.e. $M_{rr}^{(0)^{-1}} = \begin{bmatrix} 0 & M_r^{(0)^{-1}} \\ 0 & M_r^{(0)^{-1}} \end{bmatrix}$), where the single submatrix $M_r^{(0)}$ has the form as given below:

$$M_r^{(0)} = \begin{bmatrix} mI & \tilde{S}^T \\ \tilde{S} & J_f \end{bmatrix} \tag{3.56}$$

[2] In this section the superscript (0) is only meant for static deflections, otherwise the concept of the generalized coordinates ξ as first-order quantities remains intact.

$C^{(0)}_{V\Omega}$, $B^{(0)}_x$, and $B^{(0)}_u$ are reduced to zero-order states by retaining only those terms, which are related to the rigid-body motion:

$$C^{(0)}_{V\Omega} = \left[\begin{array}{c|cc} e_2 & & e_2 \\ \hline e_2 & Z_V & Z_\Omega \\ & M_V & M_\Omega \end{array}\right], \quad B^{(0)}_x = \left[\begin{array}{cc|c} & e_2 & \\ \hline Z_{R_f} & Z_{\theta_f} & e_2 \\ M_{R_f} & M_{\theta_f} & \end{array}\right]$$

$$B^{(0)}_u = \left[\begin{array}{cccc} & & e_2 & \\ \hline Z_{\delta_{el}} & Z_{\delta_a} & Z_{\delta_r} & Z_{\delta_T} \\ M_{\delta_{el}} & M_{\delta_a} & M_{\delta_r} & M_{\delta_T} \end{array}\right], \quad B_\xi = \left[\begin{array}{c} e_1^T \\ e_1^T \\ \hline Z_\xi \\ M_\xi \end{array}\right] \tag{3.57}$$

Moreover, the moment arm vectors l_f, l_i, and l_h in Eqs.(3.11–3.13) are also reduced to zero-order vectors as:

$$\tilde{l}^{(0)}_f = \tilde{r}_f C^T_f \tag{3.58}$$

$$\tilde{l}^{(0)}_i = \tilde{r}_{fi} C^T_i + C^T_i \tilde{r}_i \tag{3.59}$$

$$\tilde{l}^{(0)}_h = \tilde{r}_{fv} \left(C_h C_v\right)^T + C^T_v \tilde{r}_{vh} C^T_h + \left(C_h C_v\right)^T \tilde{r}_h \tag{3.60}$$

In most of the flight mechanics literature [26, 30, 31], instead of momenta, the equations of motion, as given in Eqs. (3.52–3.54), are solved in the form of accelerations. In Appendix G the equations of motions are simplified into the velocity states, however, this does not change the original context of the equations.

3.6.2 First-order problem

The solution of the zero-order steady-state (i.e. $x^{(0)}$, $u^{(0)}$, and $\xi^{(0)}$) enters into the first-order problem, which is a linearized state around the rigid-body perturbation and takes vibrations into account, including their effects on the overall response of the aircraft:

$$\dot{x}^{(1)}(t) = \left[A^{(1)} + C^{(1)}_{V\Omega} M^{(1)^{-1}}_{\xi\xi} + B^{(1)}_x - B^{(1)}_u G\right] x^{(1)}(t) + \begin{bmatrix} e_3 \\ F_{ext} \end{bmatrix} \tag{3.61}$$

Here F_{ext} is the external force vector caused by turbulence or pilot inputs and is obtained through the time domain solution of Eq. (3.54) as:

$$\begin{bmatrix} e_3 \\ F_{ext} \end{bmatrix} = C^{(1)}_{V\Omega} \begin{bmatrix} e_3 \\ \Delta\dot{x}^{(0)}_{R\theta}(t) \end{bmatrix} + B_x(t)^{(1)} \begin{bmatrix} e_3 \\ \Delta x^{(0)}_{R\theta}(t) \end{bmatrix} \tag{3.62}$$

$\Delta x^{(0)}_{R\theta}$ is the rigid-body perturbation over the trim condition and expressed in the vector form as $\begin{bmatrix} R^{(0)^T}_f & \theta^{(0)^T}_f & e_4 \end{bmatrix}^T$, which is solved through Eq. (3.54) or

Eqs. (G.4) and (G.5) in Appendix G[3]. e_3 is a null vector of size $(6 + m \times 1)$, and e_4 is a null vector of size $(1 \times m)$[4]. The first-order state-vector now takes its original form and adds two additional sub-vectors of generalized coordinates and their momenta:

$$x^{(1)} = \begin{bmatrix} R_f^{(1)T} & \theta_f^{(1)T} & \xi^T & p_{vf}^{(1)T} & p_{\Omega f}^{(1)T} & p_\eta^T \end{bmatrix}^T \tag{3.63}$$

The state-matrix $A^{(1)} = A[x^{(0)}, \xi^{(0)}]$ contains the partial derivatives of zero-order velocities, stiffness, and damping matrices with respect to the first-order state-vector. The coefficient matrices $C_{V\Omega}^{(1)} = C_{V\Omega}[x^{(0)}, \xi^{(0)}]$ and $B_x^{(1)} = B_x[x^{(0)}, \xi^{(0)}]$ gives the aerodynamic damping and stiffness, respectively, due to rigid-body translation and rotations, as well as the structural vibrations due to vehicle motion resulting from external disturbance, caused by a gust input or during maneuvers. $B_u^{(1)} = B_u[x^{(0)}, u^{(0)}]$ multiplied by the control gain matrix G gives the forces and moments due to first-order control inputs $u^{(1)}$, which consequently minimize the effects of external disturbance. The gain matrix G can be obtained by optimizing the performance index of linear quadratic regulator (LQR) [4, 37]:

$$J = \int_0^{t_f} \left(x^{(1)T} Q x^{(1)} + u^{(1)T} R u^{(1)} \right) dt_f \tag{3.64}$$

where t_f is the final time of the simulation. First-order control input $u^{(1)}$ is calculated as:

$$u^{(1)}(t) = -G(t) x^{(1)}(t)$$

Similar to the state-vector in Eq. (3.63), all the coefficient matrices like $A^{(1)}$, $C_{V\Omega}^{(1)}$, $B_x^{(1)}$, and $B_u^{(1)}$ take their original form as given in Eqs. (3.3), (3.8), (3.30), and (3.39), respectively. However, the coefficients related to the rigid-body motion are linearized and the process of linearization can be found in the Appendix H. The final perturbed solution will be as follows [4]:

$$\begin{aligned} \Delta x\,(t) &= \Delta x^{(0)}\,(t) + x^{(1)}\,(t) \\ \Delta u(t) &= \Delta u^{(0)}\,(t) + u^{(1)}\,(t) \end{aligned} \tag{3.65}$$

3.7 Synopsis

Equations of motion for a flexible aircraft are presented in the state-space form. The state equation is divided into coefficient matrices multiplied by the generalized state or control vector. The coefficient matrices include state coefficient

[3]It is to be noted that $\Delta x_{R\theta}^{(0)}$ in Eq. (3.62) constructs particularly the external force vector F_{ext}, otherwise the state-matrices like $A^{(1)}$, $C_{V\Omega}^{(1)}$, $B_x^{(1)}$, and $B_u^{(1)}$ are the functions of zero-order steady-state solution only (i.e. $x^{(0)}$, $u^{(0)}$, and $\xi^{(0)}$).

[4]Symbol m in case of null vectors e_3 and e_4 represents the number of shape functions used in the model reduction.

matrix, aerodynamic damping, aerodynamic stiffness and control stiffness matrix. The state-space equation is then linearized into a zero-order and first-order form, where the zero-order part takes care of the rigid-body response whose solution then enters into the first-order problem, which solves the vibrations and its effects on the overall rigid-body response of the flexible aircraft. The linearization process of key elements of the model is given in Appendix H.

Chapter 4

Flight Loads Equations

In this chapter the equations of motion are extended to predict static and dynamic loads. As given in Eq. (3.65), the loads on a flexible aircraft can also be divided into two categories, (1) static loads in a steady-state condition and (2) dynamic loads during maneuvers or as a result of external disturbances such as atmospheric turbulence.

4.1 LTI or LTV

With regard to the flight loads, first it is appropriate to choose between a linear time-invariant system (LTI) and a linear time-varying (LTV) system approach. For an LTI system it is assumed that during the maneuvers the air speed and height remain constant i.e. zero-order rigid-body velocity and position vectors do not change during the course of simulation. In other words the state-space matrices in Eqs. (3.52) and (3.61) are constructed once and held constant. This kind of scenario is assumed in steady pull-up or during a gust encounter when the aircraft does not accelerate. Although in many maneuvers like a checked and unchecked elevator deflection [38] the aircraft is subjected to a pitch acceleration [32], the author in Ref. 32 prefers to use the LTI approach. In principal the LTV approach seems more accurate than the LTI approach but on the other hand it is quite expensive in terms of numerical solution as the state-space matrices are to be updated for every time step. In Ref. 28 the authors used the LTV approach and solved the equations of motion by a discrete time numerical technique, where the model is reduced by using only the first two mode shapes. However, if the number of mode shapes in the model reduction is increased and sufficient higher frequency modes are included then the solution time in LTV approach will definitely be increased. In the present work we take the LTI approach to be most suitable however the state-space

equation presented in Chapters 2 and 3 are equally capable of being used in a LTV simulation.

4.2 Steady level flight

Steady level flight conditions for a linear time invariant (LTI) system are found by minimizing the zero-order momenta rates. It is assumed, as stated before, that before going into a maneuver or atmospheric turbulence the aircraft is flying in a purely horizontal, symmetric, and steady flight. In that case the translational momentum rate in side-slip $\dot{p}_{Vf_y}$ and bank i.e. $\dot{p}_{\Omega f_x}$ and $\dot{p}_{\Omega f_z}$ are zero. Hence, in order to obtain a constant velocity and height, only translational momenta rates in forward $\dot{p}_{Vf_x}$, plunge $\dot{p}_{Vf_z}$ and pitching $\dot{p}_{\Omega f_y}$ are to be minimized. Using the momenta in the state-vector of the Eq. (3.53), we write the quadratic cost function as:

$$J^{(0)}\left(\theta_f^{(0)}, u^{(0)}\right) = \begin{bmatrix} \dot{p}_{Vf_x}^{(0)} & \dot{p}_{Vf_z}^{(0)} & \dot{p}_{\Omega f_y}^{(0)} \end{bmatrix} W \begin{bmatrix} \dot{p}_{Vf_x}^{(0)} \\ \dot{p}_{Vf_z}^{(0)} \\ \dot{p}_{\Omega f_y}^{(0)} \end{bmatrix} \tag{4.1}$$

where W is a weighting matrix, which can be an identity matrix of order 3×3. By using an iterative optimization algorithm, in this case the simplex search method [39], the cost function given in Eq. (4.1) is minimized and that gives the trim elevator deflection δ_e, thrust settings δ_T and pitch attitude $\theta_{\Theta f}$. To verify these values, a check on the resultant horizontal and vertical forces and pitching moment at aircraft body axes O_f should find them to be zero. Figure 4.1 shows the schematic of the search algorithm used in finding the trim variables. It shows that first the Eq. (3.53) is algebraically solved, which gives the momenta rates. Based on these rates the cost function, as given in Eq. (4.1), is checked against the given minimum value (i.e. 10^{-4}). If the objective in the current iteration τ is not achieved then the optimizer proceeds to the next iteration (i.e. $\tau + 1$) with a change Δ in the design variables. This process continues till the cost function is minimized to 10^{-4}. The static deflections $\xi^{(0)}$ during the iterations are calculated by multiplying the inverse of the stiffness matrix with the generalized force vector calculated in Eqs. (2.43–2.46):

$$\xi^{(0)}(\tau) = K_\xi^{-1} \begin{bmatrix} Q_{u_\xi}^{(0)}(\tau - 1) \\ Q_{\psi_\xi}^{(0)}(\tau - 1) \end{bmatrix} \tag{4.2}$$

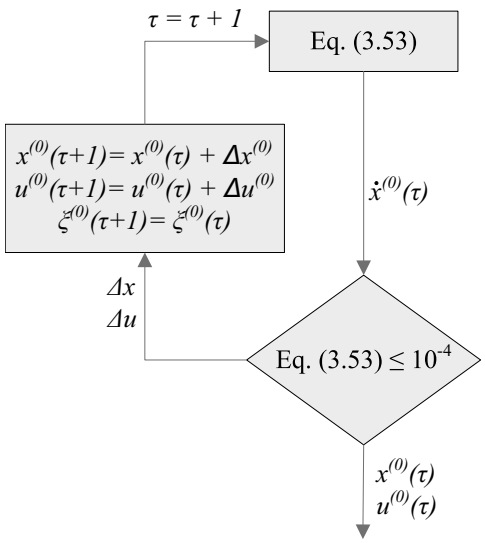

Figure 4.1: Schematic of trim algorithim.

4.2.1 Static loads

In steady level flight (i.e. $V_f^{(0)} = constant$ and $n_z = 1$), the generalized coordinates $\xi^{(0)}(\tau)$ from Eq. (4.2) are expanded to the full-order vector by using the specific rows of eigenvector D_m. The full-order vector is then multiplied with a matrix of eigenfunctions of a particular D.o.F, which gives the static deflection at each node of a component. By using the mode displacement method (MDM), which is based on the internal forces caused by the structural deformations due to aerodynamic and inertial loads [23, 40], the external static shear forces 'V_{zi_s}' and torsion moments 'M_{xi_s}' of a component 'i' are given as:

$$\begin{aligned} V_{zi_s}^{MDM}(r_i) &= \left[\phi_{u_i}(r_i) D_{u_i} + y_i \phi_{\psi_i}(r_i) D_{\psi i}\right] K_\xi \xi^{(0)}(t) \\ M_{xi_s}^{MDM}(r_i) &= \phi_{\psi_i}(r_i) D_{\psi_i} K_\xi \xi^{(0)}(t), \quad i = f, w, e \end{aligned} \tag{4.3}$$

where e.g., as given in Eq. (2.54), for the right wing bending $D_{uw}^R = D_{m(9:10,1:m)}$ and similarly for the torsion $D_{\psi w}^R = D_{m(23:24,1:m)}$.

4.3 Dynamic loads

Dynamic loads can be predicted at each node by calculating the rate of change of momentum due to elastic motions of that node:

$$\dot{p}_\eta = \frac{d}{dt}\begin{bmatrix} p_{u_i} \\ p_{\psi_i} \end{bmatrix} = \begin{bmatrix} F_{d_i} \\ T_{d_i} \end{bmatrix} \tag{4.4}$$

From Eq. (4.4) we can infer that by solving the equations of motion in the form of momenta an extra advantage is gained in simulating the dynamic loads [19, 41]. The numerical solution of Eq. (3.61) gives the first-order momenta which are then used to calculate first-order velocities. The first-order velocities can be expressed by linearizing Eq. (2.47) as given below [28], also see Appendix H:

$$p^{(1)} = M_{\xi}^{(1)} V_{\eta}^{(0)} + M_{\xi}^{(0)} V_{\eta}^{(1)} \tag{4.5}$$

Rearranging Eq. (4.5) gives the first-order velocity vector as:

$$V_{\eta}^{(1)}(t) = \left(M_{\xi}^{(0)}\right)^{-1} \left(p^{(1)}(t) - M_{\xi}^{(1)} V_{\eta}^{(0)}\right) \tag{4.6}$$

The reduced first-order velocity vector $V_{\eta}^{(1)}$ is expressed as $\left[V_f^{(1)T} \omega_f^{(1)T} \eta^T\right]^T$. After the numerical solution, Eq. (3.61) eventually acts as an algebraic equation which gives the momenta rates $\dot{p}$. It is known that the mass matrix is a function of generalized coordinates q [41], and does not depend upon the generalized velocities s (i.e. for a linear time invariant (LTI) system the time derivative of mass matrix $\dot{M}_{\xi}$ and velocity vector $\dot{V}_{\eta}^{(0)}$ around steady-state is zero), which states the time derivative of Eq. (4.6) as:

$$\dot{V}_{\eta}^{(1)}(t) = \left(M_{\xi}^{(0)}\right)^{-1} \dot{p}^{(1)}(t) \tag{4.7}$$

The reduced order dynamic loads vectors L_f and L_{η} due to rigid-body motion and elastic motion, respectively, can be expressed by the summation of forces method (SFM) and that is defined as the summation of all the aerodynamic and inertial loads [23]:

$$\begin{bmatrix} e_3 \\ L_f(t) \\ L_{\eta}(t) \end{bmatrix} = \overbrace{(A_x)\, x^{(1)}(t) + \begin{bmatrix} e_3 \\ F_{ext}(t) \end{bmatrix}}^{\text{aerodynamic loads}} - \underbrace{\begin{bmatrix} e_3 \\ \left(M_{\xi}^{(0)}\right) \dot{V}_{\eta}^{(1)}(t) \end{bmatrix}}_{\text{inertial loads}} \tag{4.8}$$

L_{η} is then expanded to a full order vector for a particular component by using the matrices of eigenvector and shape functions:

$$\begin{aligned} V_{zi_d}^{SFM}(r_i, t) &= \left[\quad \phi_{ui}(r_i) D_{ui} + y_i \phi_{\psi i}(r_i) D_{\psi i} \right] L_{\eta}^{(1)}(t) \\ M_{xi_d}^{SFM}(r_i, t) &= \phi_{\psi i}(r_i) D_{\psi i} L_{\eta}^{(1)}(t), i = f, w, e \end{aligned} \tag{4.9}$$

where 'V_{zi_d}' and 'M_{xi_d}' are the vectors of external dynamic vertical shear force and torsional moment along the $r.a$, respectively. Structural loads calculated from SFM can also be verified by using the mode displacement method (MDM) [23, 40]:

$$\begin{aligned} V_{zi_d}^{MDM}(r_i, t) &= \left[\quad \phi_{ui}(r_i) D_{ui} + y_i \phi_{\psi i}(r_i) D_{\psi i} \right] K_{\xi} \xi^{(1)}(t) \\ M_{xi_d}^{MDM}(r_i, t) &= \phi_{\psi i}(r_i) D_{\psi i} K_{\xi} \xi^{(1)}(t), i = f, w, e \end{aligned} \tag{4.10}$$

4.4 Component internal loads

Internal loads in terms of resultant shear, torsion, and bending moment are shown in Fig. 4.2. The downward shear and a bending moment that produces tension in the lower fibers is considered positive. The torsional moment on a node follows the sign convention of a particular component, see Fig 2.1. The resultant shear Q_j in Fig. 4.2 can be computed as follows [36]:

$$\begin{bmatrix} Q_1 \\ Q_2 \\ Q_3 \\ \vdots \\ Q_j \end{bmatrix} = \begin{bmatrix} 1 & 0 & 0 & \dots & 0 \\ 1 & 1 & 0 & \dots & 0 \\ 1 & 1 & 1 & \dots & 0 \\ \vdots & \vdots & \vdots & \dots & \vdots \\ 1 & 1 & 1 & \dots & 1 \end{bmatrix} \begin{bmatrix} V_{zi1} \\ V_{zi2} \\ V_{zi3} \\ \vdots \\ V_{zij} \end{bmatrix} \tag{4.11}$$

Similarly the bending moment due to the shear is expressed as:

$$\begin{bmatrix} M_1 \\ M_2 \\ M_3 \\ \vdots \\ M_j \end{bmatrix} = \begin{bmatrix} 0 & 0 & 0 & \dots & 0 \\ (r_2 - r_1) & 0 & 0 & \dots & 0 \\ (r_2 - r_1) & (r_3 - r_2) & 0 & \dots & 0 \\ \vdots & \vdots & \vdots & \dots & \vdots \\ (r_2 - r_1) & (r_3 - r_2) & (r_4 - r_3) & \dots & 0 \end{bmatrix} \begin{bmatrix} Q_1 \\ Q_2 \\ Q_3 \\ \vdots \\ Q_j \end{bmatrix} \tag{4.12}$$

The resultant torsional moment is also computed by using the analogy given in Eq. (4.11).

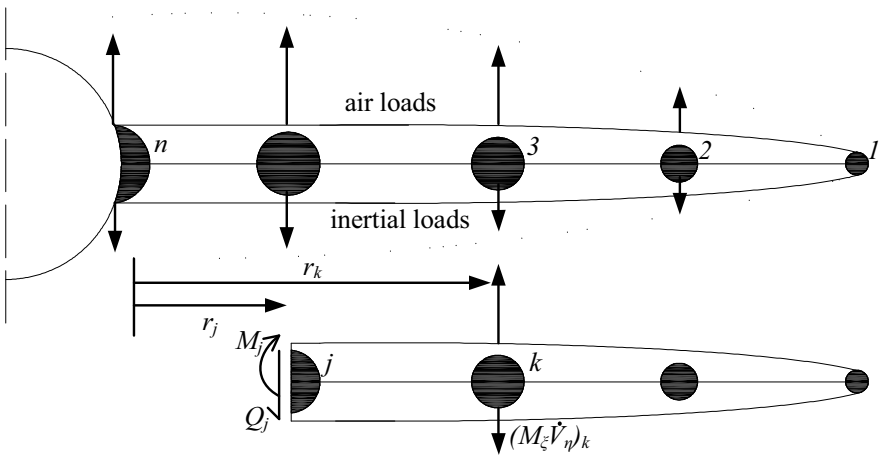

Figure 4.2: Wing resultant shear and bending.

4.5 Synopsis

The equations of motion presented in the last two chapters are further extended to structural loads equations, where it is assumed that the structural loads can be linearized into two categories; static loads during steady flight and dynamic loads due to external disturbances such as atmospheric turbulence or by pilot inputs. A quadratic cost function is used to determine the trim condition of the aircraft, by minimizing the translational and angular accelerations. After finding the trim condition in steady level flight the static structural loads are calculated by using the mode displacement method (MDM), which is based on the structural deformations. Dynamic loads due to vibrations are considered to be a first-order problem and summation of forces method (SFM) is formulated in this regard, which is based on the summation of aerodynamic, gravity and inertial forces acting on the component. Loads calculated from SFM are verified by using MDM. In the end the calculated loads are converted to component internal loads in the form of shear forces and corresponding moments.

Chapter 5

Simulation example – Part 1: Static case

In Chapters 2–4 the emphasis is put on the mathematical modeling of equations of motion, state-space form, and consequently the loads equations. This chapter gives an overview of the assembly of all mathematical equations in a computer code called DARLoads. Subsequently, a static simulation example is presented.

5.1 DARLoads

A computer code, DARLoads, has been written in MATLAB. The schematic of DARLoads is presented in Fig. 5.1. The structure of the code is divided into various functions and sub-routines such as functions that calculate mass, stiffness and damping matrices, coefficient matrices, shape functions, and graphics etc. These functions are called by the main script, whenever these are needed during the solution. It is capable of accepting the data of any aircraft of the configuration shown in Fig. 2.1. The inputs, in case of the structural model, are locations of grid points and values of lumped-masses and inertia matrices, stiffness properties of spring elements, and components' origins with their rotation matrices with respect to aircraft body-axis. For the aerodynamic model the inputs are locations of grid points of lifting strips with their aerodynamic coefficients. All the inputs are read from a spread sheet program and then saved into assigned structure arrays with particular components name and identification number (ID). For example the ID for the right wing is (3) and the structure of input routine looks like as given in Table 5.1:

After reading the aerodynamic and structural inputs, the flight conditions like nominal air speed and height are specified with arbitrary control inputs for el-

Table 5.1: Data input example

component(3).name = Right Wing;
component(3).coordinates = xlsread(input.xls, ...);
...
component(3).rotation = [0;4;90];

evator, aileron, rudder, and thrust. The structural dynamics module assembles the full-order mass, stiffness and structural damping matrices. By using these full-order mass and stiffness matrices the eigenvalue solution gives the natural frequencies and eigenvectors. Based on these eigenvectors the aircraft shape functions (ASF) are plotted and identified for the model reduction.

The rigid-body mass matrix and the aerodynamic coefficients from the inputs then constructs the zero-order state-space matrices, which include the state coefficient, aerodynamic damping, aerodynamic stiffness, and control stiffness matrices. The zero-order derivatives are then used to find the level flight trim condition. Based on the trim conditions static deformations are found and the mass matrix is updated with the effects of the static deformations. The zero-order problem is then simulated by solving the Eq. (3.52). This results in a zero-order state-vector stored in an internal database, which is to be further used in the first-order problem.

The first-order problem starts with the input of the zero-order state-vector, which, in addition to the reduced-order matrices from the structural dynamics module, makes the first-order coefficient and control gain matrices. Eq. (3.61) is solved, where for a LTI system the simulation loops proceeds to the next step (i.e. loads equations), otherwise for a LTV system, while using the discrete time numerical approach [28], the simulation proceeds to the next time step and meanwhile the mass matrix is updated with the new quasi-static deformations. The loop for the first-order problem continues for the total number of time steps, N. However, as stated in Chapter 4, only LTI is implemented so far.

The rigid-body response of the aircraft from both the zero and first-order problems is simply added and stored. Whereas the generalized coordinates and generalized momenta enter into the loads module. The Eqs. (4.3–4.12) are solved that give both static and dynamic loads on each node of the component. Based on these loads the internal shear and moments are then calculated.

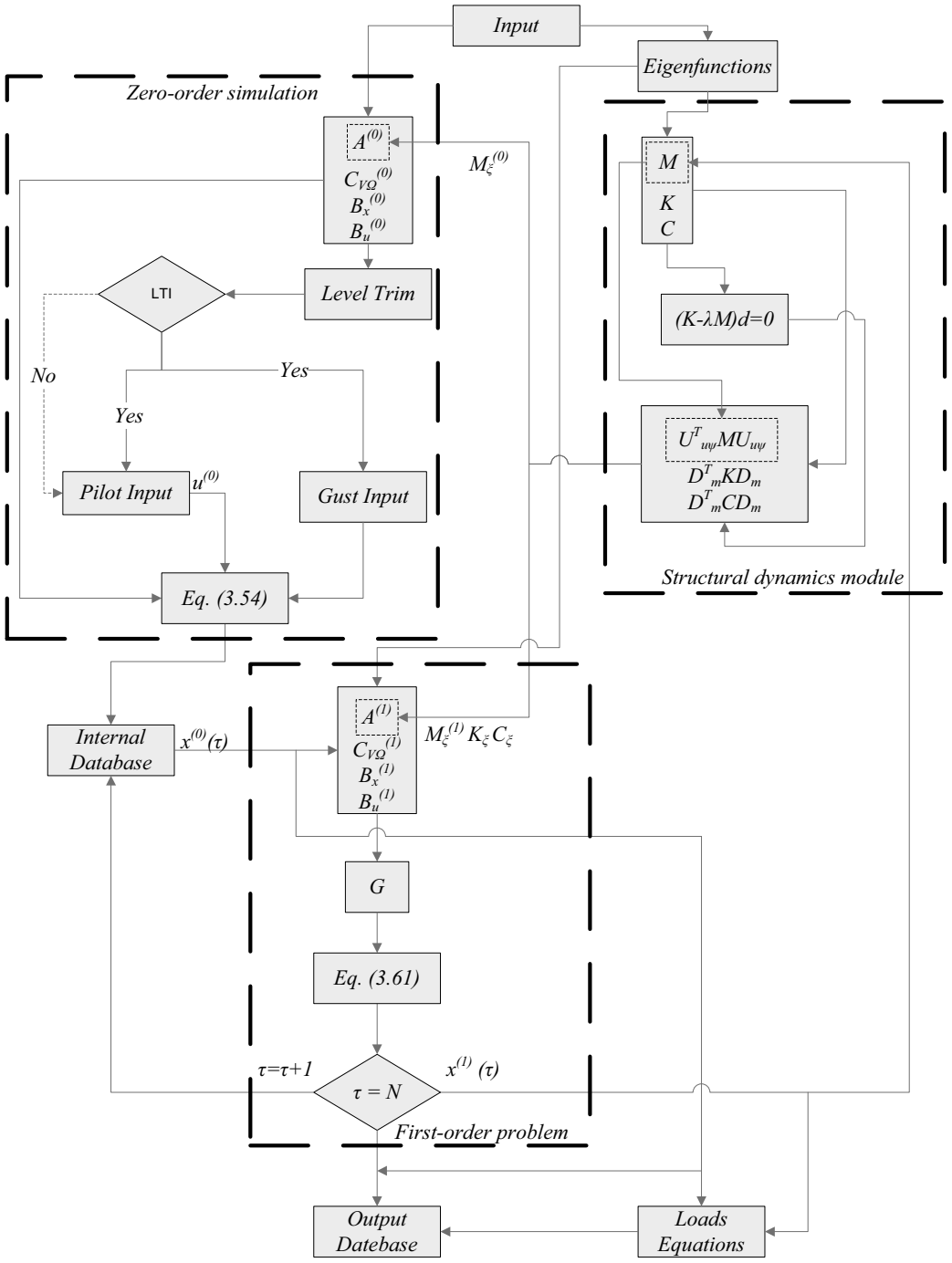

Figure 5.1: Schematic of DARLoads.

5.2 Model reduction

At this point, it is appropriate to discuss the selection of a few number of aircraft shape functions (ASF) to achieve model reduction. In Ref. 34, the authors choose the first eighteen ASF, which covers lower to higher frequencies and corresponding symmetric shapes (i.e., both symmetric and asymmetric) to reduce the model. The idea is to use sufficient number of ASF to include the effects of asymmetric shapes (i.e. particularly torsion) on the aerodynamics. Previously, in conjunction with flight controller design of a flexible aircraft, Meirovitch and Tuzcu [28] used the first two shape functions to reduce the model, which significantly retains the properties of a full-order controller. It is commonly thought that the frequencies of external disturbances, due to atmospheric turbulence, on the aircraft structure are not high enough to excite the higher structural frequencies and corresponding shapes, which therefore permits to use a few lower frequency modes. However, Bisplinghoff et al. [23] recommended considering a sufficient number of vibration modes to get an equivalency in the results from both the MDM and SFM. In the case of dynamic loads due to landing on the ground and in order to get the identical results from MDM and FSM, Bisplinghoff et al. however recommended to use all the modes of vibrations [23]. It is appropriate to recall from Section 1.3 and Appendix B that the typical orthogonal vibration modes are used to inertially decouple the structural dynamic equations, where each independent equation represents a particular mode of a component [5,14]. The ASF preserve the inertial coupling and they represent the linear combinations of component vibration modes or eigenfunctions, see Eq. (2.54). The outcome of the linear combination goes all the way from Eqs. (2.54–2.60) that makes it obvious that even the inclusion of a single ASF in Eq. (2.54) influences the dynamic response. So the contribution of each ASF on the dynamic response is to be determined. Pototzky and Perry [40] plot the frequency response of wing root bending moment (WRBM), which gives a fair idea about the contribution of each vibration mode to the dynamic response. A twin-jet aircraft is selected as a test case for response and dynamic loads over two different pilot induced maneuvers and a discrete gust, see Chapter 6. The aircraft structural and aerodynamic data are given in Ref. 4. Flight conditions for symmetric flight are presented in Table 5.2. First the aircraft is assumed to have the conventional tail configuration (CTC) and after that the aircraft is also modeled with a T-tail configuration (TTC), where the horizontal tail is moved to the tip of the vertical tail. The first twenty ASF for both tail configurations are given in Tables 5.3 and 5.4, and while the first six ASF of each tail configuration are plotted in Figs. 5.3 and 5.4[1]. It shows that change in the position of the horizontal tail to the tip of the vertical tail

[1]The higher frequency ASF are not shown here for the sake of brevity.

Table 5.2: Geometry and flight conditions

Airspeed $V^{(0)}, m–sec^{-1}$	250.0
Altitude, m	7620.0
Wing span, m	16.7
Wing root chord, m	3.287
Horizontal tail root chord, m	1.6263
Wing position r_{fw}, $[x, y, z]$	[-0.128,0,0.9736]
Vertical tail position r_{fv}, $[x, y, z]$	[-6.0698,0,-0.6099]
Horizontal tail position r_{vh} for CTC, $[x, y, z]$	[0.4964,-0.115,0]
Horizontal tail position r_{vh} for TTC, $[x, y, z]$	[2.95,0.062,0]
Aircraft total mass, Kg	5884.23
Inertia $J^{(0)}_{xx}, Kg–m^2$	20708.91
Inertia $J^{(0)}_{yy}, Kg–m^2$	64003.38
Inertia $J^{(0)}_{zz}, Kg–m^2$	79590.5
Inertia $J^{(0)}_{xy}, Kg–m^2$	0.8072
Inertia $J^{(0)}_{xz}, Kg–m^2$	-4241.35

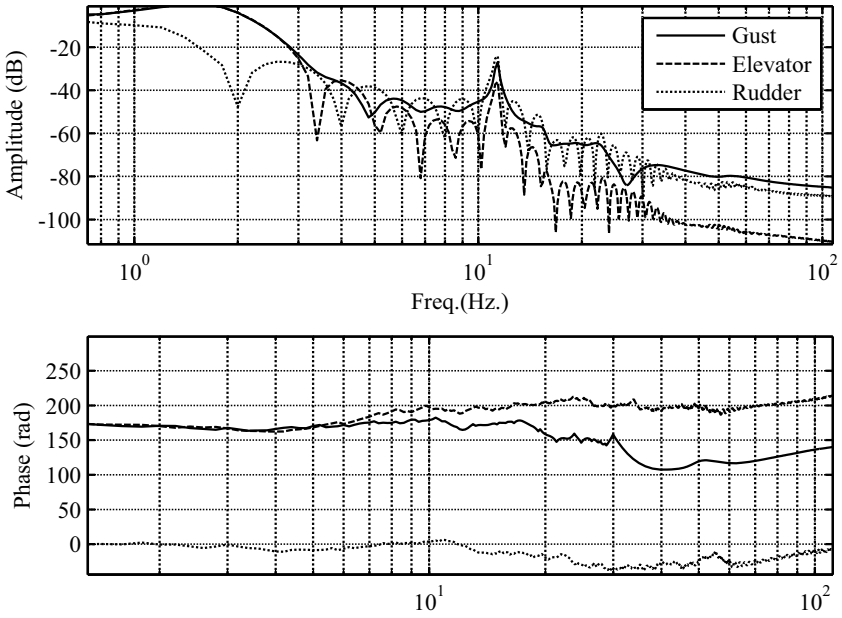

Figure 5.2: WRBM frequency response.

predominates[2] the fuselage mode in torsion, see Fig. 5.4(a). With regard to the choice of number of ASF for model reduction, the full-order aircraft models of each tail configurations are subjected, as stated above, to the gust and pilot induced maneuvers and the time response of WRBM is transformed to the frequency domain by using a Fourier transformation, see Fig. 5.2. It shows that in almost all cases the ASF up to 40Hz (i.e. first 14 ASF) significantly affect the dynamic response of the structure. However to have the greatest impact of aerodynamic forces and moments, it is thought to consider a sufficient number of ASF of lower to higher frequencies, while exhibiting both bending and torsion as predominant features in wings and horizontal tails. By using the first 18 ASF that cover the frequencies up to 46.4Hz, the full-order model in each simulation case is reduced to only 24 D.o.F i.e. 6 rigid-body and 18 elastic degrees of freedom.

5.3 Level flight trim solution

As stated in Section 5.2, a twin-jet given in Ref. 4 is selected for the simulation, where the stiffness properties of the aircraft components represent a metal airframe (i.e. with out the cross-coupling terms in the stiffness matrix). As stated in Section 1.5, the structural data of a composite aircraft is not available so the coupling effects are simulated by manipulating the $e.a$ of each wing and horizontal tail in five different cases. In first three cases, the $e.a$ of each wing and horizontal tail is drawn parallel to the $r.a$ of that particular component, where the $e.a$ with respect to $r.a$ of each component is placed in three different positions. In the fourth and fifth case, the $e.a$ of each wing and tail is drawn by intersecting the shear centers of each section from root to tip, where the shear center of a section is calculated by using Eq. (1.17). All these five cases are defined and simulated in next two sections.

5.3.1 Case 1–3: Parallel $e.a$ case

It is assumed that during a structural optimization exercise the anisotropy in the stiffness matrices of each wing and horizontal tail is negligible. However, $e.a$ of these components, while exhibiting a parallel line to that of a particular $r.a$, changes its position. For this purpose three different cases of $e.a$ position are simulated i.e. in the first case the $e.a$ of each wing and horizontal tail is placed 30.0mm in front of their particular $r.a$, in the second case these are aligned, and in the third case the $e.a$ of each wing and horizontal tail is placed

[2]Each Eigenvector of Eq. 2.52 are normalized to the unity, where the position of unity in an eigenvector of size (32×1) decides the predominance of a certain D.o.F of a component

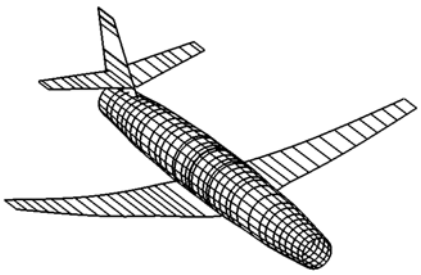

(a) 1^{st} ASF, 5.92Hz

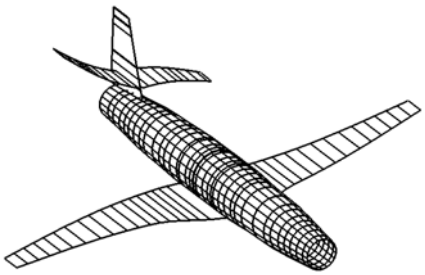

(b) 2^{nd} ASF, 8.26Hz

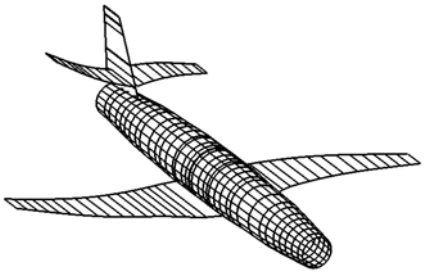

(c) 3^{rd} ASF, 10.45Hz

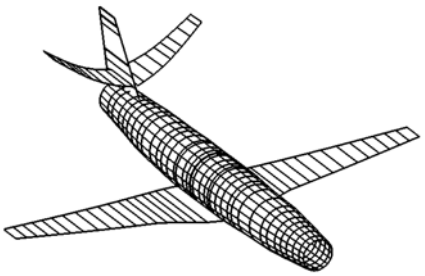

(d) 4^{th} ASF, 11.24Hz

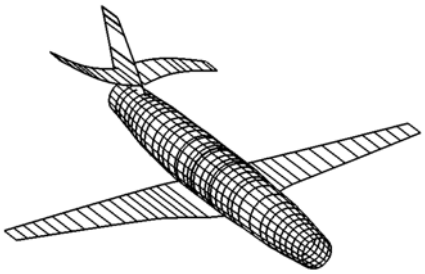

(e) 5^{th} ASF, 12.32Hz

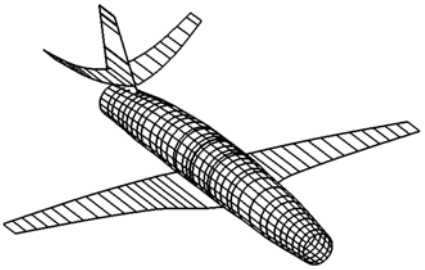

(f) 6^{th} ASF, 14.64Hz

Figure 5.3: First 6 ASF in conventional tail configuration.

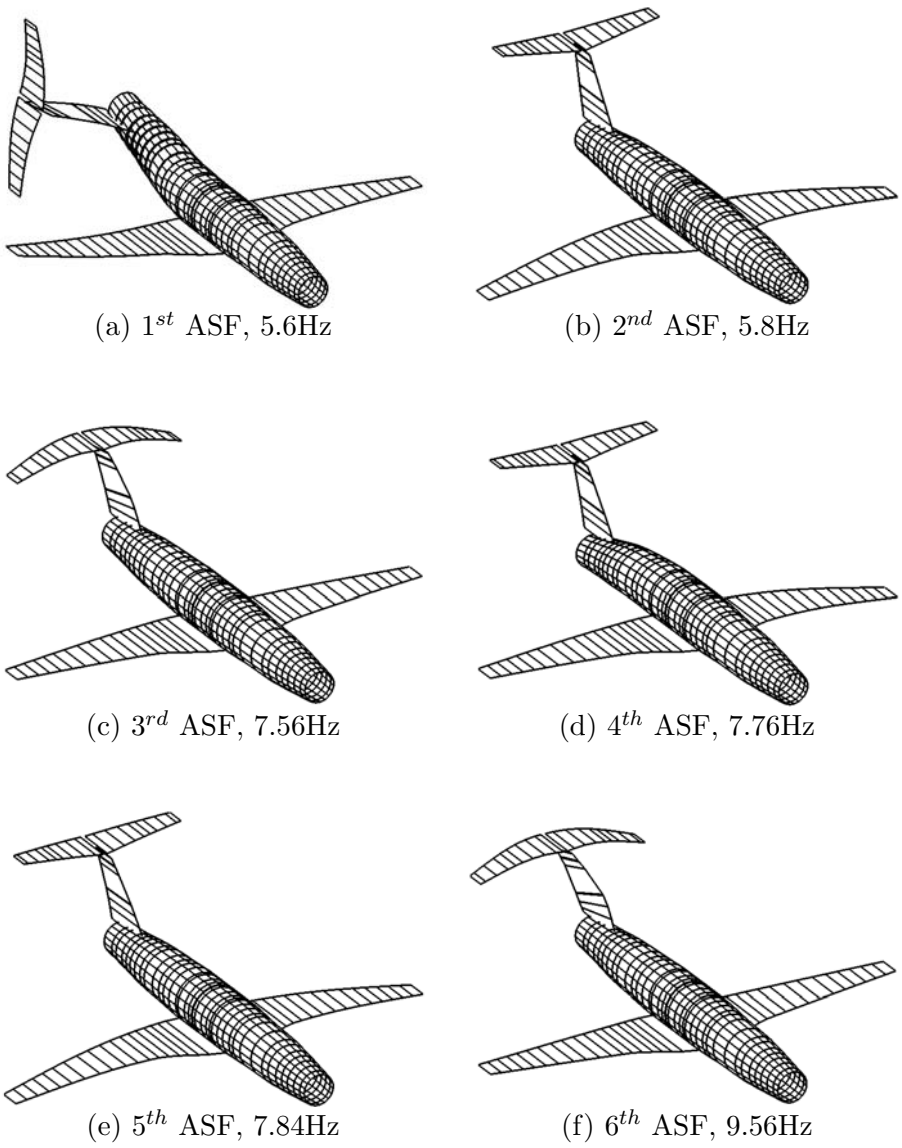

(a) 1^{st} ASF, 5.6Hz (b) 2^{nd} ASF, 5.8Hz

(c) 3^{rd} ASF, 7.56Hz (d) 4^{th} ASF, 7.76Hz

(e) 5^{th} ASF, 7.84Hz (f) 6^{th} ASF, 9.56Hz

Figure 5.4: First 6 ASF in T-tail configuration.

Table 5.3: Description of first 20 ASF (Conventional tail)

ASF No.	Freq. (Hz)	Predominate Shape[a]
1	5.92	1st symmetric W-B
2	8.26	1st asymmetric W-B
3	10.45	1st symmetric H-B
4	11.24	1st asymmetric H-B
5	12.32	2nd asymmetric H-B
6	14.64	2nd symmetric H-B
7	19.51	1st asymmetric V-B
8	20.09	1st asymmetric F-B
9	22.05	2nd asymmetric V-B
10	23.05	1st symmetric F-B
11	26.58	2nd symmetric F-B
12	27.42	2nd asymmetric W-B
13	37.72	1st asymmetric F-T
14	46.81	1st asymmetric H-T
15	49.91	2nd asymmetric H-T
16	53.02	1st symmetric H-T
17	53.37	1st asymmetric W-T
18	53.70	2nd symmetric H-T
19	62.42	3rd asymmetric H-T
20	64.60	3rd symmetric H-T

[a] B: Bending, F: Fuselage, H:Horizontal tail, T: Torsion, W: Wings, V: Vertical tail

30.0mm behind their particular $r.a$, see Table 5.5. It is to be noted that the forward or rearward directions are to be referred with respect to aircraft body axes O_f, however the sign convention of a particular y_i is taken w.r.t its local axes system O_i, see Fig. 2.1. As stated before in Section 4.2, the steady state for a purely longitudinal flight condition, as given in Table 5.2, is achieved by using an iterative optimization algorithm which balances out the forces and moments around the body axes of the aircraft by minimizing a quadratic cost function expressed in Eqs. (4.1) and (G.3) [41]. The trim elevator, aileron and rudder deflection, and throttle setting, respectively, in Case 1 are found to be $u^{(0)} = [1.55 \text{ deg}, 0, 0, 76.4\%]$. The corresponding pitch attitude $\theta^{(0)}_{f\Theta}$ is found to be 0.55 deg. The static upward bending deflection of 1.236m and 0.168m is calculated at the tip of each wing and horizontal tail, respectively. Figure 5.5 shows the change in trim solutions of pitch and elevator deflection for three cases of the elastic axis position. The change in the values of pitch-

Table 5.4: Description of first 20 ASF (T-tail)

ASF No.	Freq. (Hz)	Predominate Shape[a]
1	5.63	1st asymmetric F-T
2	5.81	1st symmetric W-B
3	7.56	1st symmetric H-B
4	7.76	1st asymmetric W-B
5	7.84	2nd asymmetric W-B
6	9.56	2nd symmetric H-B
7	10.51	2nd symmetric W-B
8	11.41	3rd symmetric H-B
9	18.71	4th symmetric H-B
10	24.11	3rd symmetric W-B
11	25.70	3rd asymmetric W-B
12	25.91	1st asymmetric V-B
13	26.78	3rd asymmetric H-B
14	36.28	2nd asymmetric F-T
15	41.12	1st symmetric H-T
16	41.78	1st asymmetric W-T
17	41.93	2nd symmetric H-T
18	46.44	1st asymmetric H-T
19	56.34	5th symmetric H-B
20	59.54	4th asymmetric H-T

[a] B: Bending, F: Fuselage, H:Horizontal tail, T: Torsion, W: Wings, V: Vertical tail

angle and elevator deflection is less than 0.1 deg and 0.66 deg, respectively, and the throttle setting is changing not more than 1.0%. It also shows that the elevator deflection decreases while the $e.a$ moves from front to the rear of $r.a$. The static torsion deflections of both wings and horizontal tails also change with the position of their particular elastic axes. Figure 5.6 shows that the local twist angles at the tip of both wing and horizontal tail increases as the $e.a$ moves from front to the rear of $r.a$. Figure 5.7 explains this phenomenon where the locations of the key points on the tip sections of both the right wing and horizontal tail are shown. It shows the actual locations of the aerodynamic centers ($a.c$), centers of mass ($c.g$), $r.a$ and the rearward position of $e.a$ i.e. Case 3 in Table 5.5. The abscissa of the Fig. 5.7 gives the section lengths in meters. In case of wing tip, the $c.g$ of the tip section is located quite close to the $r.a$ and whenever during the analysis the $e.a$ coincides or positioned in the front of $r.a$, the torque around the $e.a$ produced by weight is added to the torque produced

Table 5.5: Three cases of $e.a$ position

Case No.	y_w^R, y_e^R	y_w^L, y_e^L
1	-30.0mm	30.0mm
2	0.0mm	0.0mm
3	30.0mm	-30.0mm

by the aerodynamic loads. However, both of these torques oppose each other when the $e.a$ is positioned rearward of the $r.a$. The vertical aerodynamic force on the wing tip, at the given speed, is approximately seven times larger than its weight, which, on the other hand, due to increase in moment arm makes the twist angle a bit larger in the cases where the $e.a$ is placed ahead of the $c.g$. Similarly in the case of horizontal tail tip section the aerodynamic force, at the given speed, is approximately three times larger than its weight. The torque produced by the aerodynamic force, for all the positions of $e.a$, is deducted by the torque produced by the weight, where the moment arm of the aerodynamic force makes the horizontal tail to twist more when the $e.a$ is positioned rearward of the $r.a$. It is also noted that as the twist angle increases at the horizontal tail, the elevator deflection decreases and vice-versa. As we know that, apart from the rigid-body pitch angle and the throttle input, the lift required in trimming the aircraft is also contributed by both twist over the tailplane and the elevator deflection. So it would be correct to state that the optimization routine used here efficiently optimizes the elevator deflection against the given structural deformations.

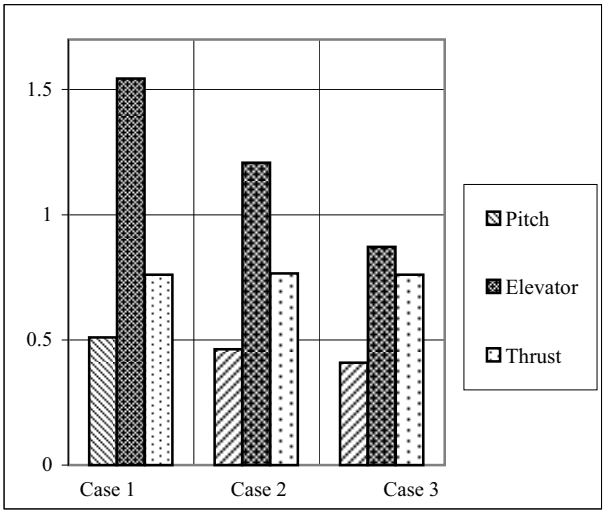

Figure 5.5: Trim variables.

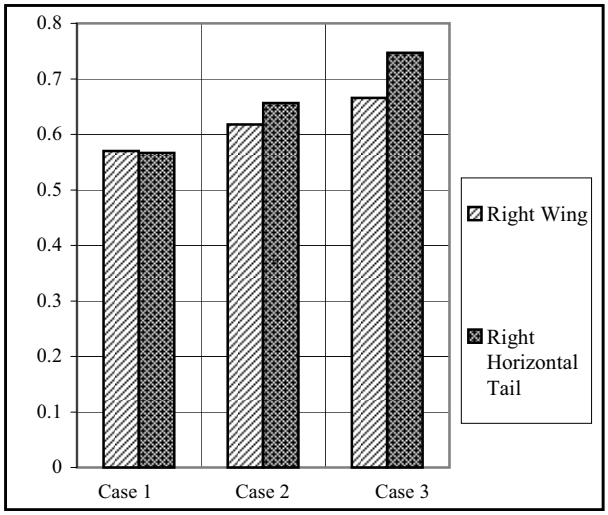

Figure 5.6: Static twist angles, deg.

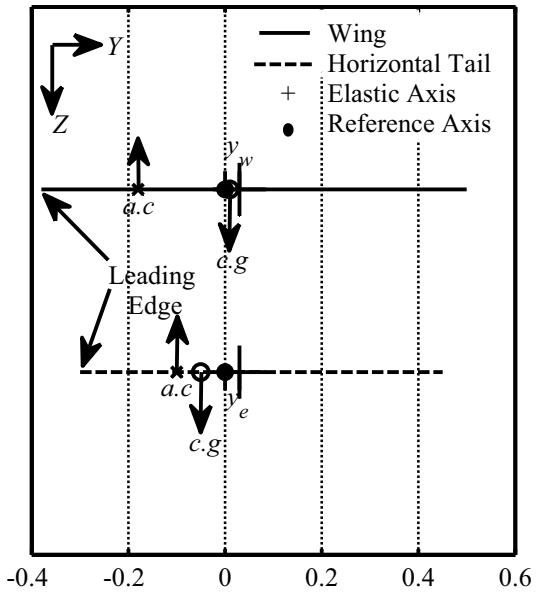

Figure 5.7: Tip sections, meters.

5.3.2 Case 4–5: Shear center case

In Case 1–3 of Section 5.3.1 the elastic axis of each wing and horizontal tail is assumed to be parallel to the corresponding reference axis of the specific component. However, in Case 4 and 5 the elastic axis of each wing and tail is derived by connecting the shear centers of each section of the component, from root to tip. The location of these shear w.r.t. the particular $r.a$ is calculated by using Eq. (1.17). It is assumed that each wing and tail, from root to tip, has a constant cross-section and the stiffness properties (i.e. EI, and GJ) along the length are the values found in Ref. 4 and given in Table 5.6. These stiffness properties are averaged over the span for the diagonal terms while the off-diagonal k terms (i.e. coupling) in Eqs. (2.19–2.21), are approximated as 10% percent of the averaged torsional stiffness GJ. In Case 4 the k term in Eq. (1.17) is considered positive, which gives a swept-back elastic axis on wings and tails. In Case 5 the k term is considered negative Eq. (1.17), which results into a swept-forward elastic axis, see Figure 5.8. Figure 5.8 also plots the positions of the mass center $c.g$ and the aerodynamic center $a.c$ along the lengths of both wing and horizontal tail. The elastic axes of each wing and horizontal tail do not remain parallel to the reference axes. In these specific wing cases the elastic axis is supposed to be out of the structural boundaries near the tip if the magintuide of k term is increased. The trimmed condition for the purely longitudinal flight condition, as given in Table 5.2, is determined by the procedure described in Section 5.3.1. The resulting elevator, aileron and rudder deflection, and the throttle setting for Case 4 and 5 are given in Table 5.7. The values for the zero-order generalized coordinates for wing and horizontal tail in bending for Case 4 are found to be:

$$q_{u_w}^{R^{(0)}} = q_{u_w}^{L^{(0)}} = \begin{bmatrix} -0.2351 & 0.0123 \end{bmatrix}^T \text{(m)} \tag{5.1}$$

$$q_{u_h}^{R^{(0)}} = q_{u_h}^{L^{(0)}} = \begin{bmatrix} -0.0270 & 0.0007 \end{bmatrix}^T \text{(m)} \tag{5.2}$$

Similarly the zero-order generalized coordinates in torsion for Case 4 are found to be:

$$q_{\psi_w}^{R^{(0)}} = \begin{bmatrix} 0.0059 & 0.0012 \end{bmatrix}^T \text{(rad)} \quad q_{\psi_w}^{L^{(0)}} = -\begin{bmatrix} 0.0059 & 0.0012 \end{bmatrix}^T \text{(rad)} \tag{5.3}$$

$$q_{\psi_h}^{R^{(0)}} = \begin{bmatrix} 0.0044 & 0.0004 \end{bmatrix}^T \text{(rad)} \quad q_{\psi_h}^{L^{(0)}} = -\begin{bmatrix} 0.0044 & 0.0004 \end{bmatrix}^T \text{(rad)} \tag{5.4}$$

Inserting the above given values in Eq. (2.7) gives the static deflections. The torsional deformation along the semi-span of wing and horizontal tail together with the mass dm and lift distributions C_{l_α} are plotted in Fig. 5.9. It shows that from root to mid span, the wing has positive twist (LE up) with maximum angles of 0.30 deg and 0.44 deg, respectively, in Case 4 and Case 5, and from mid span to tip it shows negative twist. In Case 4 of the horizontal tail a positive twist is found along the complete span with a maximum of 0.23 deg in

at the tip section. However, Case 5 of the tail gives the same kind of pattern as that of wings. The counter intuitive wing behavior is caused by the use of the averaged stiffness properties that results in a deflection pattern dominated by a higher frequency mode shape, see Fig. C.1(b) (i.e. results into $q^{R^{(0)}}_{\psi_w(2)} = 0.0012$ or $q^{L^{(0)}}_{\psi_w(2)} = -0.0012$ in Eq. (5.3)). For the horizontal tail the contribution of higher frequency modes in the static deflections is negligible. To investigate it further, the twist along the semi-span of the wing with different values of $q^{(0)}_{\psi_w(2)}$ and a constant value for $q^{(0)}_{\psi_w(1)}$ is plotted in Fig. 5.10. It shows that as the value of $q^{(0)}_{\psi_w(2)}$ increases, the higher frequency mode in torsion, as shown in Fig. C.1(b), predominates. While comparing the torsion over wing and horizontal tail, it can also be inferred that apart from the stiffness properties the length of a component also helps in exciting the higher degree modes.

5.4 Synopsis

A brief description is given of the MATLAB computer program that implements all the mathematical equations presented in the previous two chapters. A conventional metal twin jet is selected to test the software. Data of a real composite aircraft is not available and it was therefore decided to study the coupling effects on the aircraft dynamics by manipulating the $e.a$ of each wing and horizontal tail in five different cases. A selection of aircraft shape functions (ASF) is made for the model reduction. Frequency plots of the dynamic responses are used to validate the effectiveness of the selected ASF. The trimmed condition for a level flight at certain speed and height is obtained by an iterative optimization routine. The trim variables with static structural deflections are plotted for each elastic axis case. A comparison is made and conclusions are drawn for the importance of the shape of the elastic axis.

Table 5.6: Stiffness properties

Wing				Horizontal Tail			
No.	x_w	EI$\times 10^{6\,a}$	GJ$\times 10^{6\,a}$	No.	x_h	EI$\times 10^{6\,a}$	GJ$\times 10^{6\,a}$
1	0.00	31.28	30.70	1	0.00	1.12	0.69
2	0.43	27.83	30.70	2	0.06	1.08	0.67
3	0.86	24.82	29.84	3	0.35	0.90	0.60
4	1.04	23.24	28.55	4	0.81	0.66	0.49
5	1.38	19.94	25.25	5	1.26	0.47	0.38
6	1.72	16.35	21.81	6	1.63	0.35	0.30
7	2.06	13.88	18.36	7	1.90	0.27	0.23
8	2.34	12.28	15.21	8	2.24	0.20	0.16
9	2.74	10.01	12.91	9	2.64	0.13	0.12
10	3.12	8.06	11.24	10	3.03	0.093	0.085
11	3.56	6.25	9.15	11	3.23	0.078	0.062
12	4.05	4.82	6.97	Vertical Tail			
13	4.55	3.87	5.33	1	0.00	4.47	2.09
14	5.09	2.92	3.93	2	0.18	3.81	1.92
15	5.63	2.10	2.52	3	0.53	2.77	1.60
16	6.13	1.62	1.60	4	0.88	1.96	1.27
17	6.60	1.22	1.02	5	1.26	1.32	1.01
18	7.02	1.01	0.72	6	1.62	0.87	0.70
19	7.46	0.80	0.49	7	1.97	0.57	0.40
20	7.90	0.57	0.24	8	2.31	0.36	0.25
21	8.30	0.36	0.018	9	2.68	0.19	0.10
				10	2.88	0.12	0.024

[a] Units: N-m^2.

Table 5.7: Trim variables for Case 4-5

Case 4			Case 5		
$\delta_{el}^{(0)\,a}$	$\delta_T^{(0)}$	$\theta_{f\Theta}^{(0)\,a}$	$\delta_{el}^{(0)}$	$\delta_T^{(0)}$	$\theta_{f\Theta}^{(0)\,a}$
2.13	78.1%	0.686	2.77	77.3%	0.577

[a] Units: deg.

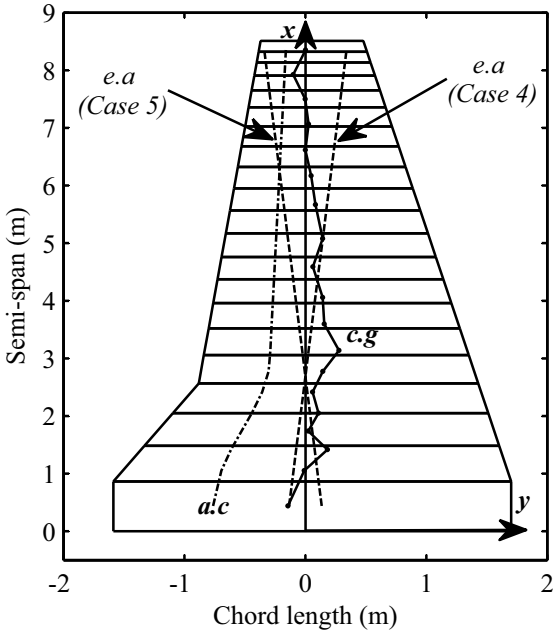

(a) Right wing

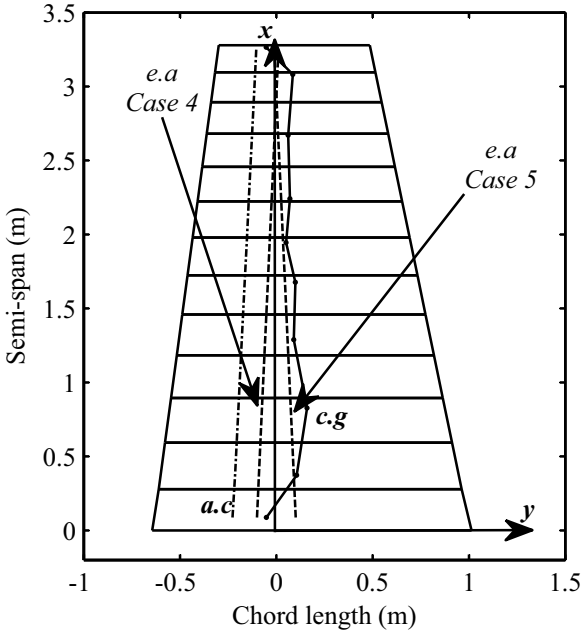

(b) Right horizontal tail

Figure 5.8: Shape of $e.a$ in Case 4 and 5.

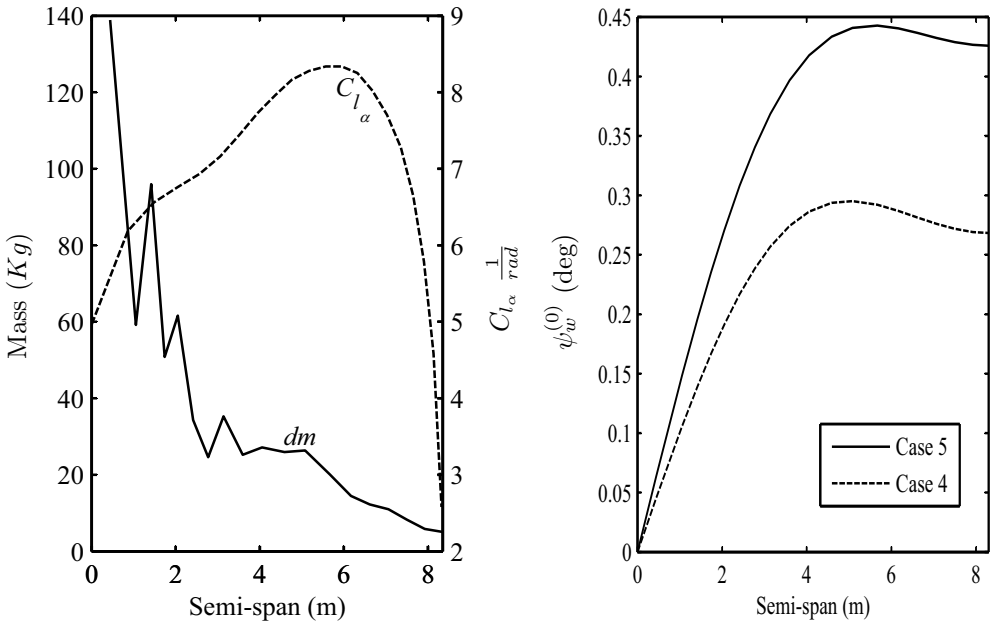

(a) Right wing

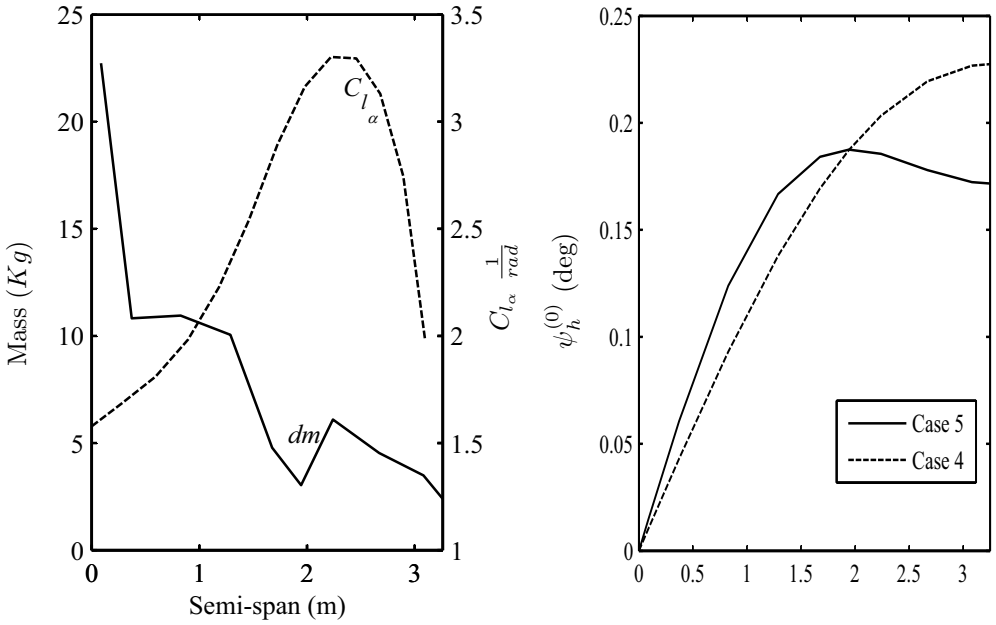

(b) Right horizontal tail

Figure 5.9: Static twist in Case 4-5 with mass and lift distribution.

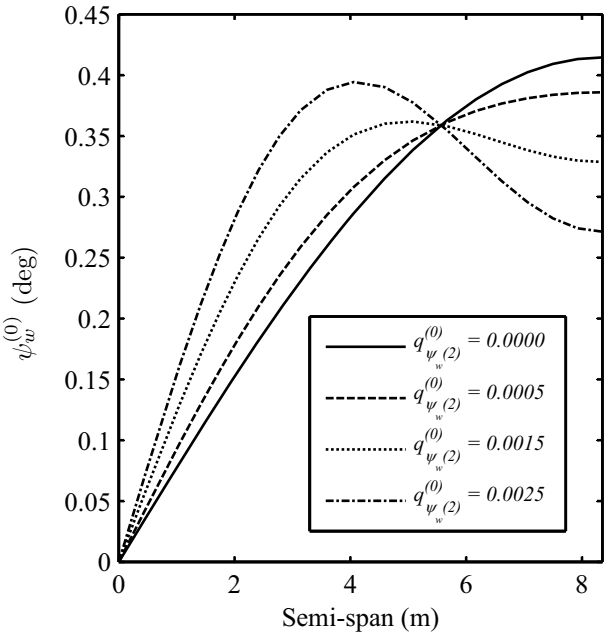

Figure 5.10: Static twist on wing with $q^{(0)}_{\psi_w(1)} = 0.0059$.

Chapter 6

Simulation example – Part 2: Dynamic case

In the previous chapter the zero-order problem for steady level flight was discussed and the coupling effects on the trim variables were studied. In this chapter the fully dynamic cases are simulated as perturbation around the steady level flight (i.e. solution of the steady state flight enters into the coefficient matrices, which are then perturbed through the external forces due to gust or pilot controls). The next sections are dedicated to the perturbation problem during a discrete gust and two pilot induced maneuvers, as given in aviation regulations [38] (i.e. checked elevator input and aileron impulse input), and results are plotted in the form of rigid-body response and structural loads.

6.1 Discrete gust

The aircraft is assumed to be subjected to symmetrical vertical gust (i.e. 1-Cosine) in level flight [38]. The level flight conditions are taken the same as those calculated in Section 5.3. The shape of the discrete gust w_g is expressed as follows [36, 38]:

$$w_g\left(x_g\right) = \frac{w_{g0}}{2}\left(1 - \cos\tfrac{2\pi x_g}{H}\right), \quad 0 \le x_g \le H \tag{6.1}$$

in which H is the gradient distance of the discrete gust. The peak gust w_{g0} is taken as 5.0m-sec^{-1}. Dynamic analysis for a conventional tail configuration is performed by first simulating the zero-order problem , as expressed in Eq. (G.7), and results in the form of plunge and pitching rates are plotted in Fig. 6.1. The external force vector, as given in Eq. (3.62), is calculated and the first-order

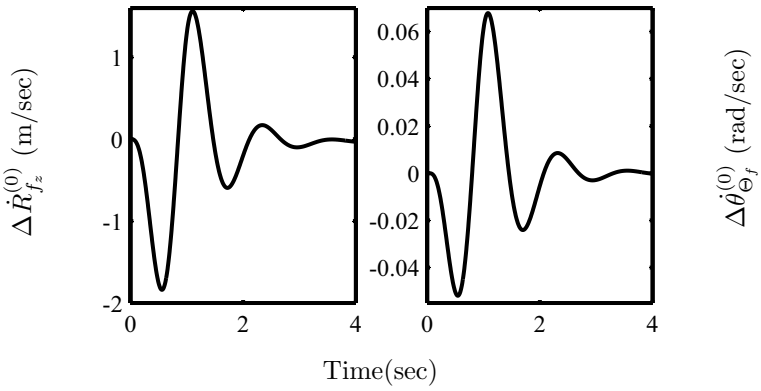

Figure 6.1: Rigid-body plunge and pitch rates during gust.

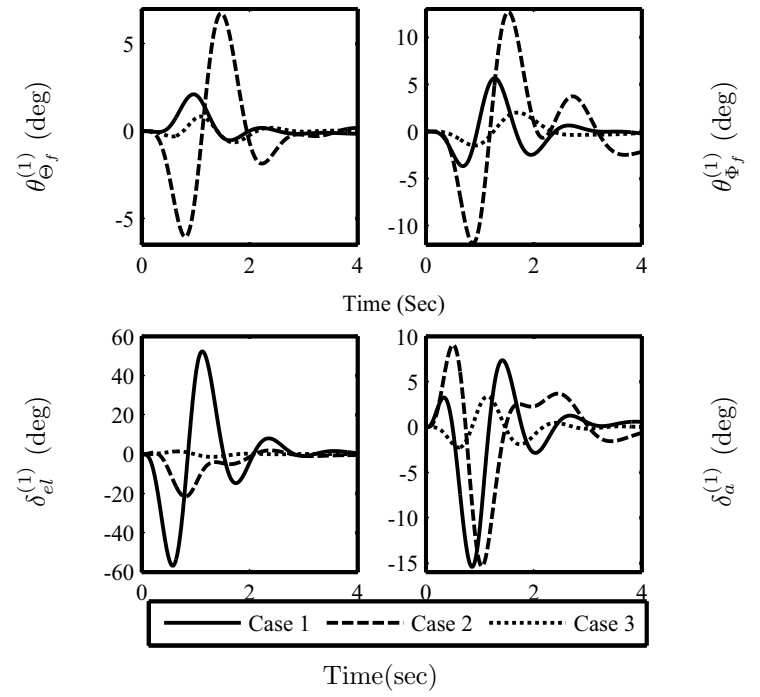

Figure 6.2: 1st order rigid-body response during gust.

problem in Eq. (3.61) is solved. Figure 6.2 shows the disturbance in rigid-body motion and consequent control inputs to minimize the perturbations. To get the structural loads, the solution of Eq. (3.61) is used in Eqs.(4.7–4.12). The

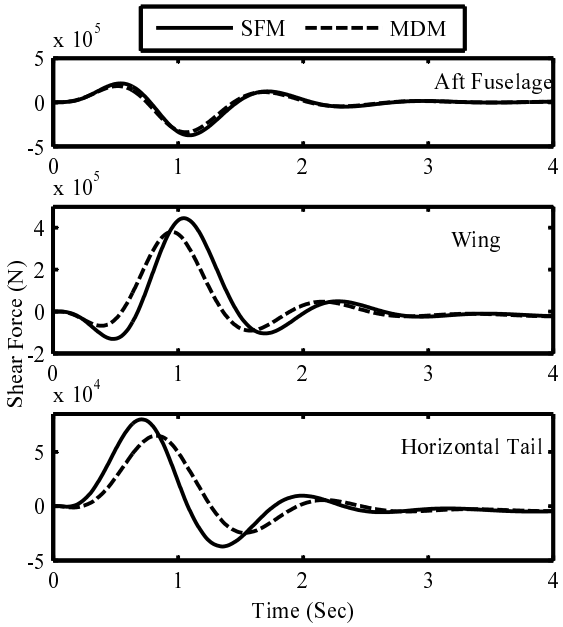

Figure 6.3: Shear forces at the root.

comparison of shear forces from the SFM and MDM load equations is presented in Fig 6.3. It shows that in case of the fuselage the results are in fair agreement, and in the case of the wings and horizontal tails the shear forces calculated from MDM are lower than those of the shear forces calculated from SFM but still these are comparable to each other.

6.1.1 Case 1–3

Figure 6.4 shows the structural deflections and dynamic loads at the wing and fuselage roots for each elastic axis position given in Table 5.5. It shows that the wing is deflecting in bending a maximum of -0.4m upward and 0.4m downward. The twist in the wing is ranging from 0.02rad upward to -0.01rad downward. The fuselage is bending vertically (i.e. in xz-plane) from 0.05m downward to -0.042m upward and twisting around 0.01rad upward and downward. Similarly Fig.6.10 shows the structural deflections and dynamic loads at the horizontal and vertical tail roots[1]. It shows that the horizontal tail is bending a max-

[1]Though the aircraft is perturbed under a purely symmetric gust input, due to nonzero J_{xy} inertia value in mass matrix the aircraft is also perturbed in the xy-plane.

imum of -0.14m upward and 0.13m downward, and twisting 0.01rad upward to -0.005rad downward. The vertical tail is bending sideways from 0.02m to -0.02m, and twisting 0.0028rad upward to -0.002rad downward.

6.1.2 Case 4–5

Only the discrete gust problem is investigated for the dynamic analysis of cases 4 and 5 (i.e. nonparallel $e.a$). The results for the right wing and right horizontal tail are presented in Fig. 6.6. One can see that the maximum bending deflection of the wing is 5.3m upwards and 4.8m downwards. The wing twist ranges from 0.18rad upwards to 0.15rad downwards. Similar results are obtained for the horizontal tail. The twist angle is most likely too large with respect to structural strength and aircraft stability. In practice, the aircraft structure would have already collapsed under these conditions. However, this example shows the importance of the right choice of the stiffness properties, especially the coupling term k, which is dependent on the lay-up sequence along the wing box. Another interesting point to be noted for case 5 is that the order of magnitude of the bending and torsion moment at the root of the horizontal tail is not as high as that of the corresponding structural deflections at the tip. It seems that the maximum moments occur somewhere near the mid-span. This is also indicated by the pattern of the high order eigenfunction shown in Fig. C.1. Although the total bending and torsion moments along the span remain the same, the scenario described above helps to increase the fatigue life of the root joints.

6.2 Checked elevator maneuver

Abrupt checked elevator maneuver is performed mainly in simulating the dynamic loads during pitching maneuver and with regard to design loads the horizontal tail during this maneuver is the most considered component [32,38]. Before the maneuver it is assumed that the aircraft flies in steady level flight and the elevator is moved rapidly in a sinusoidal motion as given below:

$$\delta_{el} = \delta_{el_{max}} \sin w_n t \tag{6.2}$$

in which $\delta_{el_{max}}$ is the maximum allowable elevator deflection during the maneuver. w_n is the elevator rate equal to the rigid-body short period mode and expressed as follows [32]:

$$w_n = \left[\left(Z_{\theta_f} M_{\Omega_f} / V_{f_x} \right) - M_{\theta_f} \right]^{\frac{1}{2}} \tag{6.3}$$

By using the numerical values given in Eq. (G.7), the elevator rate is found to be 15.7rad/sec (i.e. 2.5Hz) and elevator input is plotted in Fig. 6.7. After solving the Eq. (G.7), the first-order problem of Eq. (3.61) is solved in the same way as stated in Section 6.1. The results from both zero-order and first-order problem are plotted in Fig. 6.8 to 6.10. Figure 6.8 shows the rigid-body response during the pitching maneuver, where it shows that the aircraft bears the positive load factor n_z of around $3.0g$ during pitching up and -4.0g during pitching down[2]. Figure 6.9 shows the structural deflections and dynamic loads at the wing and fuselage roots for each elastic axis position. It shows that the wing is deflecting in bending a maximum of -1.2m upward and 1.1m downward. The twist in wing is ranging from 0.04rad upward to -0.02rad downward. Fuselage is bending vertically (i.e. in xz-plane) from 0.12m downward to -0.08m upward and twisting around 0.015rad upward and -0.02rad downward. Similarly Fig. 6.10 shows the structural deflections and dynamic loads at the horizontal and vertical tail roots. It shows that the horizontal tail is bending a maximum of -0.28m upward and 0.25m downward, and twisting 0.01rad upward to -0.006rad downward. The vertical tail is bending sideways from 0.03m to -0.04m, and twisting 0.0028rad upward to -0.0021rad downward.

6.3 Aileron impulse maneuver

In this case the aircraft with a T-Tail configuration is considered to be at steady level flight conditions, the same as assumed in Sections 6.1 and 6.2, sudden aileron input in the form of impulse is applied, see Fig. 6.11. The rigid-body response, as plotted in Fig 6.12, is converted into the time dependent first-order external force vector by using Eq. (G.7) and the first-order problem of Eq. (3.61) is solved. Figure 6.13 shows the structural deflections and dynamic loads at both right and left-half wing for each elastic axis position. Fig. 6.14 depicts the results for the aft fuselage and vertical tail deformation and loads in the xy-plane. The deflections and corresponding loads in case of wings for case 2 (i.e. when $e.a$ is aligned with the $r.a$) are quite high and the reason can be the large rolling rate, which is around 1.0rad/sec (i.e. $\approx$ 57.0deg/sec). For the other two cases the right wing has a maximum bending of around -3.0m upward with the twist ranging from 0.02rad upward to -0.025rad downward. In case of the left wing the deflections in bending are more or less the same but in torsion it is reduced as much as 0.01rad in both directions (i.e. upward and downward). The fuselage is bending sidewards (i.e. along y-axis) from 0.08m

[2]According to aviation regulations (i.e. FAR/CS-25.331(c)(2)) [38] the aircraft should not go beyond the designed load factor, which may require a digital controller to check the maximum load factor and not letting the aircraft to go beyond that point. However in this report emphasis is given to the design load cases only.

to -0.08m and twisting around 0.010rad upward and -0.012rad downward. The vertical tail is bending sidewards from 0.08m to -0.085m and twisting around 0.015rad in both directions.

6.4 Results discussion

The results clearly indicate that elastic coupling has a large influence on (1) aircraft loads, (2) the underlying rigid-body motion and (3) structural vibrations. For case 1-3, the amplitudes of the structural deformations, as well as the first order pitch $\theta^{(1)}_{f\Theta}$ and roll attitude $\theta^{(1)}_{f\Phi}$, reduce significantly when the *e.a.* is shifted rearwards with respect to the *r.a.* This seems contrary to the results of the static analysis where the twist angle at the tip increases when the *e.a.* moves from the front to the rear. The main reason is the influence of the inertial terms on the dynamic response. These terms do not have an effect on the static deformation. Thus it can be inferred that coupling can help to reduce dynamic loads. In general, the position of the *c.g.* of every section varies with respect to their respective *r.a.* Also, the position of the shear center can be different for each section on both the wings and empennage. Therefore, the results obtained for cases 4 and 5 give a better insight in how the position of the shear center affects the structural deflections and corresponding loads. The horizontal rail root bending and torsion moments are an order of magnitude lower than the structural deflections at the tip. As stated earlier, stiffness properties are assumed constant over the length of the wings, the horizontal tail surfaces and the vertical tail. In real-life, this is not the most practical solution. Nevertheless, the simulation results give a good impression of the effects of bending-torsion coupling on the aircraft response and also show the relevance of the proper mathematical modeling of the flexible aircraft dynamics.

6.5 Synopsis

After finding the steady level flight trim conditions in Chapter 5, the aircraft in this chapter is subjected to different dynamic conditions (i.e. discrete gust and two pilot induced maneuvers in pitching and rolling). For each condition the rigid-body perturbation solution is performed that is later multiplied with coefficient matrices to get the external force vector, which is used as an input for running the first-order problem. Results in the form of rigid-body disturbances and dynamic loads are extracted and plotted. It is concluded that coupling does influence the dynamic problems significantly, which opens a door for the structural optimization to achieve the loads alleviation.

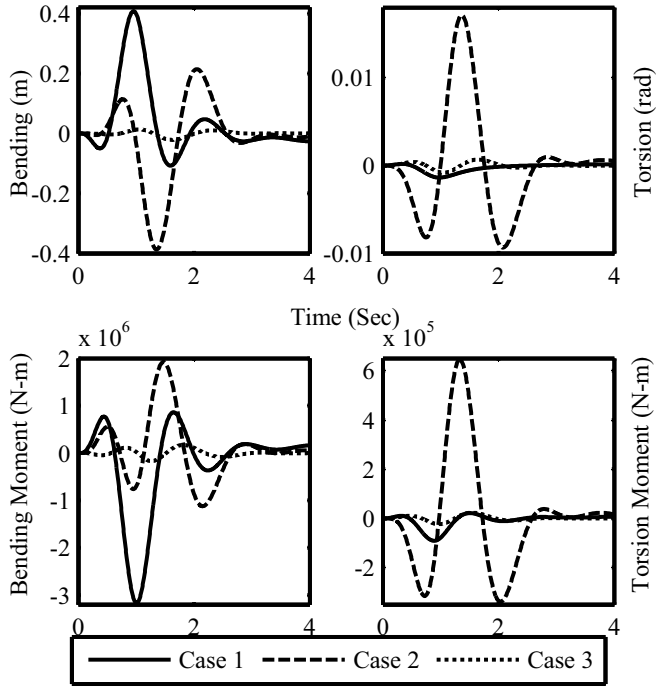

(a) Right wing

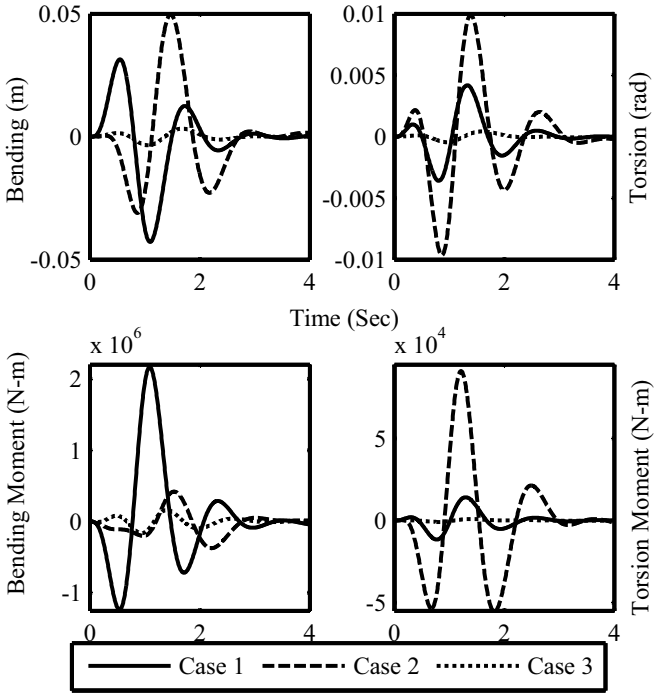

(b) Aft fuselage

Figure 6.4: 1^{st} order deflections and root loads during gust.

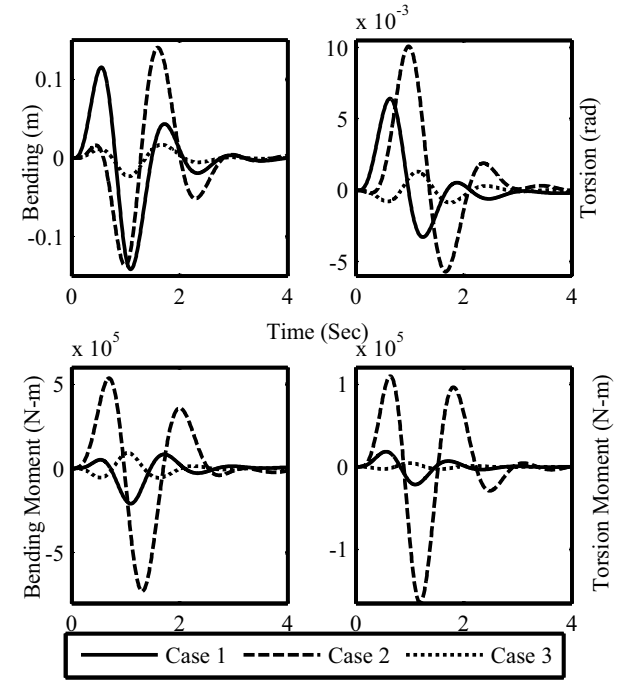

(a) Right horizontal tail

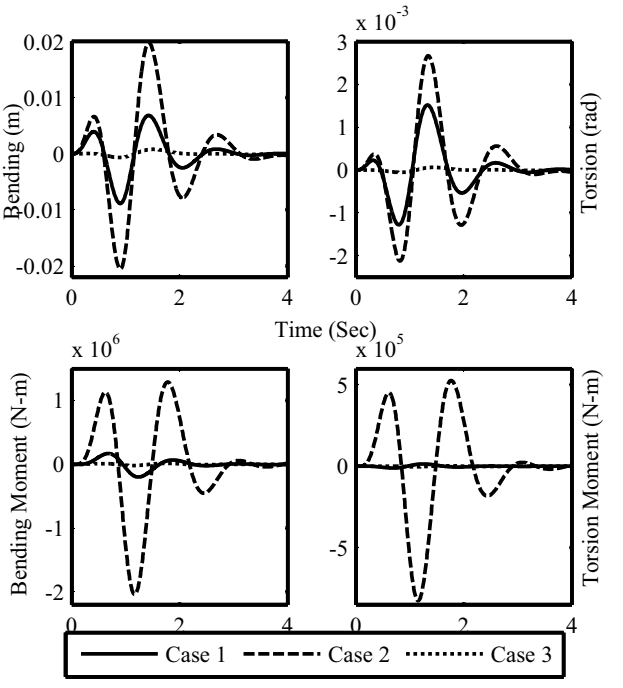

(b) Vertical tail

Figure 6.5: 1st order tip deflections and root loads during gust.

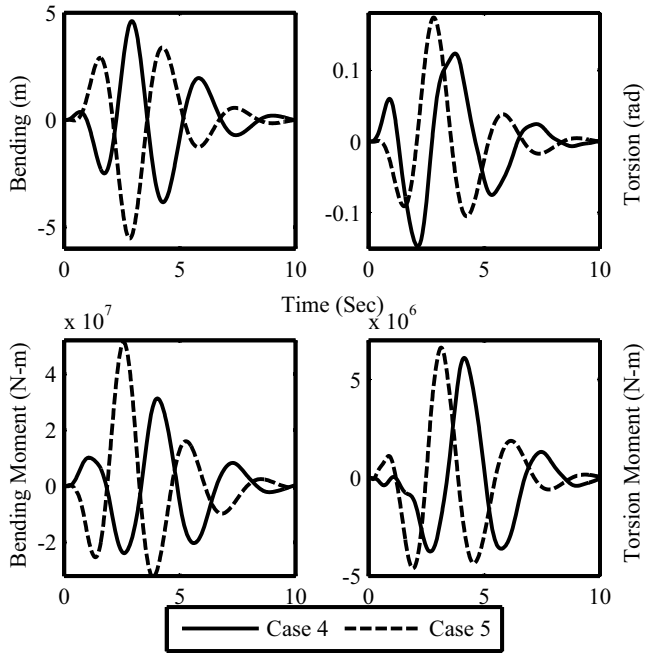

(a) Right wing

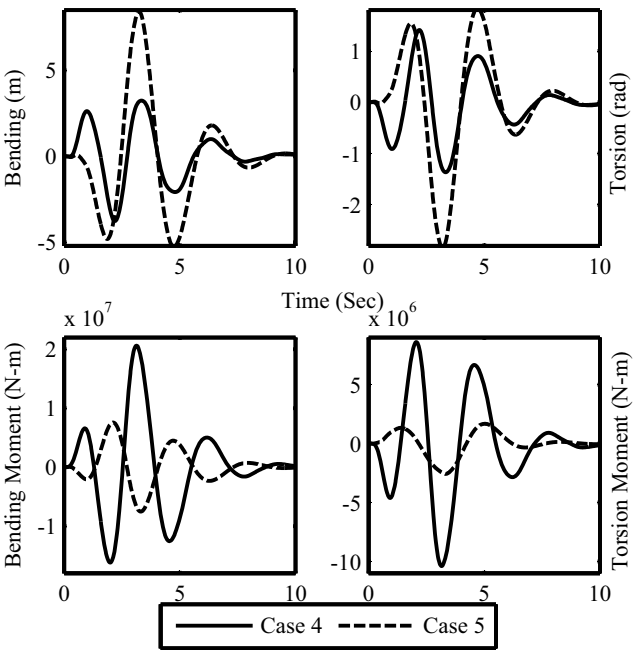

(b) Horizontal tail

Figure 6.6: 1^{st} order deflections and root loads during gust.

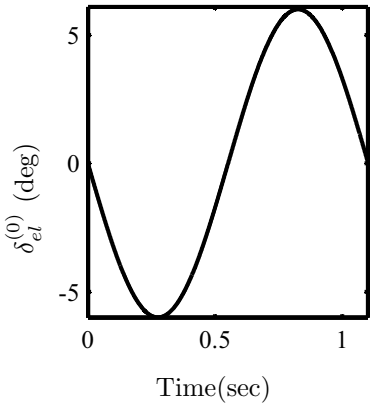

Figure 6.7: Abrupt elevator checked input.

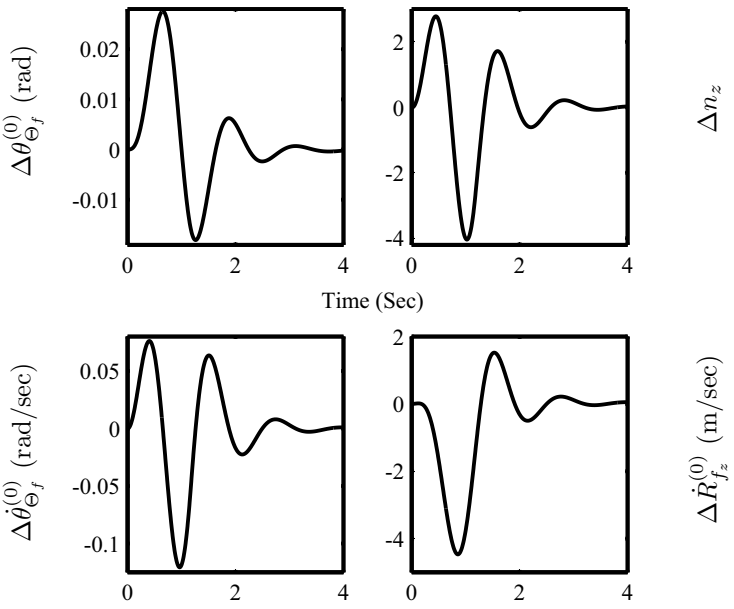

Figure 6.8: Rigid-body response during pitching maneuver.

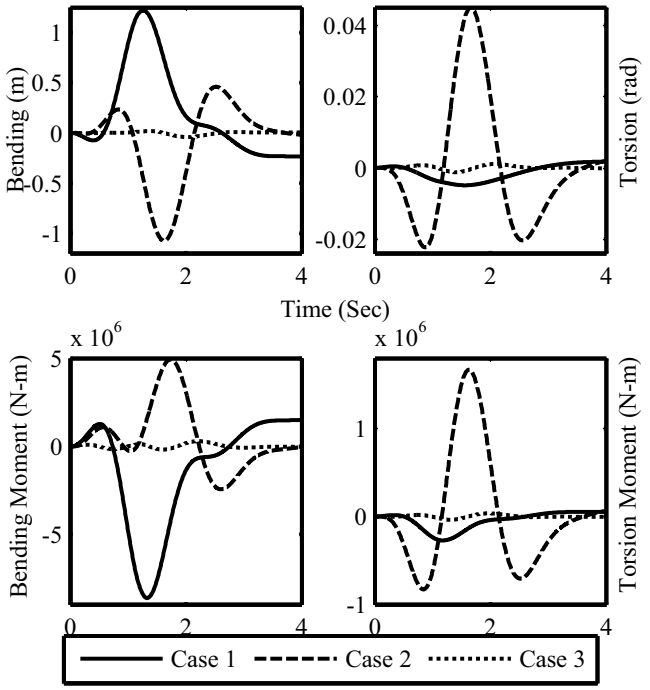

(a) Right wing

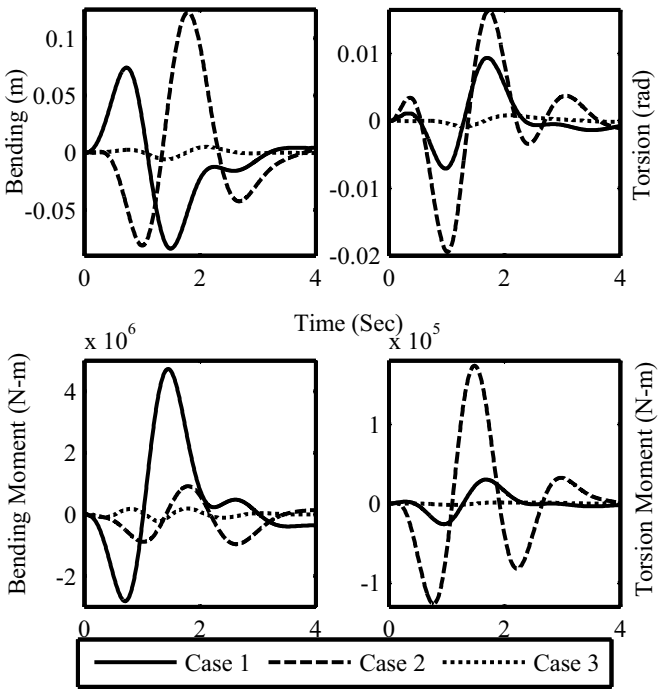

(b) Aft fuselage

Figure 6.9: 1st order deflections and root loads during pitching.

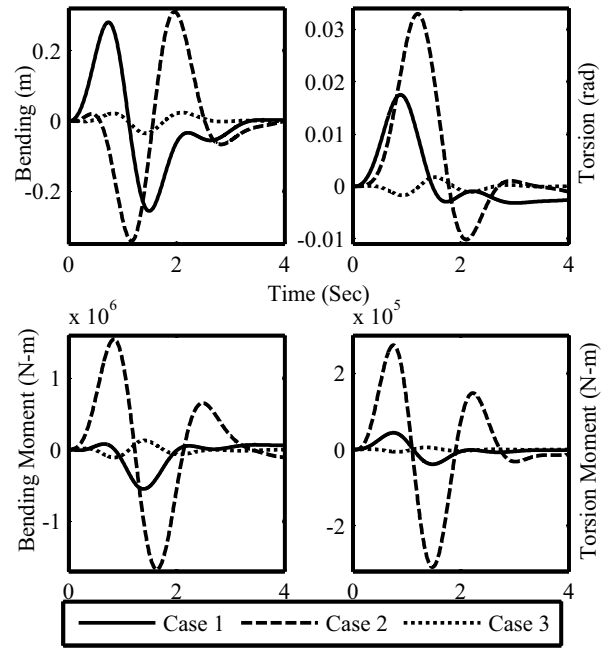

(a) Right horizontal tail

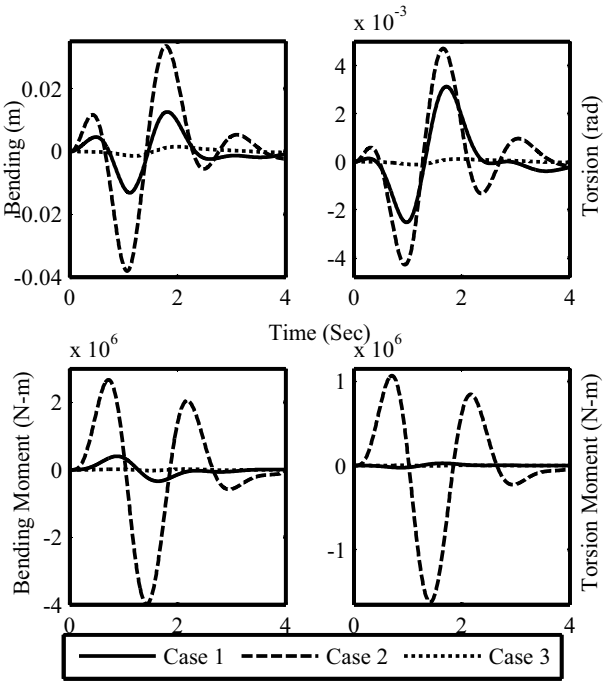

(b) Vertical tail

Figure 6.10: 1st order tip deflections and root loads during pitching.

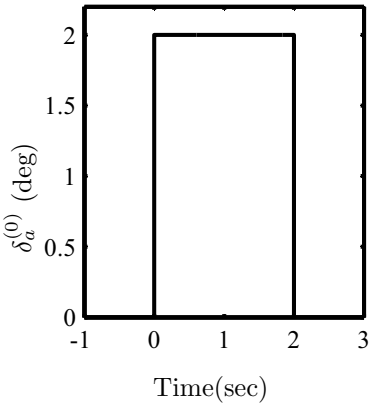

Figure 6.11: Aileron impulse input.

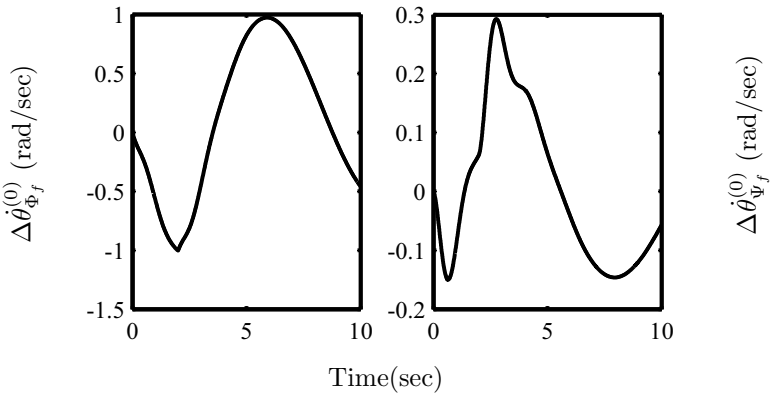

Figure 6.12: Rigid-body rolling and yawing rates during aileron impulse input.

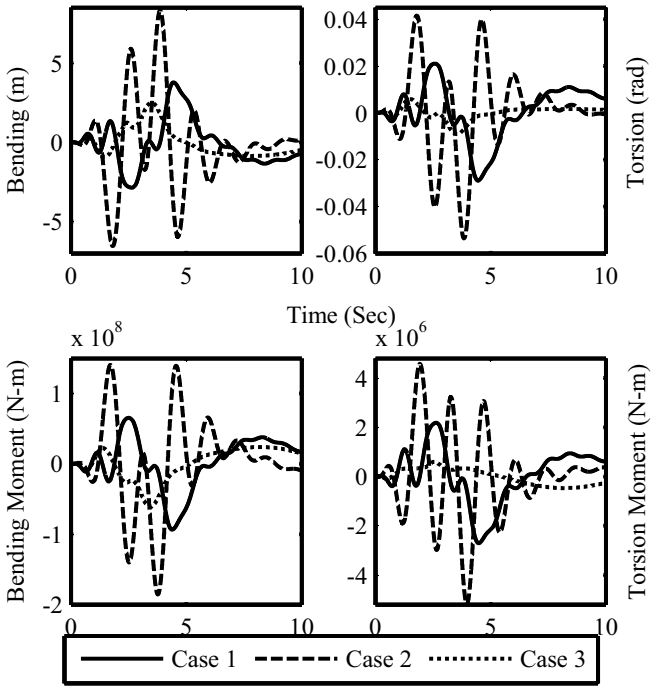

(a) Right wing

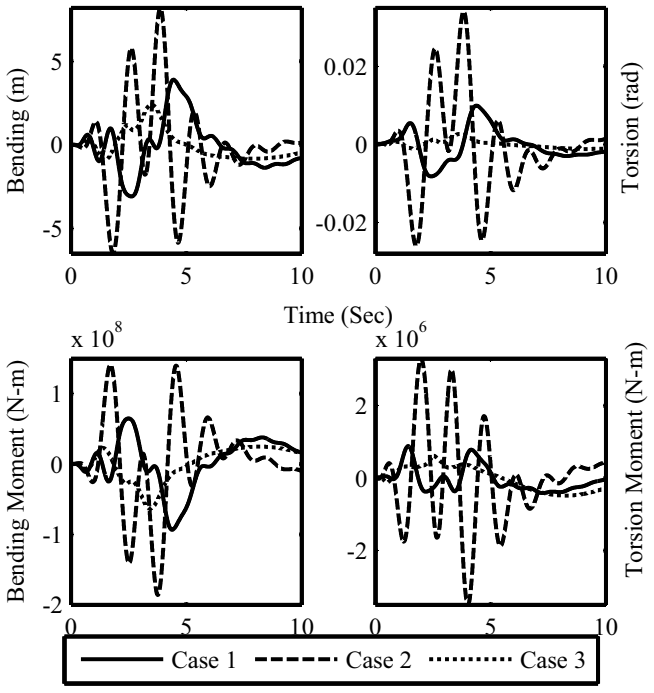

(b) Left wing

Figure 6.13: 1st order deflections and root loads during rolling.

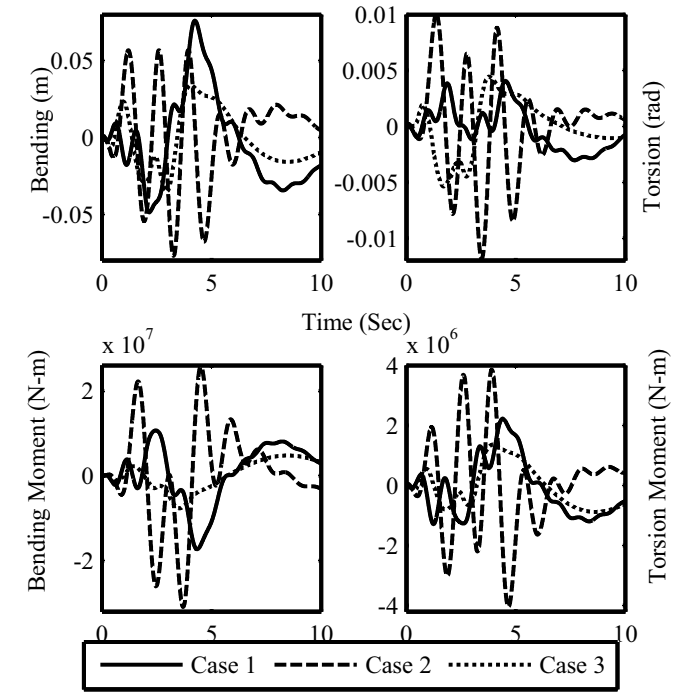

(a) Aft fuselage

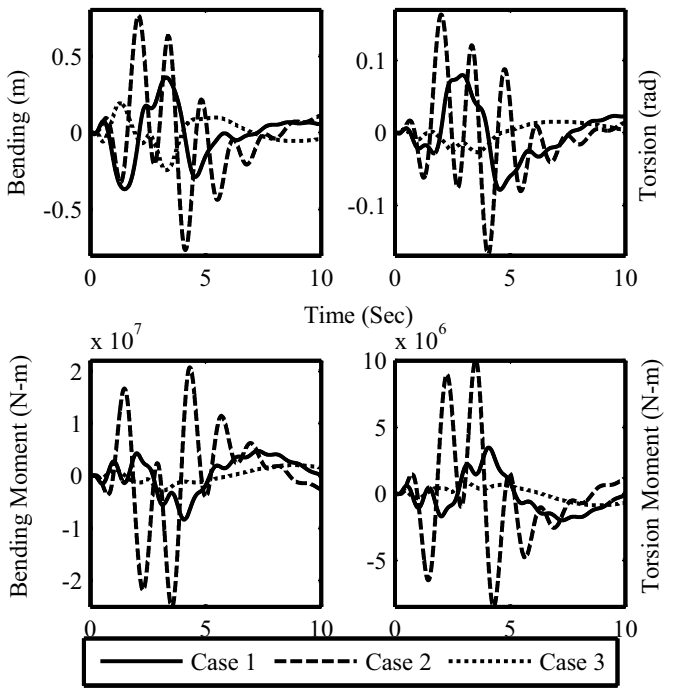

(b)Vertical tail

Figure 6.14: 1st order deflections and root loads during rolling.

Chapter 7

Conclusions

The use of fiber composite material in aircraft components results in anisotropy of the structural stiffness properties of that component and in such case the use of elastic axis $e.a$ as reference of vibration does not really decouples the bending and torsion deformations. It is also revealed that the position of a shear center of a box beam (e.g. wing box section) with symmetric-balanced laminates does not remain to be a cross-sectional property and becomes a material property. The elastic axis, which is drawn by intersecting the shear centers from root to tip, tends to get far outside from the structural boundaries. So it seemed necessary to reduce the usage of $e.a$ as the reference of vibrations. The state of the art inertially coupled equations of motion are modified to accommodate a reference axis $r.a$ other than the $e.a$ in each equivalent beam model of the aircraft component. Moreover the anisotropic material properties are also accommodated in the stiffness matrix. This modification requires to rederive the mathematical model from top to bottom (i.e. from the expression of a section deformation to the formation of structural dynamics matrices and further down to state-space matrices and structural loads equations). A small executive twin jet is selected for the simulation in a few static (i.e. steady level flight) and dynamic conditions (i.e. discrete gust and pilot induced maneuvers). Due to the nonavailability of the composite aircraft data the coupling effects on the response of the aircraft are studied by manipulating the $e.a$ of each wing and horizontal tail of the metal aircraft in five different cases of numerical examples. The modified equations of motion were found to be very useful in this regard, which show that the coupling plays a significant role in the dynamics of the fully flexible aircraft. It shows different effects both in static and dynamic conditions. Those effects were not clearly known because the $e.a$ was either used as the reference of vibrations or the modeling and simulation of the $e.a$ position was restricted to a wing in flutter analysis. Although for a structural design engineer the cases of $e.a$ positions, given herein, do not seem to be a

proper way of doing an analysis, it does give a fair picture in conceptual or preliminary design. However, the modified equations remove the necessity of using an elastic axis as a reference of vibration in fiber composite aircrafts and open a door for an optimization problem to optimize the position of $e.a$, which should result in minimized vibrations due to the coupling effects.

7.1 Recommendations

A multidisciplinary design optimization (MDO) of an aircraft during the preliminary design phase can be formulated as a multiobjective problem (e.g. minimum weight, controllability, minimum drag, and etc.) with multivariables (e.g. fiber orientations, position of aircraft components w.r.t. aircraft CG, sweep angle, and etc.) This sort of MDO problem is quite possible while using the global sensitivity equations (GSE) approach. GSE, which are gradient based Jacobian equations make it possible to internally couple the disciplines of structures, aerodynamics, and controls in a single optimization framework. During the optimization solution structural dynamics matrices (i.e. mass, stiffness and structural damping matrices) are updated in each iteration. Each new stiffness and mass matrix in an iteration give new sets of dynamic loads. The mathematical model presented herein is equally capable of handling this kind of problem, for example, while using the gradient-based optimization routines, if one of the objectives is to minimize the vibrations and consequent loads then the loads equations based on stiffness (i.e. MDM) can easily be differentiated to a structural design variable that yields the loads sensitivity of the each relevant design variable. During the preliminary design phase this sort of exercise will yield a minimum stiffness requirement for each aircraft component against the dynamic loads. During the advanced design phases, when the geometry of the aircraft components is more or less fixed, some latest optimization techniques like genetic algorithm can be used to optimize the layer configurations of a fiber composite component under a static load case. The resultant stiffness and mass properties can later be compared with a minimum requirement of a stable system.

While looking at the scope of the mathematical modeling in general and structural dynamics in particular of a flexible aircraft, the development presented in this report does not end here. The generic equations of motion can be used for any type of aircraft, but the formulation of its subparts like mass and stiffness matrices vary with the configuration. The model presented in this report is capable of simulating the dynamics of any conventional aircraft, which are believed to well remain as the dominant design for at least next two decades. Looking at the proposed alternatives like the blended wing-body (BWB) or the Prandtlplane, a robust framework will be required in the future to automate

the process of constructing the structural dynamics part of the inertially coupled equations of motion. This will reduce the purpose of lengthy and complex analytical mathematical modeling. A commercial finite element software can be a good choice, which would automatically construct the structural dynamics matrices and it may also require a kind of internal programming (e.g. Direct Matrix Abstraction Programing in Nastran). However this exercise may have its own limitations for each and every different aircraft configuration, which may require some changes in programming and it would not serve as a fully automated optimization framework but at least it will work for a fixed configuration at a time.

The knowledge based engineering (KBE) tools like design and engineering engine (DEE), being developed by DAR group of Faculty of Aerospace Engineering in Delft University, is a best example in the automation of MDO problem in aircraft preliminary design phase. The above discussion leads us to a conclusion that DARLoads can be accommodated in the DEE framework and the use of GSE can be the best approach to couple the various analysis tools like CFD and FEA.

Appendix A

Static condensation

The aircraft beam model shown in Fig 2.1 is usually created by using the static condensation or Guyan reduction technique [42], where the full-order finite element structural model of any component like wings, fuselage or empennage are condensed to lumped mass and stiffness elements [36]. Without going into the detailed theory of static condensation, only a brief description of modeling a condensation problem is presented with an example of using the superelements approach in MSC.Nastran software [43].

A.1 Superelement modeling

Fig A.1(a) shows a fuselage section structure discretized into several panels along the circumference, where it is assumed that each stiffened panel is represented by a a straight panel with equivalent stiffness and material properties [44,45]. Modeling the structure with equivalent panels saves a considerable solution time and it terms of accuracy this practice is also quite reliable especially with reference to aeroelastic predictions [46]. Each section along the fuselage length (i.e., a distance between from one fuselage frame to the next) is modeled as a superelement (SE) by using the SESET bulk data entry, where the grids at the root of that section represent its interior points and the grids at the tip acts as its exterior points to the next section, see Fig A.1(a). Figure A.1(b) shows the superelement tree from root to the tip superelement. By using the rigid body element, RBE2 or RBE3, the stiffness and mass properties of the section are condensed to the grid at neutral axis. These rigid-body elements typically give a rigid connection between an independent node (i.e. condensation node at neutral axis) to other dependent nodes on the fuselage (i.e. exterior points or nodes). The RBE2 does not allow a relative motion between the dependent and independent nodes, whereas the RBE3 allows a rel-

ative motion of a certain D.o.F as the weighted average of the displacement of the other D.o.F. The output data from the MSC.Nastran is written out in *output4* format, which is then read by MATLAB to get mass and stiffness matrices of the structure.

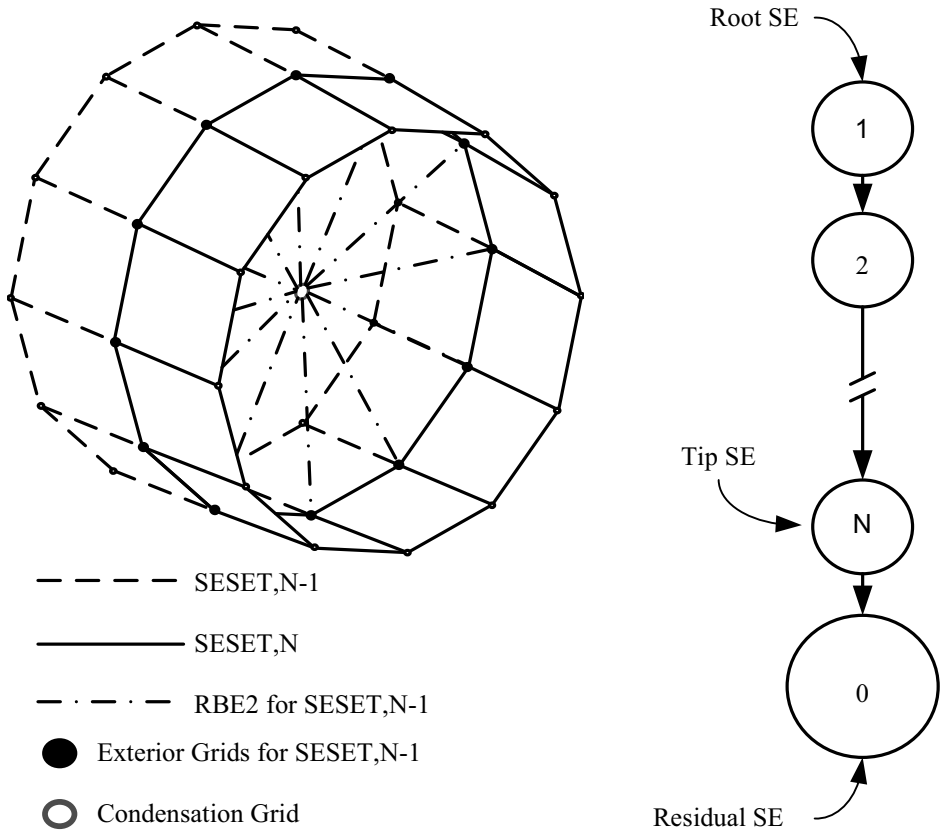

(a) Equivalent shell modeling. (b) Superelement tree.

Figure A.1: Superelement modeling.

A.2 A wing-box example

A composite wing-box, as shown in Fig. A.2, is modeled in MSC.Nastran by using several CQUAD elements, which are then divided into two superelements (SE). The layers configurations with material and geometrical properties are given in Ref. 8 and presented herewith in Table A.1. The free-body diagram shows the formation of the SE tree, where the nodes connecting SE1 and SE2

Table A.1: Wing-box layers configuration and stiffness properties

Configuration[a]		Ref. 8[b]			MSC.Nastran[b]		
Flanges	Webs	EI	GJ	k	EI	GJ	k
$[0/90]_3$	$[0/90]_3$	13.1	2.34	0	12.73	2.02	0
$[15]_6$	$[15/-15]_3$	22.53	5.26	5.85	14.90	2.51	3.0

[a] Mechanical properties: $E_{11} = 14.19$GPa, $E_{22} = 9.8$GPa, $G_{12} = 6.14$GPa, $\mu = 0.42$, ply thickness = 0.127mm, width = 0.0242m, height = 0.014m.
[b] Units: kg-m^2.

act as external nodes (i.e., *ASET*) for SE1 and internal nodes (i.e., *OSET*) to SE2. By using the SOL103 solution option in MSC.Nastran the stiffness and mass properties are condensed, and the results are presented and compared with those of Ref. 8 in Table A.1. It shows that in the first test case the error is not more than the 2.8%, whereas the error increases to 33% for the second case. The reason can be the use of type of rigid-body elements (i.e., RBE2) and it can be improved by using the RBE3 element. However, we concentrate only on to the static condensation approach while using a commerical finite element software. Moreover, it can easily be observed that slight change in ply angle on left and right sides of the web gives the material anisotropy, which causes the coupled vibrations. Although the orthogonality, as shown in Eq. (B.4), decouples the equations of motion in Eqs. (B.1–B.3), the present example shows that these are not actually fully decoupled and the material anisotropy somehow keeps the coupling intact.

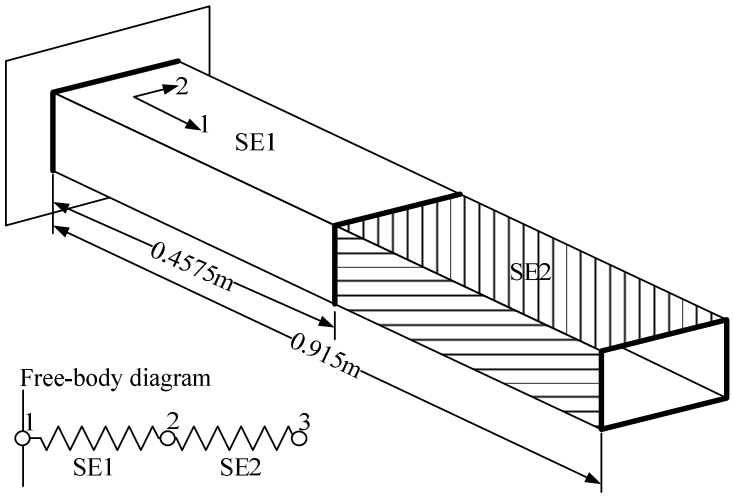

Figure A.2: Composite wing-box.

Appendix B

Inertially decoupled equations of motion

The rigid-body motion of the flexible aircraft is normally observed w.r.t. two types of the axes system (i.e. inertial and aircraft body axes). The positions of the aircraft in translation R_f and rotation θ_f are defined w.r.t to the inertial axes, whereas aircraft motion in the form of rigid-body velocities (i.e. V_f as translational velocity vector and Ω_f as angular velocity vector) are defined w.r.t aircraft body axes. Elastic motion in the form of structural generalized velocities (i.e. $\dot{q}_u$ in bending and $\dot{q}_\psi$ in torsion) of the aircraft components are defined w.r.t. a component's local axes system. The dynamic response of the aircraft is solved by the numerical solution of the equations of motion, which can be inertially coupled equations of motion (i.e. with a nondiagonal mass matrix) or inertially decoupled equations of motion (i.e. with a diagonal mass matrix). Inertially coupled equations of motion for a flexible aircraft derived in Ref. 14 and 25 are reproduced here with a brief description of the formulation.

$$\dot{R}_f = C_{If}^T V_f, \quad \dot{\theta}_f = E_{If}^{-1} \Omega_f \tag{B.1}$$

$$\dot{V}_f = \frac{F_f}{m} - \tilde{\Omega}_f V_f, \quad \dot{\Omega}_f = \frac{M_f - \tilde{\Omega}_f J_f \Omega_f}{J_f} \tag{B.2}$$

$$\ddot{q}_i + \omega_i^2 q_i = \frac{Q}{M}, \quad i = 1, 2, 3, \ldots \tag{B.3}$$

in which the Eqs. (B.1) and (B.2) relate to the rigid-body motion with respect to inertial and aircraft body axes, respectively. Eq. (B.3) is related to the elastic motion where ω_i represents the vibration frequency for the ith mode. It is to be noted that the Eqs. (B.1–B.2) are inertially decoupled and the only coupling

between the equations comes through the force vectors i.e. F_f, M_f, and Q. The inertial decoupling results from the the constraints of practical mean axes [14]. One of the constraints is the use of orthogonal modes, which makes the mass matrix a diagonal matrix, like in the following expression decoupling between the bending and torsion degrees arises as follows:

$$M_{ij} = \int_{Di} \phi_{u_i} \phi_{\psi_i} dm_i \equiv 0 \tag{B.4}$$

whereas the submatrices of mass matrix given in Eqs. (2.15) and (E.2–E.54) contradicts the above expression and holds the coupling between the two different D.o.F.

Appendix C

Eigenfunctions for a fixed-free beam

To calculate the structural deflections over the length of a fixed-free beam (i.e. cantilever beam), as given in Eq. (2.7), the eigenfunctions ϕ_u in bending and ϕ_ψ in torsion are multiplied with generalized coordinates of corresponding D.o.F. (i.e. q_u and q_ψ, respectively). Eigenfunctions used in this report do not represent typical natural modes of vibration, which are orthogonal with respect to mass distribution of the beam, see Eq. (B.4). However, each eigenfunction does hold two important properties of natural modes (i.e. shape of a vibration mode, and the corresponding natural frequency). Eigenfunctions are the functions of position r_x along the length of a beam and in bending these are expressed as follows [4]:

$$\phi_u(r_x) = \cosh\frac{\beta_{L_n} r_x}{L} - \cos\frac{\beta_{L_n} r_x}{L} + \frac{\sin\beta_{L_n} - \sinh\beta_{L_n}}{\cos\beta_{L_n} + \cosh\beta_{L_n}} \times \left(\sinh\tfrac{\beta_{L_n} r_x}{L} - \sin\tfrac{\beta_{L_n} r_x}{L}\right) \tag{C.1}$$

in which L is the total length of a beam. The values of β_{L_n} are given by the abscissas of the points of intersection of the curves, which are plotted as a solution of transcendental equation of cantilever beam, see Fig. 3-4 of Ref. 23. For first two vibration shapes in bending (i.e. $n = 1, 2$), the values of intersection points are given as $\beta_{L_n} = \begin{bmatrix}0.597\pi & 1.49\pi\end{bmatrix}$, where the corresponding normalized shapes are plotted in Fig. C.1(a). Similarly eigenfunctions in torsion are expressed as follows:

$$\phi_\psi(r_x) = \sin\frac{(2n-1)\pi r_x}{2L} \tag{C.2}$$

The shapes of first two normalized shapes in torsion are plotted in Fig. C.1(b).

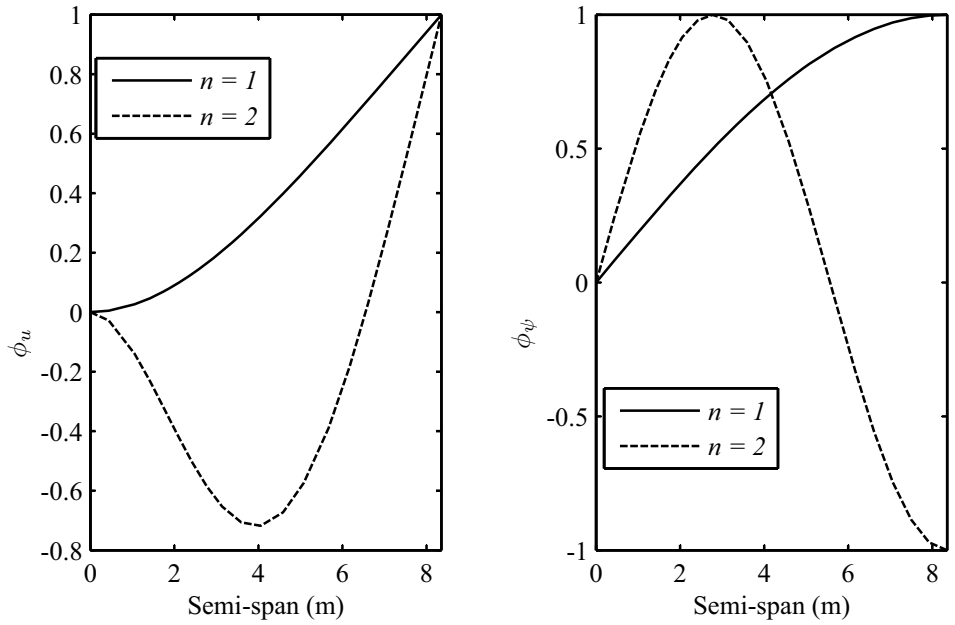

(a) Bending (b) Torsion

Figure C.1: First two vibration mode shapes

Appendix D

Transformation matrices

All the transformation or rotation matrices from inertial axes to aircraft body axes in both translation and rotation are obtained through the sequence of Euler rotations i.e. yaw θ_{Ψ_f} about the z-axis, pitch θ_{Θ_f} about the y-axis and lastly roll θ_{Φ_f} about the x-axis. Same analogy is adopted in the case of transformation from aircraft body axes O_f to a component local axes O_i. The quasi rotation matrices from inertial axes to the aircraft body axes is translation and rotation is expressed as [4]:

$$C_{If} = \begin{bmatrix} c\theta_{\Psi_f} c\theta_{\Theta_f} & s\theta_{\Psi_f} c\theta_{\Theta_f} & -s\theta_{\Theta_f} \\ c\theta_{\Psi_f} s\theta_{\Theta_f} s\theta_{\Phi_f} - s\theta_{\Psi_f} c\theta_{\Phi_f} & s\theta_{\Psi_f} s\theta_{\Theta_f} s\theta_{\Phi_f} + c\theta_{\Psi_f} c\theta_{\Phi_f} & c\theta_{\Theta_f} s\theta_{\Phi_f} \\ c\theta_{\Psi_f} s\theta_{\Theta_f} c\theta_{\Phi_f} + s\theta_{\Psi_f} s\theta_{\Phi_f} & s\theta_{\Psi_f} s\theta_{\Theta_f} c\theta_{\Phi_f} - c\theta_{\Psi_f} s\theta_{\Phi_f} & c\theta_{\Theta_f} c\theta_{\Phi_f} \end{bmatrix} \tag{D.1}$$

$$E_{If} = \begin{bmatrix} 1 & 0 & -s\theta_{\Theta_f} \\ 0 & c\theta_{\Phi_f} & c\theta_{\Theta_f} s\theta_{\Phi_f} \\ 0 & -s\theta_{\Phi_f} & c\theta_{\Theta_f} c\theta_{\Phi_f} \end{bmatrix} \tag{D.2}$$

in which s = sin and c = cos. The component transformation matrices used in the simulation examples of Chapter 5 and 6 are as follows:

$$C_f^F = \begin{bmatrix} 1 & 0 & 0 \\ 0 & 1 & 0 \\ 0 & 0 & 1 \end{bmatrix} \quad C_f^A = \begin{bmatrix} -1 & 0 & 0 \\ 0 & -1 & 0 \\ 0 & 0 & 1 \end{bmatrix}$$

$$C_w^R = \begin{bmatrix} 0 & 0.9976 & -0.0698 \\ -1 & 0 & 0 \\ 0 & 0.0698 & 0.9976 \end{bmatrix} \quad C_w^L = \begin{bmatrix} 0 & -0.9976 & -0.0698 \\ 1 & 0 & 0 \\ 0 & -0.0698 & 0.9976 \end{bmatrix}$$

$$C_v = \begin{bmatrix} -0.4808 & 0 & -0.8768 \\ -0.8768 & 0 & 0.4808 \\ 0 & 1 & 0 \end{bmatrix}$$

$$C_h^R = \begin{bmatrix} 0.1653 & -0.0234 & 0.9860 \\ 0.4719 & 0.8797 & -0.0582 \\ -0.8660 & 0.4749 & 0.1564 \end{bmatrix} \quad C_h^L = \begin{bmatrix} 0.1653 & -0.0234 & -0.9860 \\ -0.4719 & -0.8797 & -0.0582 \\ -0.8660 & 0.4749 & -0.1564 \end{bmatrix}$$

Appendix E

Mass matrix terms

The structural mass matrix is constructed by using the velocity terms Eqs. (2.9) and (2.13– 2.14) in the kinetic energy expression of Eq. (2.2). The coefficients resulting from the product of velocities construct the global mass matrix. A complete listing of submatrices and arrays of the mass matrix of a flexible aircraft is given in Ref. 4 except for the modified submatrices and arrays due to bending-torsion coupling and T-Tail configuration, which are presented here. Before that it is appropriate to briefly elaborate the structure of the mass matrix as given in Eq. (2.15). As given in Eq. (2.15) the mass matrix is divided into (8×8) arrays, where not all the array exhibit the same size but they make a full-order mass matrix of size (38×38). The size of each array depends upon the size of the coupling terms. For instance the coupling between the rigid-body motion in translation V_f and empennage bending D.o.F is stored in the array M_{15} of size (3×6), in which the number of rows (i.e. 3) originates from the size of V_f and similarly the number of columns (i.e. 6) originates from the size of generalized coordinates in bending D.o.F of empennage in Eq. (2.4). Similarly in Eq. (E.1), with the conjunction of two shape functions per D.o.F of a component in Eqs. (2.7) and (2.4), the array M_{88} of size (6×6) couples the torsion D.o.F of each horizontal tail to the vertical tail and vice-versa.

$$M_{88} = \begin{bmatrix} M_{88_{(1,1)}} & M_{88_{(1,2)}} & M_{88_{(1,3)}} \\ M_{88_{(2,1)}} & M_{88_{(2,2)}} & M_{88_{(2,3)}} \\ M_{88_{(3,1)}} & M_{88_{(3,2)}} & M_{88_{(3,3)}} \end{bmatrix} \tag{E.1}$$

in which each submatrix consists of a size (2×2). $M_{88_{(1,1)}}$, $M_{88_{(2,2)}}$, and $M_{88_{(3,3)}}$ defines the inertial terms in torsion D.o.F of vertical tail, right and left horizontal tails, respectively. $M_{88_{(1,2)}}$ and $M_{88_{(1,3)}}$ represent the effects of torsion of right and left horizontal tails on the vertical tail, respectively, and vice-versa in

submatrices $M_{88_{(2,1)}}$ and $M_{88_{(3,1)}}$[1]. Supposedly there is no structural coupling between the two horizontal tails so the submatrices $M_{88_{(2,3)}}$ and $M_{88_{(3,2)}}$ are the null matrices of size (2×2).

E.1 Inertia matrices

By using the Eqs. (3.11–3.13)[2], the first moment of inertia and the inertia matrix of a deformed aircraft are defined as follows:

$$\tilde{S} = \sum_{i=f,e,w} \int_{D_i} \tilde{l}_i dm_i \tag{E.2}$$

$$J_f = \sum_{i=f,e,w} \int_{D_i} \tilde{l}_i^T \tilde{l}_i dm_i \tag{E.3}$$

E.2 V_f-Bending coupling

The effects of deformations in bending D.o.F of fuselage, wing, or empennage beams on the rigid-body velocity in translation V_f are taken into account in arrays M_{13}, M_{14}, or M_{15} of Eq. (2.15), respectively, and vice-versa i.e. the effect of V_f on the bending D.o.F are taken into account in arrays M_{31}, M_{41}, or M_{51}. The array M_{15} is not affected at all but the submatrices related to horizontal tail in bending in arrays M_{13} and M_{15} are changed. By using Table 3.1[3]:

$$M_{13_{(1,2)}} = \left(C_h C_v\right)^T \int_{D_h} \Phi_{u_{fh}} d_{m_h} \tag{E.4}$$

$$M_{15_{(1,2)}} = \left(C_h^R C_v\right)^T \int_{D_h^R} \Phi_{u_h} d_{m_h} \tag{E.5}$$

$$M_{15_{(1,3)}} = \left(C_h^L C_v\right)^T \int_{D_h^L} \Phi_{u_h} d_{m_h} \tag{E.6}$$

[1] $M_{88_{(2,1)}}$ and $M_{88_{(3,1)}}$ are simply equal to $M_{88_{(1,2)}}^T$ and $M_{88_{(1,3)}}^T$, respectively. The same analogy is applied to the rest of the submatrices and arrays.

[2] It is to be noted that while computing the full-order mass matrix the products of transformation matrices and the vector of reduced-order generalized coordinates i.e. $D_{u_i}\xi$ and $D_{\psi_i}\xi$ of a particular component in Eqs. (3.11–3.13) are simply replaced by full-order generalized coordinate q_{u_i} and q_{ψ_i}, respectively.

[3] While constructing a full-order matrix, again the transformation matrices D_{u_i} or D_{ψ_i} are omitted in the eigenfunctions Φ_{u_i} or Φ_{ψ_i}.

E.3 V_f-Torsion coupling

The coupling of deformations in the torsion D.o.F of fuselage, wing, or empennage beams on the rigid-body velocity in translation V_f are taken into account in arrays M_{16}, M_{17}, or M_{18} of Eq. (2.15), respectively. The modified expressions are given as:

$$M_{16} = C_f^T \int_{D_f} \Phi_{\psi_f} d_{m_f} + \sum_{i=w,v} C_i^T \int_{D_i} \Phi_{\psi_{fi}} d_{m_i} + \left(C_h C_v\right)^T \int_{D_h} \Phi_{\psi_{fh}} d_{m_h} \tag{E.7}$$

$$M_{17} = C_w^T \int_{D_w} \Phi_{\psi_w} d_{m_w} \tag{E.8}$$

$$M_{18_{(1,1)}} = C_v^T \int_{D_v} \left(\Phi_{\psi_{vh}} + \Phi_{\psi_v}\right) d_{m_v} \tag{E.9}$$

$$M_{18_{(1,2)}} = \left(C_h^R C_v\right)^T \int_{D_h^R} \Phi_{\psi_h} d_{m_h} \tag{E.10}$$

$$M_{18_{(1,3)}} = \left(C_h^L C_v\right)^T \int_{D_h^L} \Phi_{\psi_h} d_{m_h} \tag{E.11}$$

E.4 Ω_f-Bending coupling

The effects of deformations in the bending D.o.F of fuselage, wing, or empennage beams on the rigid-body velocity in rotation Ω_f are taken into account in arrays M_{23}, M_{24}, or M_{25} of Eq. (2.15), respectively. The modified expressions are as follows:

$$M_{23_{(1,2)}} = \int_{D_h} \tilde{l}_h \Phi_{u_{fh}} d_{m_h} \tag{E.12}$$

$$M_{25_{(1,1)}} = \int_{D_v} \tilde{l}_v \left(\Phi_{u_{vh}} + \Phi_{u_v}\right) d_{m_v} \tag{E.13}$$

$$M_{25_{(1,2)}} = \int_{D_h^R} \tilde{l}_h \Phi_{u_h} d_{m_h} \tag{E.14}$$

$$M_{25_{(1,3)}} = \int_{D_h^L} \tilde{l}_h \Phi_{u_h} d_{m_h} \tag{E.15}$$

E.5 Ω_f-Torsion coupling

The coupling of deformations in the torsion D.o.F of fuselage, wing, or empennage beams on the rigid-body velocity in rotation Ω_f are taken into account in arrays M_{26}, M_{27}, or M_{28} of Eq. (2.15), respectively. The modified expressions are given as:

$$M_{26} = \int_{D_f} \tilde{l}_f \Phi_{\psi_f} d_{m_f} + \sum_{i=e,w} \int_{D_i} \tilde{l}_i \Phi_{\psi_{fi}} d_{m_i} \tag{E.16}$$

$$M_{27} = \int_{D_w} \tilde{l}_w \Phi_{\psi_w} d_{m_w} \tag{E.17}$$

$$M_{28_{(1,1)}} = \int_{D_v} \tilde{l}_v \Phi_{\psi_v} d_{m_v} + \int_{D_h} \tilde{l}_h \Phi_{\psi_{vh}} d_{m_h} \tag{E.18}$$

$$M_{28_{(1,2)}} = \int_{D_h^R} \tilde{l}_h \Phi_{\psi_h} d_{m_h} \tag{E.19}$$

$$M_{28_{(1,3)}} = \int_{D_h^L} \tilde{l}_h \Phi_{\psi_h} d_{m_h} \tag{E.20}$$

E.6 Bending–Bending coupling

The coupling of deformations in the bending D.o.F of fuselage are inertially coupled to the bending of wing, or empennage beams and vice-versa. The array M_{33} represents the effect of fuselage bending on itself and moreover the wings and empennage beams. Similarly the effects of bending of each wing on itself and fuselage beams are as follows:

$$M_{33} = \int_{D_f} \Phi_{u_f}^T \Phi_{u_f} d_{m_f} + \sum_{i=e,w} \int_{D_i} \Phi_{u_{fi}}^T \Phi_{u_{fi}} d_{m_i} \tag{E.21}$$

$$M_{34} = \int_{D_w} \Phi_{u_{fw}}^T \Phi_{u_w} d_{m_w} \tag{E.22}$$

$$M_{44_{(1,1)}} = \int_{D_w^R} \Phi_{u_w}^T \Phi_{u_w} d_{m_w} \tag{E.23}$$

$$M_{44_{(2,2)}} = \int_{D_w^L} \Phi_{u_w}^T \Phi_{u_w} d_{m_w} \tag{E.24}$$

As the bending in the horizontal tail affects the fuselage through the vertical tail so the array M_{35} is portioned as follows:

$$M_{35_{(1,1)}} = \Phi_{u_{fv}}^T \left[\int_{D_v} \Phi_{u_v} dm_v + \int_{D_h} \Phi_{u_{vh}} dm_h \right] \tag{E.25}$$

$$M_{35_{(1,2)}} = \int_{D_h^R} \Phi_{u_{fh}}^T \Phi_{u_h} d_{m_h} \tag{E.26}$$

$$M_{35_{(1,3)}} = \int_{D_h^L} \Phi_{u_{fh}}^T \Phi_{u_h} d_{m_h} \tag{E.27}$$

The coupling in mass matrix between the bending in vertical and horizontal tails is given as:

$$M_{55_{(1,1)}} = \int_{D_v} \Phi_{u_v}^T \Phi_{u_v} d_{m_v} + \sum_{L,R} \int_{D_h} \Phi_{u_{vh}}^T \Phi_{u_{vh}} d_{m_h} \tag{E.28}$$

$$M_{55_{(1,2)}} = \int_{D_h^R} \Phi_{u_{vh}}^T \Phi_{u_h} d_{m_h} \tag{E.29}$$

$$M_{55_{(1,3)}} = \int_{D_h^L} \Phi_{u_{vh}}^T \Phi_{u_h} d_{m_h} \tag{E.30}$$

$$M_{55_{(2,2)}} = \int_{D_h^R} \Phi_{u_h}^T \Phi_{u_h} d_{m_h} \tag{E.31}$$

$$M_{55_{(3,3)}} = \int_{D_h^L} \Phi_{u_h}^T \Phi_{u_h} d_{m_h} \tag{E.32}$$

It is to be noted that there is no direct inertial effect of bending in each wing or horizontal tail on the other wing or horizontal tail but their coupling in bending comes through the array M_{33}. Therefore the arrays $M_{44_{(1,2)}}$ or $M_{44_{(2,1)}}$ for wings and $M_{55_{(2,3)}}$ or $M_{55_{(3,2)}}$ of horizontal tails are the null matrices of each (2×2). Moreover wing and empennage beams are also not directly connected to each other and again, as stated, the coupling comes through the fuselage (i.e. the array M_{33}), whereas the arrays M_{45} or M_{54} are the null matrices of each (4×4).

E.7 Torsion-Bending coupling

The bending D.o.F of each component is inertially coupled to its torsion D.o.F and vice-versa. In case of the fuselage the arrays M_{36}, M_{37}, and M_{38} represents

the effect of fuselage, wings and empennage torsion, respectively on the bending D.o.F of the fuselage. The array M_{47} represent the coupling of the wing torsion and the wing bending, and similarly the array M_{58} for the empennage beams. The analogy of null matrices in the arrays $M_{55_{(2,3)}}$ and $M_{55_{(3,2)}}$, as stated above, also works in case of the arrays $M_{47_{(1,2)}}$ or $M_{47_{(2,1)}}$ for wings and $M_{58_{(2,3)}}$ or $M_{58_{(3,2)}}$ of horizontal tails.

$$M_{36} = \int_{D_f} \Phi_{u_f}^T \Phi_{\psi_f} d_{m_f} + \sum_{i=e,w} \int_{D_i} \Phi_{u_{fi}}^T \Phi_{\psi_{fi}} d_{m_i} \tag{E.33}$$

$$M_{37} = \int_{D_w} \Phi_{u_{fw}}^T \Phi_{\psi_w} d_{m_w} \tag{E.34}$$

$$M_{38_{(1,1)}} = \Phi_{u_{fv}}^T \left[\int_{D_v} \Phi_{\psi_v} dm_v + \int_{D_h} \Phi_{\psi_{vh}} dm_h \right] \tag{E.35}$$

$$M_{38_{(1,2)}} = \int_{D_h^R} \Phi_{u_{fh}}^T \Phi_{\psi_h} d_{m_h} \tag{E.36}$$

$$M_{38_{(1,3)}} = \int_{D_h^L} \Phi_{u_{fh}}^T \Phi_{\psi_h} d_{m_h} \tag{E.37}$$

$$M_{47} = \int_{D_w} \Phi_{u_w}^T \Phi_{\psi_w} d_{m_w} \tag{E.38}$$

$$M_{58_{(1,1)}} = \int_{D_v} \Phi_{u_v}^T \Phi_{\psi_v} d_{m_v} + \sum_{L,R} \int_{D_h} \Phi_{u_{vh}}^T \Phi_{\psi_{vh}} d_{m_h} \tag{E.39}$$

$$M_{58_{(1,2)}} = \int_{D_h^R} \Phi_{u_{vh}}^T \Phi_{\psi_h} d_{m_h} \tag{E.40}$$

$$M_{58_{(1,3)}} = \int_{D_h^L} \Phi_{u_{vh}}^T \Phi_{\psi_h} d_{m_h} \tag{E.41}$$

$$M_{58_{(2,2)}} = \int_{D_h^R} \Phi_{u_h}^T \Phi_{\psi_h} d_{m_h} \tag{E.42}$$

$$M_{58_{(3,3)}} = \int_{D_h^L} \Phi_{u_h}^T \Phi_{\psi_h} d_{m_h} \tag{E.43}$$

E.8 Torsion-Torsion coupling

$$M_{66} = \int_{D_f} \Phi_{\psi_f}^T \Phi_{\psi_f} d_{m_f} + \sum_{i=e,w} \int_{D_i} \Phi_{\psi_{fi}}^T \Phi_{\psi_{fi}} d_{m_i} + J_f \tag{E.44}$$

$$M_{67} = \int_{D_w} \Phi_{\psi_{fw}}^T \Phi_{\psi_w} d_{m_w} \tag{E.45}$$

$$M_{68_{(1,1)}} = \Phi_{\psi_{fv}}^T \left[\int_{D_v} \Phi_{\psi_v} dm_v + \int_{D_h} \Phi_{\psi_{vh}} dm_h \right] \tag{E.46}$$

$$M_{68_{(1,2)}} = \int_{D_h^R} \Phi_{\psi_{fh}}^T \Phi_{\psi_h} d_{m_h} \tag{E.47}$$

$$M_{68_{(1,3)}} = \int_{D_h^L} \Phi_{\psi_{fh}}^T \Phi_{\psi_h} d_{m_h} \tag{E.48}$$

$$M_{77} = \int_{D_w} \Phi_{u_w}^T \Phi_{\psi_w} d_{m_w} + J_w \tag{E.49}$$

$$M_{55_{(1,1)}} = \int_{D_v} \Phi_{\psi_v}^T \Phi_{\psi_v} d_{m_v} + \sum_{L,R} \int_{D_h} \Phi_{\psi_{vh}}^T \Phi_{\psi_{vh}} d_{m_h} + J_v \tag{E.50}$$

$$M_{88_{(1,2)}} = \int_{D_h^R} \Phi_{\psi_{vh}}^T \Phi_{\psi_h} d_{m_h} \tag{E.51}$$

$$M_{88_{(1,3)}} = \int_{D_h^L} \Phi_{\psi_{vh}}^T \Phi_{\psi_h} d_{m_h} \tag{E.52}$$

$$M_{88_{(2,2)}} = \int_{D_h^R} \Phi_{\psi_h}^T \Phi_{\psi_h} d_{m_h} + J_h \tag{E.53}$$

$$M_{88_{(3,3)}} = \int_{D_h^L} \Phi_{\psi_h}^T \Phi_{\psi_h} d_{m_h} + J_h \tag{E.54}$$

Appendix F

α–β Definitions

From Fig. F.1 we can define the angle of attack α of a strip of the wing or the horizontal tail as a function of rigid-body pitch θ_{Θ_f}, flight path $-\gamma = \frac{V_{z_f} - V_\xi + l_i \Omega_{f_\Theta}}{V_{f_x}}$, structural generalized velocities $s = \dot{q}$ or $\eta = \dot{\xi}$ in reduced order, and the torsion angle ψ of the strip:

$$\alpha_i - \frac{V_\xi}{V_{f_x}} = \theta_{\Theta_f} - \gamma + \frac{\dot{\xi}}{V_{f_x}} + \psi(r_i) \tag{F.1}$$

$$\alpha_i = \theta_{\Theta_f} + \frac{V_{f_z} - V_\xi + l_i \Omega_{f_\Theta} + \dot{\xi}}{V_{f_x}} + \psi_i(r_i), \quad i = f, h, w \tag{F.2}$$

in which V_ξ is the vertical component of the downwash in horizontal tail only.

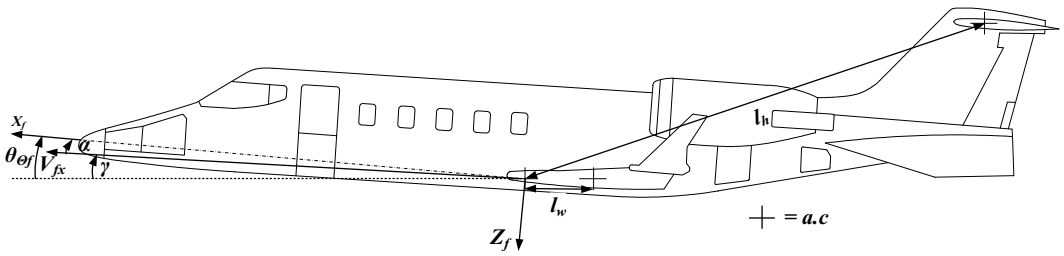

Figure F.1: Aircraft in pitch and plunge.

Similarly from Fig F.2 we can also define the side-slip angle β of a strip of the vertical tail or the fuselage as a function of rigid-body yaw θ_{Ψ_f}, flight path ζ,

structural generalized velocities $\eta = \dot{\xi}$, and the torsion angle ψ of the strip:

$$\beta_i = \theta_{\Psi_f} - \zeta + \frac{\dot{\xi}}{V_{f_x}} + \psi(r_i) \tag{F.3}$$

$$\beta_i = \theta_{\Psi_f} + \frac{V_{f_y} + l_i \Omega_{f_\Psi} + \dot{\xi}}{V_{f_x}} + \psi, \quad i = f, v \tag{F.4}$$

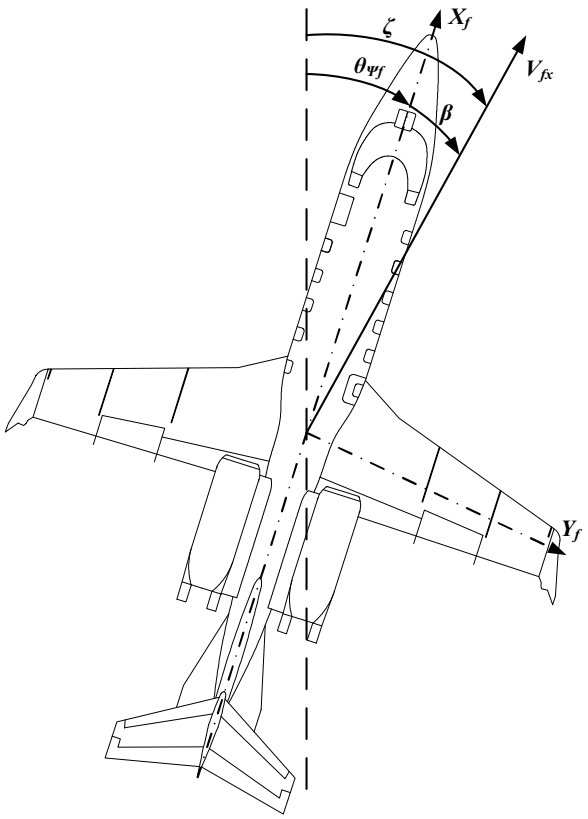

Figure F.2: Aircraft in side-slip.

Appendix G

Simplified form for rigid-body equations

It is a quite common practice in most of the flight mechanics literature [26, 30, 31] that, instead of momenta, the equations of motion representing rigid-body motion are solved in the form of velocity rates. In this Appendix the equations of motion for the rigid-body motion, as given in Eq. (3.52), are simplified so that these can be solved in terms of accelerations. However the simplification does not change the original context of the Eq. (3.52) but, as required by the airworthiness regulations [38], it only helps to solve the acceleration at the aircraft body axes. By using the last two expressions of Eq. (2.48), Eq. (3.52) for a LTI system can be written as:

$$
\begin{aligned}
M_r\ddot{x}^{(0)}(t) &= M_r \begin{bmatrix} -\widetilde{\Omega_f^{(0)}} & 0 \\ -\widetilde{V_f^{(0)}} & -\widetilde{\Omega_f^{(0)}} \end{bmatrix} \dot{x}^{(0)}(t) + C_{V\Omega}^{(0)}\dot{x}^{(0)}(t) + B_x^{(0)}x^{(0)}(t) + B_u^{(0)}u^{(0)}(t) \\
\ddot{x}^{(0)}(t) &= \begin{bmatrix} -\widetilde{\Omega_f^{(0)}} & 0 \\ -\widetilde{V_f^{(0)}} & -\widetilde{\Omega_f^{(0)}} \end{bmatrix} \dot{x}^{(0)}(t) + \frac{C_{V\Omega}^{(0)}}{M_r}\dot{x}^{(0)}(t) + \frac{B_x^{(0)}}{M_r}x^{(0)}(t) + \frac{B_u^{(0)}}{M_r}u^{(0)}(t)
\end{aligned}
\tag{G.1}
$$

in which the state vector $x^{(0)}$ is expressed as $\begin{bmatrix} R_f^{(0)T} & \theta_f^{(0)T} \end{bmatrix}^T$.

G.1 Steady-state equations

During the trim condition analysis, it is assumed that plunging and pitching rates are zero so the Eq. (G.1) is written for this particular problem as:

$$\ddot{x}^{(0)}(t) = \begin{bmatrix} -\widetilde{\Omega_f^{(0)}} & 0 \\ -V_f^{(0)} & -\widetilde{\Omega_f^{(0)}} \end{bmatrix} \dot{x}^{(0)}(t) + \frac{B_x^{(0)}}{M_r} x^{(0)}(t) + \frac{B_u^{(0)}}{M_r} u^{(0)}(t) \tag{G.2}$$

Similarly, the quadratic cost function in finding the trim variables, as given in Eq. (4.1), is also transformed to the following expression:

$$J^{(0)}\left(\theta_f^{(0)}, u^{(0)}\right) = \begin{bmatrix} \dot{R}_{f_x}^{(0)} & \dot{R}_{f_z}^{(0)} & \dot{\theta}_{f_\Theta}^{(0)} \end{bmatrix} W \begin{bmatrix} \dot{R}_{f_x}^{(0)} \\ \dot{R}_{f_z}^{(0)} \\ \dot{\theta}_{f_\Theta}^{(0)} \end{bmatrix} \tag{G.3}$$

G.2 Perturbation equations

Rigid-body perturbation over a steady-state due to a discrete gust is expressed as follows, where it is assumed that steady-state flight variables (i.e. rigid-body velocities and control inputs) are kept constant:

$$\Delta\ddot{x}^{(0)}(t) = \frac{C_{V\Omega}^{(0)}}{M_r} \Delta\dot{x}^{(0)}(t) + \frac{B_x^{(0)}}{M_r} \Delta x^{(0)}(t) + \frac{B_{w_g}^{(0)}}{M_r} w_g(t) \tag{G.4}$$

in which $B_{w_g}^{(0)}$ is the stiffness due to the gust and in this case it can be taken the same as the aerodynamic stiffness but without the gravity terms in Eqs. (3.31) and (3.32). The perturbation equation for a pilot induced maneuvers around the steady-state condition are given as:

$$\Delta\ddot{x}^{(0)}(t) = \frac{C_{V\Omega}^{(0)}}{M_r} \Delta\dot{x}^{(0)}(t) + \frac{B_x^{(0)}}{M_r} \Delta x^{(0)}(t) + \frac{B_u^{(0)}}{M_r} \Delta u^{(0)}(t) \tag{G.5}$$

G.3 Decoupling

The Eqs. (G.4) and (G.5) are further decoupled into two equations (i.e. pure symmetric and pure asymmetric rigid-body motions)[1]. The equation of motion

[1] This assumption is not considered to be true for a non-zero first moment inertia matrix $\tilde{S}$ and a non-zero J_{xy} inertia in mass matrix M_r. However in the present case, just for an approximation and simplicity, these variables are assumed to be zero. Otherwise one should solve the Eqs. (G.4) and G.5 as a whole.

representing a purely symmetric perturbation is given as:

$$\begin{bmatrix} \ddot{R}^{(0)}_{f_z}(t) \\ \ddot{\theta}^{(0)}_{f_\Theta}(t) \end{bmatrix} = \begin{bmatrix} m & 0 \\ 0 & J_{yy} \end{bmatrix}^{-1} \left(\begin{bmatrix} Z_{V_z} & Z_{\Omega_\Theta} \\ M_{V_z} & M_{\Omega_\Theta} \end{bmatrix} \begin{bmatrix} \dot{R}^{(0)}_{f_z}(t) \\ \dot{\theta}^{(0)}_{f_\Theta}(t) \end{bmatrix} + \begin{bmatrix} 0 & Z_{\theta_\Theta} \\ 0 & M_{\theta_\Theta} \end{bmatrix} \begin{bmatrix} R^{(0)}_{f_z}(t) \\ \theta^{(0)}_{f_\Theta}(t) \end{bmatrix} + \begin{bmatrix} 0 & Z_{w_{g_i}} \\ 0 & M_{w_{g_i}} \end{bmatrix} w_g(t) + \begin{bmatrix} Z_{\delta_{el}} \\ M_{\delta_{el}} \end{bmatrix} \delta^{(0)}_{el}(t) \right) \tag{G.6}$$

After the trim solution of the flight conditions given in Table 5.2 the numerical values in the Eq. (G.6), as used in the simulation example of Chapter 6, are as follows:

$$\begin{bmatrix} \ddot{R}^{(0)}_{f_z}(t) \\ \ddot{\theta}^{(0)}_{f_\Theta}(t) \end{bmatrix} = \begin{bmatrix} 5884.23 & 0 \\ 0 & 64003.38 \end{bmatrix}^{-1} \left(\begin{bmatrix} -15843.00 & -7923.89 \\ -4980.57 & -47510.37 \end{bmatrix} \begin{bmatrix} \dot{R}^{(0)}_{f_z}(t) \\ \dot{\theta}^{(0)}_{f_\Theta}(t) \end{bmatrix} + \begin{bmatrix} 0 & -3962739.43 \\ 0 & -1755796.38 \end{bmatrix} \times \begin{bmatrix} R^{(0)}_{f_z}(t) \\ \theta^{(0)}_{f_\Theta}(t) \end{bmatrix} + \begin{bmatrix} 0 & -14638.13 \\ 0 & 267.49 \end{bmatrix} w_{g_w}(t) + \begin{bmatrix} 0 & -1209.68 \\ 0 & -7250.19 \end{bmatrix} w_{g_h}(t) + \begin{bmatrix} -45279.47 \\ -278097.15 \end{bmatrix} \delta^{(0)}_{el}(t) \right) \tag{G.7}$$

Similarly for an asymmetric motion due to a rudder or aileron input the numerical values are as follows:

$$\begin{bmatrix} \ddot{R}^{(0)}_{f_y}(t) \\ \ddot{\theta}^{(0)}_{f_\Phi}(t) \\ \ddot{\theta}^{(0)}_{f_\Psi}(t) \end{bmatrix} = \begin{bmatrix} 5884.23 & 0 & 0 \\ 0 & 20708.91 & -4241.35 \\ 0 & -4241.35 & 79590.5 \end{bmatrix}^{-1} \left(\begin{bmatrix} 1012.54 & 0 & 6849.01 \\ 1874.04 & -86805.7593 & -5161.90 \\ -6563.81 & 283942.1731 & 2830.7422 \end{bmatrix} \begin{bmatrix} \dot{R}^{(0)}_{f_y}(t) \\ \dot{\theta}^{(0)}_{f_\Phi}(t) \\ \dot{\theta}^{(0)}_{f_\Psi}(t) \end{bmatrix} + \begin{bmatrix} 0 & 64618.66 & 253168.02 \\ 0 & -1355.13 & 468612.39 \\ 0 & -32099.194 & -1641309.694 \end{bmatrix} \begin{bmatrix} R^{(0)}_{f_y}(t) \\ \theta^{(0)}_{f_\Phi}(t) \\ \theta^{(0)}_{f_\Psi}(t) \end{bmatrix} + \begin{bmatrix} -5091.77 & -34178.20 \\ -445738.90 & -63263.63 \\ -445.00 & 221580.17 \end{bmatrix} \begin{bmatrix} \delta^{(0)}_a(t) \\ \delta^{(0)}_r(t) \end{bmatrix} \right) \tag{G.8}$$

Appendix H

Linearization process

While ignoring the higher order terms, the first-order Taylor's series is expressed as [29]:

$$f\left(x,y\right) \cong \overbrace{f\left(x^{(0)},y^{(0)}\right)}^{\text{zero-order problem}} + \overbrace{\frac{\partial f\left(x^{(0)},y^{(0)}\right)}{\partial x}y^{(0)} + \frac{\partial f\left(x^{(0)},y^{(0)}\right)}{\partial y}x^{(0)}}^{\text{first-order problem}}$$
$$\cong f\left(x^{(0)},y^{(0)}\right) + x^{(1)}y^{(0)} + x^{(0)}y^{(1)} \tag{H.1}$$

Using the analogy of first-order problem in Eq. (H.1), the Eqs. (2.48) and (2.60) will take a form as:

$$\begin{gathered}
\dot{R}_f^{(1)} = C_{If}^{(0)T}V_f^{(1)} + C_{If}^{(1)T}V_f^{(0)},\ \dot{\theta}_f^{(1)} = {E_{If}^{(0)}}^{-1}\Omega_f^{(1)} - {E_{If}^{(0)}}^{-1}E_{If}^{(1)}{E_{If}^{(0)}}^{-1}\Omega_f^{(0)} \\
\dot{\xi} = \eta \\
\dot{p}_{v_f}^{(1)} = -\tilde{\Omega}_f^{(1)}p_{v_f}^{(0)} - \tilde{\Omega}_f^{(0)}p_{v_f}^{(1)} + F^{(1)} \\
\dot{p}_{\Omega_f}^{(1)} = -\tilde{V}_f^{(1)}p_{v_f}^{(0)} - \tilde{V}_f^{(0)}p_{v_f}^{(1)} - \tilde{\Omega}_f^{(1)}p_{\Omega_f}^{(0)} - \tilde{\Omega}_f^{(0)}p_{\Omega_f}^{(1)} + M^{(1)} \\
\dot{p}_\eta = \frac{\partial T}{\partial \xi}^{(1)} - K_\xi\xi - C_\eta\eta + Q_\eta
\end{gathered} \tag{H.2}$$

in which the vectors of $F^{(1)}$, $M^{(1)}$, and Q_η result from the coefficient matrices $C_{V\Omega}^{(1)}$, $B_x^{(1)}$, and $B_u^{(1)}$ of Eq. (3.61) and their linearization process is presented in the next section of this Appendix. As far as the coefficient matrix $A^{(1)}$ is concerned readers are referred to Ref. 28 for the complete description of the matrix as its linearized state is not expressed for the sake of conciseness. However, due to the modification in the mathematical model, presented in the Chapter 2, a few submatrices particular to $\frac{\partial T}{\partial \xi}^{(1)}$ in $A^{(1)}$ are presented here but before that it is also necessary to express the linearization of absolute velocities of each component.

H.1 First-Order velocity expressions

H.1.1 Fuselage

The absolute velocity expression in Eq. (2.9) is also linearized into zero-order and first-order velocity expressions. The zero-order velocity expression, with superscript (0), simply represents a purely rigid-body motion i.e. without the effects of structural deformations. Whereas the first-order velocity expression, with superscript (1), represents the disturbance over the zero-order velocity vector due to vibrations or generalized velocities η.

$$\bar{V}_f^{(0)} = C_f V_f^{(0)} + \tilde{r}_f^T C_f \Omega_f^{(0)} \tag{H.3}$$

$$\bar{V}_f^{(1)} = C_f V_f^{(1)} + \tilde{r}_f^T C_f \Omega_f^{(1)} + \left(\widetilde{\phi_{u_f} D_{u_f}}\xi + \tilde{y}_f \widetilde{\phi_{\psi_f} D_{\psi_f}}\xi\right)^T C_f \Omega_f^{(0)} + \Phi_f \eta \tag{H.4}$$

in which the expression for the eigenvector Φ_f is given in Eq. (3.29).

H.1.2 Wing and vertical tail

Similar to Eqs (H.3–H.4), the absolute velocity expression for wings and vertical tail in Eq. (2.13) is also segregated into zero-order and first-order forms as follows, respectively:

$$\bar{V}_i^{(0)} = C_i V_f^{(0)} + \left(C_i \tilde{r}_{f_i}^T + \tilde{r}_i^T C_i\right) \Omega_f^{(0)} \tag{H.5}$$

$$\begin{aligned} \bar{V}_i^{(1)} &= C_i V_f^{(1)} + \left(C_i \tilde{r}_{f_i}^T + \tilde{r}_i^T C_i\right) \Omega_f^{(1)} \\ &+ \begin{bmatrix} C_i \left(\widetilde{\phi_{u_{fi}} D_{u_f}}\xi + \tilde{y}_f \widetilde{\phi_{\psi_{fi}} D_{\psi_f}}\xi\right)^T \\ + \left(\widetilde{\phi_{u_i} D_{u_i}}\xi + \tilde{y}_i \widetilde{\phi_{\psi_i} D_{\psi_i}}\xi\right)^T C_i \end{bmatrix} \Omega_f^{(0)} + \Phi_i \eta \end{aligned} \tag{H.6}$$

in which the expression for the eigenfunction Φ_i is given in Eqs. (3.27–3.28).

H.1.3 Horizontal tail

The absolute velocity expression for horizontal tail in Eq. (2.14) is segregated into zero-order and first-order forms as follows, respectively:

$$\bar{V}_h^{(0)} = C_h C_v V_f^{(0)} + \left(C_h C_v \tilde{r}_{f_v}^T + C_h \tilde{r}_{v_h}^T C_v + \tilde{r}_h^T C_h C_v\right) \Omega_f^{(0)} \tag{H.7}$$

$$\bar{V}_h^{(1)} = C_h C_v V_f^{(1)} + \left(C_h C_v \tilde{r}_{f_v}^T + C_h \tilde{r}_{v_h}^T C_v + \tilde{r}_h^T C_h C_v\right) \Omega_f^{(1)} + \begin{bmatrix} C_h C_v \left(\widetilde{\phi_{u_{fv}} D_{u_f}} \xi + \tilde{y}_f \widetilde{\phi_{\psi_{fv}} D_{\psi_f}} \xi\right)^T \\ +C_h \left(\widetilde{\phi_{u_{vh}} D_{u_v}} \xi + \tilde{y}_i \widetilde{\phi_{\psi_{vh}} D_{\psi_v}} \xi\right)^T C_v \\ + \left(\widetilde{\phi_{u_h} D_{u_h}} \xi + \tilde{y}_h \widetilde{\phi_{\psi_h} D_{\psi_h}} \xi\right)^T C_h C_v \end{bmatrix} \Omega_f^{(0)} + \Phi_h \eta \tag{H.8}$$

in which the expression for the eigenvector Φ_h is given in Eq. (3.26)

H.2 T_ξ coefficients

The expression of kinetic energy in Eq. (2.2) with linearized velocity expressions can be written as:

$$T = \frac{1}{2} \sum_{i=f,e,w} \int \left(\bar{V}_i^{(0)} + \bar{V}_i^{(1)}\right)^T \left(\bar{V}_i^{(0)} + \bar{V}_i^{(1)}\right) dm_i \tag{H.9}$$

Now using the Eqs. Eq. (H.9), and (H.3–H.8) in Eqs. (2.50) and (2.51) and rearranging brings us:

$$\left(\frac{\partial T}{\partial \xi}\right)^{(1)} = A_\xi \xi + A_V V_f^{(1)} + A_\Omega \Omega_f^{(1)} + A_\eta \eta \tag{H.10}$$

where the coefficient matrices w.r.t ξ, $V_f^{(1)}$, $\Omega_f^{(1)}$, and η are as follows:

$$\begin{aligned} A_\xi = &\int_{D_f} \phi_{u\psi_f}^T \left(\widetilde{C_f \Omega_f}^{(0)}\right)^T \left(\widetilde{C_f \Omega_f^{(0)}}\right) \phi_{u\psi_f} dm_f + \sum_{i=w,v} \phi_{u\psi_{fi}}^T \tilde{\Omega}_f^{(0)T} \\ &\times \int_{D_i} \left[\tilde{\Omega}_f^{(0)} \phi_{u\psi_{fi}} + C_i^T \left(\widetilde{C_i \Omega_f^{(0)}}\right) \phi_{u\psi_i}\right] dm_i + \phi_{u\psi_{fv}}^T \tilde{\Omega}_f^{(0)T} \times \\ &\int_{D_h} \tilde{\Omega}_f^{(0)} \phi_{u\psi_{fv}} + \left(C_h C_v\right)^T \left[\left(\widetilde{C_h C_v \Omega_f^{(0)}}\right) \phi_{u\psi_i} + C_h \left(\widetilde{C_v \Omega_f^{(0)}}\right) \phi_{u\psi_{vh}}\right] dm_h \\ &+ \sum_{i=w,v} \phi_{u\psi_i}^T \left(\widetilde{C_i \Omega_f^{(0)}}\right)^T \int_{D_i} \left[C_i \tilde{\Omega}_f^{(0)} \phi_{u\psi_{fi}} + \left(\widetilde{C_i \Omega_f^{(0)}}\right) \phi_{u\psi_i}\right] dm_i \\ &+ \left[\phi_{u\psi_{vh}}^T C_h^T \left(\widetilde{C_v \Omega_f^{(0)}}\right)^T + \phi_{u\psi_h}^T \left(\widetilde{C_h C_v \Omega_f}\right)^T\right] \\ &\times \int_{D_h} \left[C_h C_v \tilde{\Omega}_f^{(0)} \phi_{u\psi_{fv}} + C_h \left(\widetilde{C_v \Omega_f^{(0)}}\right) \phi_{u\psi_{vh}} + \left(\widetilde{C_h C_v \Omega_f^{(0)}}\right) \phi_{u\psi_h}\right] dm_h \end{aligned} \tag{H.11}$$

$$A_V = \int_{D_f} \phi_{u\psi_f}^T \left(\widetilde{C_f \Omega_f^{(0)}}\right)^T dm_f + \sum_{i=w,v} \int_{D_i} \left[\phi_{u\psi_{fi}}^T \tilde{\Omega}_f^{(0)T} + \phi_{u\psi_i}^T \left(\widetilde{C_i \Omega_f^{(0)}}\right)^T C_i\right] dm_i$$
$$+ \int_{D_h} \phi_{u\psi_{fv}}^T \tilde{\Omega}_f^{(0)T} + \left[\phi_{u\psi_{vh}}^T C_h^T \left(\widetilde{C_v \Omega_f^{(0)}}\right)^T + \phi_{u\psi_h}^T \left(\widetilde{C_h C_v \Omega_f^{(0)}}\right)^T\right] C_h C_v dm_h \tag{H.12}$$

$$A_\Omega = \int_{D_f} \phi_{u\psi_f}^T \left(\widetilde{C_f \Omega_f^{(0)}}\right)^T \tilde{l}_f^T dm_f + \sum_{i=w,v} \int_{D_i} \left[\phi_{u\psi_{fi}}^T \tilde{\Omega}_f^{(0)T} C_i^T + \phi_{u\psi_i}^T \widetilde{C_i \Omega_f^{(0)}}^T\right] \tilde{l}_i^T dm_i$$
$$+ \int_{D_h} \left[\phi_{u\psi_{fv}}^T \tilde{\Omega}_f^{(0)T} \left(C_h C_v\right)^T + \phi_{u\psi_{vh}}^T C_h^T \left(\widetilde{C_v \Omega_f^{(0)}}\right)^T + \phi_{u\psi_h}^T \left(\widetilde{C_h C_v \Omega_f^{(0)}}\right)^T\right] \tilde{l}_h^T dm_h \tag{H.13}$$

$$A_\eta = \int_{D_f} \phi_{u\psi_f}^T \left(\widetilde{C_f \Omega_f^{(0)}}\right)^T \phi_f dm_f + \sum_{i=w,v} \int_{D_i} \left[\phi_{u\psi_{fi}}^T \tilde{\Omega}_f^{(0)T} C_i^T + \phi_{u\psi_i}^T \widetilde{C_i \Omega_f^{(0)}}^T\right] \phi_i dm_i$$
$$+ \int_{D_h} \left[\phi_{u\psi_{fv}}^T \tilde{\Omega}_f^{(0)T} \left(C_h C_v\right)^T + \phi_{u\psi_{vh}}^T C_h^T \left(\widetilde{C_v \Omega_f^{(0)}}\right)^T + \phi_{u\psi_h}^T \left(\widetilde{C_h C_v \Omega_f^{(0)}}\right)^T\right] \phi_h dm_h \tag{H.14}$$

$$\begin{aligned} \phi_{u\psi_{fi}} &= \phi_{u_{fi}} D_{u_f} + \tilde{y}_f \phi_{\psi_{fi}} D_{\psi_f} \\ \phi_{u\psi_{vh}} &= \phi_{u_{vh}} D_{u_v} + \tilde{y}_v \phi_{\psi_{vh}} D_{\psi_v} \\ \phi_{u\psi_i} &= \phi_{u_i} D_{u_i} + \tilde{y}_i \phi_{\psi_i} D_{\psi_i} \end{aligned} \tag{H.15}$$

H.3 Linearization of coefficient matrices

In this section the coefficient matrices $A_{V\Omega}$, B_x, and B_u are linearized. Keeping in view the consiceness in the document, it is thought to present only one example of linearization. The rest of the equations are linearized in the same way as that of the example and presented without the derivations.

H.3.1 w.r.t. V_f

Starting with the linearization of the Eq. (3.9) while assuming that in case of vertical lift the V_{f_z} gives the damping as:

$$Z_{V_{li}} V_{f_z} = \frac{\rho V_{f_x}}{2} \int \left(c_i C_i^T Z_{V_{\alpha i}}\right) dD_i V_{f_z} \tag{H.16}$$

From the Taylor's series expansion:

$$Z_{V_{li}}^{(1)} V_f^{(1)} = \frac{\rho}{2}\left(V_{f_x}^{(0)} V_{f_z}^{(1)} + V_{f_z}^{(0)} V_{f_x}^{(1)}\right) \int \left(c_i C_i^T Z_{V_{\alpha i}}\right) dD_i \tag{H.17}$$

$$\Rightarrow \frac{\rho}{2} C_i^T \int c_i \begin{bmatrix} Z_{V_{\alpha i}} V_{f_z}^{(0)} & e_1^T & Z_{V_{\alpha i}} V_{f_x}^{(0)} \end{bmatrix} dD_i \begin{bmatrix} V_{f_x}^{(1)} \\ 0 \\ V_{f_z}^{(1)} \end{bmatrix} \tag{H.18}$$

$$Z_{V_{li}}^{(1)} = \frac{\rho}{2} C_i^T \int c_i \begin{bmatrix} Z_{V_{\alpha i}} V_{f_z}^{(0)} & e_1^T & Z_{V_{\alpha i}} V_{f_x}^{(0)} \end{bmatrix} dD_i \tag{H.19}$$

Similarly for the side force:

$$Z_{V_{si}}^{(1)} V_f^{(1)} = \frac{\rho}{2} C_i^T \int c_i \begin{bmatrix} Z_{V_{\beta i}} V_{f_y}^{(0)} & Z_{V_{\beta i}} V_{f_x}^{(0)} & e_1^T \end{bmatrix} dD_i \begin{bmatrix} V_{f_x}^{(1)} \\ V_{f_y}^{(1)} \\ 0 \end{bmatrix} \tag{H.20}$$

$$Z_{V_{si}}^{(1)} = \frac{\rho}{2} C_i^T \int c_i \begin{bmatrix} Z_{V_{\beta i}} V_{f_y}^{(0)} & Z_{V_{\beta i}} V_{f_x}^{(0)} & e_1^T \end{bmatrix} dD_i \tag{H.21}$$

The matrix of first-order aerodynamic damping in translation is:

$$Z_{V_v}^{(1)} = \sum_{i=f,v} \int Z_{V_{si}}^{(1)} dD_i + \sum_{i=h,w} \int Z_{V_{li}}^{(1)} dD_i \tag{H.22}$$

The moment due to aerodynamic damping in translation, as expressed in Eq. (3.10), is linearized as:

$$M_V^{(1)} = \sum_{i=f,v} \int \tilde{l}_i^{(0)} C_i Z_{V_{si}}^{(1)} + \tilde{l}_i^{(1)} C_i Z_{V_{si}}^{(0)} dD_i + \sum_{i=h,w} \int \tilde{l}_i^{(0)} C_i Z_{V_{li}}^{(1)} + \tilde{l}_i^{(1)} Z_{V_{li}}^{(0)} dD_i \tag{H.23}$$

in which the moment vectors $\tilde{l}_i^{(0)}$ are defined in Eqs. (3.58–3.60) and $\tilde{l}_i^{(1)}$ corresponds to the structural deformations in Eqs. (3.11–3.13), which are functions of generalized coordinates ξ. So Eq. (H.23) is reduced to:

$$M_{V_v}^{(1)} = \sum_{i=f,v} \int \tilde{l}_i^{(0)} C_i Z_{V_{si}}^{(1)} dD_i + \sum_{i=h,w} \int \tilde{l}_i^{(0)} C_i Z_{V_{li}}^{(1)} dD_i \tag{H.24}$$

whereas $\tilde{l}_i^{(1)}$ part of the Eq. (H.23) is separated as[1]:

$$M_{\xi_v} = -\frac{\rho V_{f_x}^{(0)}}{2} \left[\sum_{i=f,v} \int \left(\widetilde{C_i^T c_i Z_{V_{\beta i}}} \right) \frac{\partial l_i^{(1)}}{\partial \xi} dDi + \sum_{i=h,w} \int \left(\widetilde{C_i^T c_i Z_{V_{\alpha i}}} \right) \frac{\partial l_i^{(1)}}{\partial \xi} dDi \right] \tag{H.25}$$

[1]The property of skew symmetry: $\tilde{a}b = -\tilde{b}a$ and $\tilde{a}^T b = \tilde{b}a$

Repeating the process of linearization as given in Eqs. (H.16–H.25), the aerodynamic damping and stiffness in Eqs. (3.18) and (3.31–3.32), respectively, and control stiffness in Eqs. (3.40–3.50), are linearized where the parts that are a function of $V_f^{(1)}$ are collected and form the first-order aerodynamic damping due to rigid-body translation as:

$$
\begin{aligned}
Z_V^{(1)} = Z_{V_v}^{(1)} &- \rho\tilde{\theta}_f^{(0)} \left(\sum_{i=h,w} \int C_i^T \begin{bmatrix} Z_{V_{\alpha h}}^T \\ e_1 \\ e_1 \end{bmatrix}^T dD_h + \sum_{i=f,v} \int C_i^T \begin{bmatrix} Z_{V_{\beta v}}^T \\ e_1 \\ e_1 \end{bmatrix}^T dD_v \right) \\
&- \frac{\rho}{2}\tilde{\Omega}_f^{(0)} \left(\int \|l_h\|^{(0)} (C_h C_v)^T \begin{bmatrix} Z_{V_{\alpha h}}^T \\ e_1 \\ e_1 \end{bmatrix}^T dD_h + \int \|l_v\|^{(0)} C_v^T \begin{bmatrix} Z_{V_{\beta v}}^T \\ e_1 \\ e_1 \end{bmatrix}^T dD_v \right) \\
&+ \rho \left(\begin{aligned} & C_v^T C_h^T \int c_h \delta_{el}^{(0)} \begin{bmatrix} 0 & 0 & 0 \\ 0 & 0 & 0 \\ C_{l_{\delta_{el}}} & 0 & 0 \end{bmatrix} dD_h + C_w^T \int c_w \delta_a^{(0)} \begin{bmatrix} 0 & 0 & 0 \\ 0 & 0 & 0 \\ C_{l_{\delta_a}} & 0 & 0 \end{bmatrix} dD_w \\ & + C_v^T \int c_v \delta_r^{(0)} \begin{bmatrix} 0 & 0 & 0 \\ C_{l_{\delta_r}} & 0 & 0 \\ 0 & 0 & 0 \end{bmatrix} dD_v \end{aligned} \right)
\end{aligned}
\tag{H.26}
$$

$$
\begin{aligned}
M_V^{(1)} = M_{V_v}^{(1)} &- \rho\tilde{\theta}_f^{(0)} \left(\sum_{i=h,w} \int \tilde{l}_i^{(0)} C_i^T \begin{bmatrix} Z_{V_{\alpha h}}^T \\ e_1 \\ e_1 \end{bmatrix}^T dD_h + \sum_{i=f,v} \int \tilde{l}_i^{(0)} C_i^T \begin{bmatrix} Z_{V_{\beta v}}^T \\ e_1 \\ e_1 \end{bmatrix}^T dD_v \right) \\
&- \frac{\rho}{2}\tilde{\Omega}_f^{(0)} \left(\int \tilde{l}_h^{(0)} \|l_h\|^{(0)} (C_h C_v)^T \begin{bmatrix} Z_{V_{\alpha h}}^T \\ e_1 \\ e_1 \end{bmatrix}^T dD_h + \int \tilde{l}_v^{(0)} \|l_v\|^{(0)} C_v^T \begin{bmatrix} Z_{V_{\beta v}}^T \\ e_1 \\ e_1 \end{bmatrix}^T dD_v \right) \\
&+ \rho \left(\begin{aligned} & C_v^T C_h^T \int \tilde{l}_h^{(0)} c_h \delta_{el}^{(0)} \begin{bmatrix} 0 & 0 & 0 \\ 0 & 0 & 0 \\ C_{l_{\delta_{el}}} & 0 & 0 \end{bmatrix} dD_h + C_w^T \int \tilde{l}_w^{(0)} c_w \delta_a^{(0)} \begin{bmatrix} 0 & 0 & 0 \\ 0 & 0 & 0 \\ C_{l_{\delta_a}} & 0 & 0 \end{bmatrix} dD_w \\ & + C_v^T \int \tilde{l}_v^{(0)} c_v \delta_r^{(0)} \begin{bmatrix} 0 & 0 & 0 \\ C_{l_{\delta_r}} & 0 & 0 \\ 0 & 0 & 0 \end{bmatrix} dD_v \end{aligned} \right)
\end{aligned}
\tag{H.27}
$$

H.3.2 w.r.t. Ω_f

Using the same analogy as given in Eqs. (H.16–H.25), the Eqs. (3.18) and (3.19) are linearized as:

$$Z_{\Omega}^{(1)} = Z_{\Omega}^{(0)} \tag{H.28}$$

$$M_{\Omega}^{(1)} = \sum_{i=h,v} \tilde{l}_i^{(0)} C_i Z_{\Omega_i}^{(0)} \tag{H.29}$$

in which $Z_{\Omega}^{(0)}$ means the solution of Eq. (3.18) by taking into account the zero-order values of $V_f^{(0)}$ and $l_i^{(0)}$.

H.3.3 w.r.t. θ_f

Similarly the Eqs. (3.31) and (3.32) are also linearized by using the analogy of Eqs. (H.16–H.25):

$$Z_{\theta_f}^{(1)} = Z_{\theta}^{(0)} \tag{H.30}$$

$$M_{\theta_f}^{(1)} = \sum_{i=f,e,w} \tilde{l}_i^{(0)} C_i Z_{\theta_i}^{(0)} \tag{H.31}$$

Similarly the $Z_{\theta}^{(0)}$ means the computation of Eq. (3.31) by taking into account the zero-order values of $V_f^{(0)}$, $\theta_f^{(0)}$, and $l_i^{(0)}$.

H.3.4 w.r.t. δ_i

The aerodynamic stiffness due to the control inputs are also linearized by using the analogy of Eqs. (H.16–H.25):

$$Z_{\delta_i}^{(1)} = Z_{\delta_i}^{(0)} \tag{H.32}$$

$$M_{\delta_i}^{(1)} = \tilde{l}_i^{(0)} C_i Z_{\delta_i}^{(0)} \tag{H.33}$$

$Z_{\delta}^{(0)}$ is also computed by taking into account the zero-order values of $V_f^{(0)}$ and $R_{f_z}^{(0)}$ in Eqs. (3.40–3.51).

H.3.5 w.r.t. ξ

In addition to the aerodynamic moment due to torsion in Eq. (3.35), the linearization of the aerodynamic damping and stiffness coefficients, as given in

Sections H.3.1 to H.3.4, also adds some additional terms in Eq. (3.35), e.g. Eq.(H.25). So after the linearization Eq. (3.35) is updated to:

$$
\begin{aligned}
M_\xi = \text{Eq. (3.35)} - \frac{\rho V_{f_x}^{(0)}}{2} & \begin{pmatrix} \int \|l_h\|^{(0)} c_h \left(\widetilde{\begin{bmatrix} e_1 \\ Z_{V_{\alpha h}}^T \\ e_1 \end{bmatrix}^T} \Omega_f^{(0)} \right) \frac{\partial l_h^{(1)}}{\partial \xi} dD_h \\ - \int \|l_v\|^{(0)} c_v \left(\widetilde{\begin{bmatrix} e_1 \\ e_1 \\ Z_{V_{\beta v}}^T \end{bmatrix}^T} \Omega_f^{(0)} \right) \frac{\partial l_v^{(1)}}{\partial \xi} dD_v \end{pmatrix} \\
+\text{Eq. (H.25)} - \frac{\rho V_{f_x}^{(0)^2}}{2} & \begin{pmatrix} C_v^T C_h^T \int c_h \delta_{el}^{(0)} \widetilde{\begin{bmatrix} 0 \\ 0 \\ C_{l_{\delta_{el}}} \end{bmatrix}} \frac{\partial l_h^{(1)}}{\partial \xi} dD_h \\ + C_w^T \int c_w \delta_a^{(0)} \widetilde{\begin{bmatrix} 0 \\ 0 \\ C_{l_{\delta_a}} \end{bmatrix}} \frac{\partial l_w^{(1)}}{\partial \xi} dD_w \\ + C_v^T \int c_v \delta_r^{(0)} \widetilde{\begin{bmatrix} 0 \\ C_{l_{\delta_r}} \\ 0 \end{bmatrix}} \frac{\partial l_v^{(1)}}{\partial \xi} dD_v \end{pmatrix} \\
- \sum_{i=f,e,w} \frac{\rho V_{f_x}^{(0)}}{2} & \int c_i \left(\widetilde{\begin{bmatrix} e_1 \\ (C_i^T Z_{V_{\alpha_i}})^T \\ (C_i^T Z_{V_{\beta_i}})^T \end{bmatrix}^T} \theta_f^{(0)} \right) \frac{\partial l_i^{(1)}}{\partial \xi} dD_i \\
- \sum_{i=f,e,w} & \int \left(\widetilde{\begin{bmatrix} \frac{\partial C_{If}}{\partial \theta_{\Phi_f}} & \frac{\partial C_{If}}{\partial \theta_{\Theta_f}} & \frac{\partial C_{If}}{\partial \theta_{\Psi_f}} \end{bmatrix}} \begin{bmatrix} 0 \\ 0 \\ g \end{bmatrix} \right) \frac{\partial l_i^{(1)}}{\partial \xi} dm_i
\end{aligned}
\tag{H.34}
$$

Bibliography

[1] Mayuresh J. Patil, Dewey H. Hodges, and Carlos E. S. Cesnik. Nonlinear aeroelasticity and flight dynamics of high-altitude long-endurance aircraft. *J of Aircraft*, vol.38(1):pp.88–94, 2001.

[2] Chistopher Shearer and Carlos E. S. Cesnik. Nonlinear flight dynamics of very flexible aicraft. *J of Aircraft*, vol.44(5):pp.1528–1545, 2007.

[3] Chistopher Shearer and Carlos E. S. Cesnik. Trajectory control for very flexible aircraft. *J of Guidance, Control and Dynamics*, vol.31(2):pp.340–357, 2008.

[4] Ilhan Tuzcu and Leonard Meirovitch. Integrated approach to the dynamics and control of maneuvering flexible aircraft. Technical report, NASA/CR-2003-211748, 2003.

[5] J. Hofstee, T. Kier, C. Cerulli, and G. Looye. A variable fully flexible dynamic response tool for special investigations (varloads). In *Proceedings of the International Forum on Aeroelasticity and. Structural Dynamics*, Amsterdam, The Netherlands, June 4-6, 2003.

[6] Dewey H. Hodges. *Nonlinear Composite Beam Theory*, chapter 4, pages 71–88. Progress in Astronautics and Aeronautics, AIAA, Reston, VA, 2006.

[7] Dulnath D. Wijayratne. Validation of design and analysis techniques of tailored composite structures. Technical report, NASA/CR-2004-212650, December 2004.

[8] Ramesh Chandra, Alan Stemple, and Inderjit Chopra. Thin-walled composite beams under bending, torsional, and extensional loads. *J of Aircraft*, 27(7):pp. 619–626, 1990.

[9] L. P. Kollar and G. S. Springer. *Mechanics of Composite Stuctures*, chapter Chapter 3. Cambridge University Press, Cambridge UK, 2003.

[10] C. Hong and I. Chopra. Aeroelastic stability analysis of a composite rotor blade. *J of American Helicopter Society*, 30(2):pp. 57–67, 1985.

[11] Edward Smith and Inderjit Chopra. Formulation and evaluation of an analytical model for composite box-beams. *J of American Helicopter Society*, 36(3):pp. 23–35, July 1991.

[12] I. Lottati. Flutter and divergence aeroelastic characteristics for composite forward swept cantilevered wing. *J of Aircraft*, 22, 1985.

[13] Shijun Guo, Wenyuan Cheng, and Degang Cui. Aeroelastic tailoring of composite wing structures by laminate layup optimization. *AIAA Journal*, 44(12):pp. 3146–3149, December 2006.

[14] M. R. Waszak and D. K. Schmidt. Flight dynamics of aeroelastic vehicles. *J of Aircraft*, 25(6):pp. 563–571, June 1988.

[15] R. D. Milne. Dynamics of the deformable aeroplane. Technical report, R&M 3345, British Aeronautical Research Council, 1964.

[16] C.S. Buttrill, T.A. Zeiler, and P.D. Arbuckle. Nonlinear simulation of a flexible aircraft in maneuvering flight. In AIAA Paper 87-2501-CP, editor, *AIAA Flight Simulation Technologies Conference*, Monterey, CA, USA, August 1987.

[17] Eric W. Weisstein. *CRC Concise Encyclopedia of Mathematics*, page 250. Chapman and Hall/CRC, 2nd edition, December 2002.

[18] R. J. Allemang and D. L. Brown. Experimental modal analysis and dynamic component synthesis-system modeling techniques. Technical report, AFWAL-TR-87-3069, AF Wright Aeronautical Laboratries, 1987.

[19] Haroon A. Baluch, Ronald Slingerland, and M. J. L. van Tooren. Dynamic loads optimization during atmospheric turbulence on a flexible aircraft. In Royal Aeronautical Society, editor, *Proceedings of Young Persons Aerodynamic Conference*, Bristol UK, October 29-30, 2006.

[20] Michel van Tooren. Multi-objective design of moveables of aircraft(modair); requirements specifications. Technical report, Delft University of Technology, 2008.

[21] Gunter Endres. A fine balance. *Flight International*, (5111):pp. 24–37, 30 Oct.–5 Nov. 2007.

[22] Leonard Meirovitch. *Principles and Techniques of Vibrations*, chapter 4.4. Prentice Hall, New Jersey, USA, 2000.

[23] L. R. Bisplinghoff, H. Ashley, and R. L. Halfman. *Aeroelasticity*, pages 62–69,641–684. Dover Publications, New York, 1996.

[24] Dewey H. Hodges. Bending-torsion divergence of a clamped-clamped composite wing. *J of Aircraft*, 44(6):pp. 2070–2072, Nov.-Dec. 2007.

[25] M. R. Waszak, C. S. Buttrill, and D. K. Schmidt. Modeling and model simplification of aeroelastic vehicles: An overview. Technical report, NASA TM-107691, 1992.

[26] Robert F. Stengel. *Flight Dynamics*, chapter 2,3, pages 57–240. AIAA Education Series, 2004.

[27] Leonard Meirovitch and Ilhan Tuzcu. Time simulations of the response of maneuvering flexible aircraft. *J of Guidance, Control and Dynamics*, 27(5):pp. 814–828, Sept.-Oct. 2004.

[28] Leonard Meirovitch and Ilhan Tuzcu. Control of flexible aircraft executing time-dependent maneuvers. *J of Guidance, Control and Dynamics*, 28(6):pp. 1291–1300, Nov-Dec. 2005.

[29] Erwin Kreyszig. *Advanced Engineering Mathematics*, chapter 8.4, pages 350–351. John Wiley and Sons Inc., New Jersey, USA, 2006.

[30] Bernard Etkin and Lloyd D. Reid. *Dynamics of Flight Stability and Control*, chapter Chapter 4,5. Jhon Wiley and Sons, Inc., 1996.

[31] Louis V. Schmidt. *Introduction to Aircraft Flight*, chapter 4, pages 107–110. AIAA Education Series, 1998.

[32] Ted L. Lomax. *Structural Loads Analysis for Commercial Transport Aircraft: Theory and Practice*, chapter 2, pages 19–26. AIAA Education Series, 1996.

[33] Christopher Shearer and G. Looye. Modified generalized alpha method for integrating governing equations of very flexible aircraft. In *Proceedings of the 47th AIAA/ASME/ASCE/AHS/ASC Structures, Structural Dynamics, and Materials Conference 14th AIAA/ASME/AHS Adaptive Structures Conference*, Rhode Island, USA, May 1-4, 2006.

[34] Haroon A. Baluch and Michel van Tooren. Modified inertially coupled equations of motion for a flexible aircraft with coupled vibrations. *J of Aircraft*, 46(1):pp. 107–115, 2009.

[35] Brian L. Stevens and Frank L. Lewis. *Aircraft Control and Simulation*, chapter 4. Wiley-Interscience, second edition, 2003.

[36] Jan R. Wright and Jonathan E. Cooper. *Introduction to Aircraft Aeroelasticity and Loads*, chapter 16, pages 303–305. AIAA Education Series, 2007.

[37] J. Sobieszczanski-Sobieski, C. L. Bloebaum, and P. Hajela. Sensitivity of control-augmented structure obtained by a system decomposition method. *AIAA Journal*, 29(2):pp. 264–270, 1991.

[38] Anonymous. Certification specifications for large aeroplanes. Technical report, CS-25, EASA, October 2003.

[39] J.C. Lagarias, J. A. Reeds, M. H. Wright, and P. E. Wright. Convergence properties of the nelder-mead simplex method in low dimensions. *SIAM Journal of Optimization*, 9(1):pp. 112–147, 1998.

[40] A. S. Pototzky and B. Perry. New and existing techniques for dynamic loads analysis of flexible airplanes. *J of Aircraft*, 23(4):pp. 340–347, April 1986.

[41] H. A. Baluch, Lisandrin P., R. Slingerland, and M. van Tooren. Effects of flexibility on aircraft dynamic loads and structural optimization. In *45th AIAA Aerospace Sciences Meeting and Exhibit*, Reno, USA, 8-11 January 2007.

[42] Guyan R.J. Reduction of stiffness and mass matrices. *AIAA Journal*, 3(2):pp. 380, 1965.

[43] The MacNeal-Schwendler Corporation. *MSC.NASTRAN 2001 Superelement User's Guide*. 2001.

[44] Collier C.S. Stiffness, thermal expansion, and thermal bending formulation of stiffened, fiber-reinforced composite panels. In AIAA, editor, *AIAA/ASME/ASCE/AHS/ACS 34th Structures, Dynamics, & Materials Conference*, La Jolla, CA, April 19-22 1993. Paper No. AIAA-93-1569.

[45] Collier C.S. Thermoelastic formulation of stiffened, unsymmetric composite panels for finite element analysis of high speed aircraft. In *AIAA/ASME/ASCE/AHS/ACS 35th Structures, Dynamics & Materials Conference*, Hilton Head, SC, April 18-20 1994. Paper AIAA 94-1579.

[46] Paolo Lisandrin and Michel van Tooren. High-order finite elements reduced models for use in a flutter design tool. *J of Aircraft*, 42(3):pp. 748–754, May-June 2005.

Summary

Aeroelastic Loads Modeling
for
Composite Aircraft Design Support

by Haroon A. Baluch

The use of fiber composite material is getting common in the aircraft industry. Previously their use was quite common only in the light weight aircrafts and in the true sense most of the time the home builders or hobbyists were the forerunners in using these types of materials. The main reason behind this is the ease of manufacturing and its lower cost. We also see that in that period the manufacturers of large airplanes are always reluctant to use the fiber composite material and restricted most of the time to the parts that were less critical to loads. Contrary to that we see a change in late 80s and early 90s that few of these manufacturers start using the fiber composite materials in tail-section which was quite encouraging to the world of aircraft engineering and especially to the fiber composite industry. The start of 21st century gives another break through in the sense that, apart from tail section, two of the major manufacturers come up with fiber composite fuselages i.e. the fuselages of A380 and B787. The manufacturers of executive jets have already started producing the complete fiber composites airframes and we expect that those days are not far away when the wings of large airplanes will also be made of fiber composites.

With regard to the simulation of structural vibrations and consequent aeroelastic loads in aircraft components, the use of elastic axis $e.a$ as reference of vibrations is quite common. The $e.a$ decouples the bending and torsion degrees of freedom (D.o.F) during the dynamic analysis. The use of the $e.a$ to decouple the bending and torsion in vibration analysis does not work for fiber composite structures with anisotropic material properties. Anisotropic material proper-

ties often result in an elastic axis that is either discontinuous or far outside the real aircraft. Existing mathematical models of flexible aircraft dynamics do not address this issue. In this report, state of the art inertially coupled equations of motion of a flexible aircraft are modified. For each of the equivalent beam model of the fuselage, wings, and tail structure a particular fixed reference axis $r.a$ is used for vibrations instead of elastic axis. Since no decoupling can be used, the beam deflections become a function of both bending and twist. The resulting displacements are expanded to the expressions of beam generalized velocities. Apart from the inclusion of the coupling effects, it is also thought to modify the structural dynamics model that, apart from the conventional tail configuration, should also accommodate the analysis of T-Tail configuration aircraft. These developments modify the expressions of kinetic and strain energies and subsequent global mass and stiffness matrices, state-space coefficient matrices.

The modified model is then linearized into zero-order problem (i.e. rigid-body maneuvers) and first-order problem (i.e. vibrations and their effects on the rigid-body response of the aircraft). The equations of motion are then expanded to the structural loads equations, which are based on the summation of forces method (SFM) and mode displacement method (MDM). SFM is based on the summation of all the aerodynamic, gravity, and inertial forces on a component. Whereas the MDM is based on the structural deformations caused by the external forces. The results computed from SFM can be verified by comparing to those of the results from the MDM.

A computer code, DARLoads, is written to simulate the dynamics of the flexible aircraft and all the equations given in this report are programmed in MATLAB software. An executive twin-jet is selected for the simulation. Due to the non-availability of the composite aircraft data the coupling effects on the response of the aircraft are studied by manipulating the $e.a$ of each wing and horizontal tail of the metal aircraft in five different cases of numerical examples. In first three cases, the $e.a$ of each wing and horizontal tail is drawn parallel to the $r.a$ of that particular component, where the $e.a$ with respect to $r.a$ of each component is placed in three different positions. In the fourth and fifth case, the $e.a$ of each wing and tail is drawn by intersecting the shear centers of each section from root to tip. The aircraft is trimmed at the given air speed and altitude for each $e.a$ case, which shows that the coupling affects the trim variables significantly (i.e. elevator and thrust inputs, and the pitch angle) and moreover the static deflections. For each optimized trim condition the aircraft is subjected to different dynamic conditions, which include the discrete gust and abrupt checked elevator maneuver with a conventional tail configuration, and impulse aileron input with a T-tail configuration. The results in the form of rigid-body response and consequent structural loads show the same kind of scenario as observed in the static case (i.e. during trim solution). It shows that

the position of elastic axis has significant effects on the dynamics of the fully flexible composite aircraft.

Lastly, it is concluded that the present work opens a door for a multidisciplinary design optimization (MDO) problem, where the position of $e.a$ can be optimized for minimized vibrations. Moreover, to reduce the purpose of lengthy and complex analytical mathematical modeling, a robust framework is required to automate the construction of structural dynamics part of the equations of motion for the more advanced design like BWB and Prandtlplane. Otherwise the the mathematical model presented in this report will restricted to only conventional composite aircraft, which on the other hand, are believed to remain in service for at least next two to three decades.

Samenvatting

Bepaling van Aero-elastische Belastingen
in het
Ontwerp van Composiet Vliegtuigen

door Haroon A. Baluch

Het gebruik van fiber composiet materiaal wordt steeds gebruikelijk in de luchtvaartindustrie. Voorheen was het gebruik ervan vrij vaak alleen in het lichte gewicht van vliegtuigen en in de meest ware zin van de tijd de woning bouwers of hobbyisten waren de voorlopers in het gebruik van deze types van materialen. De belangrijkste reden hiervoor is het gemak van het productieproces en de lagere kosten. Verder zien we dat in die periode de fabrikanten van grote vliegtuigen zijn altijd huiverig voor het gebruik van de glasvezel composiet materiaal en beperkt het merendeel van de tijd tot de delen die waren minder kritische lading. In tegenstelling tot dat zien we een verandering in de late jaren'80 en vroege jaren'90 dat maar weinig van deze fabrikanten start met het gebruik van de glasvezel composiet materialen in tail-afdeling en dat was bemoedigend naar de wereld van vliegtuigen engineering en vooral aan de glasvezel composiet industrie. Het begin van de 21ste eeuw geeft een andere doorbraak in de zin dat, afgezien van de staart sectie, twee van de belangrijkste fabrikanten komen met fiber composiet rompen dwz de rompen van de A380 en B787. De fabrikanten van executive jets zijn reeds begonnen met de productie van de complete fiber composieten casco's en we verwachten dat deze dagen zijn niet ver weg als de vleugels van grote vliegtuigen zullen ook worden gemaakt van fiber composieten.

Met betrekking tot de simulatie van trillingen en de daaruit voortvloeiende structurele aroelastische lading in het vliegtuig onderdelen, het gebruik van elastische as *e.a* als referentie van trillingen is niet homogeen. De ea decouples de buiging en torsie graden van vrijheid (D.o.F) tijdens de dynamische

analyze. Het gebruik van de *e.a* te ontkoppelen van de buig-en torsie in vibratieanalyse werkt niet voor fiber composiet constructies met anisotrope materiaal eigenschappen. Anisotroop materiaal eigenschappen die vaak resulteren in een elastische as die een discontinue of ver buiten de echte vliegtuigen. Bestaande wiskundige modellen van flexibele luchtvaartuigen dynamics niet op dit onderwerp. In dit verslag, state of the art traagheids gekoppelde vergelijkingen van de beweging van een flexibele vliegtuigen worden gewijzigd. Voor elk van de lichtbundel gelijk model van de romp, vleugels, staart en de structuur van een bepaalde vaste referentie-as *r.a* wordt gebruikt voor trillingen in plaats van elastische as. Aangezien er geen ontkoppeling kan worden gebruikt, de lichtbundel verleggingen een functie van zowel buigen en draaien. De daaruit voortvloeiende verschuivingen worden uitgebreid tot de uitdrukkingen van de boomkorvisserij gegeneraliseerde snelheden. Naast het opnemen van de koppeling van effecten is het ook aan gedacht om de structurele dynamica model dat, afgezien van de staart conventionele configuratie, moet ook aan het onderzoek van T-Tail configuratie vliegtuigen. Deze ontwikkelingen passen uitingen van de kinetische energie en de stam en de daaropvolgende wereldwijde massa en stijfheid matrices, state-space coëfficiënt matrices.

Het gewijzigde model is in linearized dan nul-orde-probleem (dat wil zeggen stijve romp manoeuvers) en eerste-orde-probleem (dat wil zeggen trillingen en hun effecten op de stijve romp respons van het vliegtuig). De vergelijkingen van de beweging wordt vervolgens uitgebreid naar de structurele lasten vergelijkingen, die zijn gebaseerd op de sommering van de strijdkrachten methode (SFM) en modus verplaatsing methode (MDM). SFM is gebaseerd op de som van alle arodynamische, zwaartekracht, en inertielle krachten op een onderdeel. Overwegende dat de MDM is gebaseerd op de structurele vervormingen als gevolg van de externe krachten. De resultaten lopen vanaf SFM kan worden geverifieerd door middel van een vergelijking met die van de resultaten van het MDM.

Een computer-code, DARLoads, is geschreven voor de simulatie van de dynamiek van de flexibele vliegtuigen en alle vergelijkingen in dit rapport zijn geprogrammeerd in MATLAB software. Een uitvoerend tweemotorig straalvliegtuig is gekozen voor de simulatie. Vanwege de nonavailability van de composiet vliegtuigen gegevens van de koppeling op de respons van het vliegtuig worden bestudeerd door het verplaatsen van de positie van *e.a* met betrekking tot de *r.a* van elke vleugel en de horizontale staart. Het vliegtuig is bij het gegeven gegarneerd lucht snelheid en hoogte voor elke positie *e.a*, waaruit blijkt dat de koppeling effecten hebben een significant effect op de trim (ie een lift en stuwkracht input en de pitch hoek) en bovendien de statische doorbuiging. Voor elk geoptimaliseerd trim conditie van het vliegtuig wordt blootgesteld aan verschillende dynamische omstandigheden, waaronder de discrete en plotselinge windvlaag gecontroleerd lift manoeuvreren met een conventionele staart con-

figuratie en impuls rolroer ingangssignaal met een T-staart-configuratie. De resultaten in de vorm van stijve romp respons en de daaruit voortvloeiende structurele lasten vertonen dezelfde soort scenario zoals waargenomen in het statische geval is (dwz tijdens trim-oplossing). Hieruit blijkt dat de positie van elastische as significante effecten heeft op de dynamiek van de volledig flexibele composiet vliegtuigen.

Tot slot is het conclulded dat het huidige werk opent een deur voor een multidisciplinair ontwerp-optimalisatie (MDO) probleem, waar de positie van *e.a* kan worden geoptimaliseerd voor geminimaliseerd trillingen. Bovendien, om het doel van lange en complexe analytische wiskundige modellering, een robuust raamwerk nodig is voor het automatiseren van de bouw van de structurele dynamica deel van de vergelijkingen van de beweging voor de meer geavanceerde ontwerp graag BWB en Prandtlplane. Anders wordt het wiskundig model gepresenteerd in dit verslag zal beperkt blijven tot alleen de klassieke composiet vliegtuigen, die aan de andere kant, zijn vermoedelijk in gebruik blijven gedurende ten minste komende twee tot drie decennia.

Publications

Journal archives

Haroon Baluch and Michel van Tooren, Modified inertially coupled equations of motion for flexible aircraft with coupled vibrations, AIAA Journal of Aircraft, vol.46(1):107–115, 2009.

Conference proceedings

Haroon Baluch and Michel van Tooren, Multidisciplinary Design of Flexible Aircraft, Collaborative Product and Service Life Cycle Management for a Sustainable World (pp. 375-385). Springer Verlag London Ltd./ Queen's University Belfast (Won best paper award).

Haroon Baluch, Michel van Tooren, and Joost Schut, Design Tradeoffs for Fiber Composite Fuselages under Dynamic Loads using Structural Optimization,(AIAA-2008-2055), 49th AIAA SDM Conference, 7-10 April 2008, Schaumburg IL, USA.

Haroon Baluch and Michel van Tooren, Modified inertially coupled equations of motion for a flexible aircraft with bending-torsion coupled beams, (IF-095-Baluch-Coupling), International Forum on Aeroelasticity and Structural Dynamics (IFASD), 18-20 June 2007, Stockholm Sweden.

Haroon Baluch, et al., Effects of flexibility on aircraft dynamic loads and structural optimization, (AIAA-2007-768), 45th AIAA Aerospace Sciences Conference, 8-11 January 2007, Reno USA.

Haroon Baluch and Michel van Tooren, Dynamic loads optimization during atmospheric turbulence on a flexible aircraft, Royal Aeronautical Society Young Persons Conference, 30-31 October 2006, Bristol UK.

Acknowledgments

In the name of Allah the most gracious, the most beneficent.

First of all I would like to thank Prof. Michel van Tooren for his kind support and guidance. I really enjoyed working with him as a student. During the research he was always very supportive of my ideas and gave much freedom to decide about the next level of the research. I found him a very good teacher, boss and a very humble human being.

I would also like to thank all the members of the exam committee that they took their time to read my thesis and gave some useful comments for the improvement. In this regard, Dr. Ilhan Tuzcu's support during the early days of my Ph.D. is unforgettable.

I would like to thank all the staff members of Faculty of Aerospace in Delft, especially my present and past colleagues in DAR: Mrs. Lin, Marilena, Hans, Monqiue, Chiara, Lars, Jessica, Stefan, Meng, Maarten, Dennis, Dries, Sander, Maslina, Marcel, Prof. van Holten and Ronald Slingerland (Late), and most importantly Giampietro, Joost, Paolo, Gianfranco, and Jochem. I am also thankful to Wim with regard to his help on Latex, Mark for his timely and very useful inputs on the writing, and Michiel for his constant support on various issues related to IT and computer systems. Gandert being a room mate in the Faculty was best to me.

Some of my friends with whom I spent a great time in Holland: Hisham, Nadeem Shirazi, Qaiser Butt, Omer Naeem, Shareef Khan, Naveed, Zubair, Zeshan, Mehfooz, Tariq, Laiq, and Abbas Abdul Hakeem.

Some of very good friends of mine to whom I owe a respect: Syed Waqar, Humayun Qureshi, Inam, Yasir, Baqar, Sanaullah, Anwar, and Sajid Noor. I would also like to thank all those officials who directly or indirectly were involved in my scholarship matters, especially to Dr. Nisar, Iftikhar Ahmad, Javed Aslam, Altaf Saleemi, Nadeem, Naseer, and Mureed.

My former teachers who have lots of contribution on my career: my late Grand-

father who himself was an engineer and taught me the Mathematics, Dr. Akhtar Nawaz and Dr. Afzaal Malik in EME-NUST, Ms. Marry in Convent Jhelum, Mr. Ali Haider, Mr. Nasir, and Mrs. Talat in FG Jhelum, Maj (Late) Altaf and Mr. Tariq Ahmed in MCJ.

Fareed Bhai and Zia Bhai (Late) for their sincere advices during difficult times. Uncle Riaz and Aunt Naseem with Eman and Rizwan Bhai were always very dear to me.

My brothers Zuhair Bhai, Muazzam Shaheed and Dr. Wuqaas, and my beloved sisters Saleha and Aapo (Dr. Asma) who always stood along with me, and offered what they could do in terms of moral and physical support. I feel proud of them. My parents, Ami and Abu, who are the living source of encouragement and righteousness to me. Perhaps, there are no words available to me through which I can pay my gratitudes for every thing that they have done for me. Without their prayers success is difficult to achieve.

No one, however, helped more directly and continuously in completing my Ph.D. than my wife Uzma. She shared all the burdens and good times over this period. Without the love and support of Uzma and my sons; Muazzam (MuJ) and Ibrahim (Ibri) this thesis could not have been written. To Uzma and kids I indebted a deep affection.

About the Author

Haroon was born on the 26th of November 1976 in Peshawar, Pakistan. He did his early primary education in Convent School Jhelum and later in FG Public Jhelum. He passed his secondary in pre-engineering from MCJ. Later in early 1995 he started his bachelor of engineering in Mechanical at College of EME in National University of Sciences and Technology (NUST) Rawalpindi, Pakistan. After passing his BE in late 1998, he enrolled for Masters in the same institution and graduated in mid 2000.

Meanwhile in late 1999, he also started working in AERO Pakistan as a design engineer and worked on the designing of light aircraft components. In April 2004, he got the scholarship from the Pakistani Government to pursue his PhD research in Delft University. In December 2004 he started his PhD under the supervision of Prof. dr. Michel van Tooren at Design, Integration and Operation of Aircraft and Rotorcraft (DAR) group of Faculty of Aerospace Engineering in Delft University.

During his PhD he also worked on a few industrial projects namely STABCON and ModAir. In STABCON, he worked on the modeling of the equations of motion of wind turbines and simulated the rigid response of the twin blade wind turbine. In ModAir, sponsored by Stork Fokker, he is simulating the dynamic response of the Fokker-100 passenger aircraft.